Development of Scale-Up Methodologies for Pharmaceutical Crystallization Processes

Dissertation presented for the Doctor of Philosophy degree in Refining, Petrochemical and Chemical Engineering

by

Ameessa Viliam Tulcidas

Supervisors: Prof. Fernando Rocha
Dr. Bruno Santos
Dr. Sylwin Pawlowski

December 2019

This work was developed for NORTE-08-5369-FSE-000042, co-financed by FSE (Fundo Social Europeu), under North's Regional Operational Program (Norte 2020).

UNIÃO EUROPEIA

Fundo Social Europeu

Acknowledgments

Firstly, I would like to thank my supervisors Prof. Fernando Rocha, Dr. Sylwin Pawlowski and industrial coordinator Dr. Bruno Santos, for the guidance provided. I also would like to acknowledge NORTE2020 for this Ph.D. research grant, since this work was a result of the project Operation NORTE-08-5369-FSE-000042 supported by Norte Portugal Regional Operational Program (NORTE 2020), under the PORTUGAL 2020 Partnership Agreement, through the European Social Fund (ESF). This work was financially supported by project UID/EQU/00511/2019 - Laboratory for Process Engineering, Environment, Biotechnology and Energy – LEPABE funded by national funds through FCT/MCTES (PIDDAC). I would also like to acknowledge the director of this doctoral program, Prof. Fernando Martins, for always being available to solve any grant-related issues.

Major thanks to Rafael Antunes and his R&D Products group members Nuno Torres, Isabel Martins, Margarida Figueiredo, Carmelina Frazão, Sérgio Silva, Sara Sequeira (my dearest SEM images provider), Joana Fernandes, Sara Cardoso (my dearest ex-coworker), Patrícia Serrano and many others who gave me chemical and analytical support.

I would also like to thank Rui Loureiro and the Process Chemistry Development group members for lending me their fume hoods and also giving me the training to operate with the reactors, Huber, FBRM probe and many more: Albertina Dias, Alexandra Vaz, Ana Cruz, André Carlos, António Henriques, Daniel Filipe Santos, Filipe Ataíde, Emília Leitão, Jorge Ferreira, José Pereira, Lucinda Conceição, Maria de Fátima Carvalho, Ricardo Mendonça, Ricardo Rosa, Rui Campos, Sílvia Cecília and many others.

Huge thanks to Miguel Cansado for taking some time from his busy schedule to share knowledge on how to create engaging presentations (this world definitely needs more humble leaders willing to teach and spread knowledge).

Many thanks also to João Bandarra and his Technical Services group for providing help, fume hoods and analytical support: Cláudio Leal, Gilda Lameira, João Rafael (PDG), João Lavrado, Marco António Silva, Paulo Glória, Pedro Borges and anyone I might have forgotten to mention.

Big thanks to Pedro Santos and his group members João Sequeira and Susana Medinas for giving me product and data.

I would also like to express my gratitude to Filipe Neves, Susana Nascimento and the remaining Pilot Plant team members. Especially to Maria Inês Lopes (aka 1000), Margarida Coutinho and Gonçalo Poeiras, for always giving a pat on my back after excessive venting. I must also thank Pilot Plant's B22

Formulation group for the laughter and friendly environment provided. Will definitely miss José Palma Oliveira aka Palm Olive's singing.

To my friends and ex-colleagues from the analytical department, a huge thank you for the kind words and positivity shown. Thanks, Lúcia Sousa and Ricardo Gonçalves for the help provided in the analytical field. Huge thanks to António Serôdio for the discussion about particle size. Thanks Catarina Vieira and Inês Silva for injecting my HPLC samples when I lost my access to the software.

I would also like to express gratitude towards all my fellow students and the Innovation team of Hovione.

Last but not the least, I would like to thank my ENGIQ family (Ana, André, Churro, Fred, Patrícia, Pedro and Tiago) for the discussions and gatherings; Diogo for the countless emotional support given and my family.

Abstract

The scale-up of crystallization processes is extremely challenging. Increase of equipment size leads to a decrease of surface area to volume ratio and development of temperature and/or concentration gradients, which, in turn, can affect the API (active pharmaceutical ingredients) crystals' properties (e.g. particle size distribution (PSD), crystal habit, etc.). Challenges such as the formation of fines and consequent loss of yield are reported at scale-up and therefore it becomes critical to understand and control the crystallization processes in order to obtain API with the desired properties.

This thesis aims at a better understanding of pharmaceutical crystallization processes and the development of methodologies that can help overcome the previously mentioned challenges. Hence, two case studies were considered, which embrace challenging crystallization techniques: evaporative crystallization followed by cooling and anti-solvent crystallization.

The first case study highlights the relevant aspects to be taken into consideration in the early stages of the development of a crystallization process. It reports the attempts in modifying the crystal habit and increasing the particle size of an API in a laboratory-scale evaporative followed by cooling crystallization. Ostwald ripening phenomenon was induced while monitoring the particle dimensions and population throughout the time with a Process Analytical Technology (PAT) tool. The solubility and supersolubility curves were determined to obtain the Metastable Zone Width (MSZW) and to further quantify the supersaturation attained in the process. Experiments with lower supersaturation and seeding were performed to attempt crystal growth, using the desired process solvent. Additionally, polymorphic stability, crystal habit, and size assessment studies were carried out in a different solvent system. It was found that working at a temperature above the melting point of the API seems to lead to the most stable polymorph, with a different crystal habit, size, and an acceptable purity, as desired.

The second case study addresses an anti-solvent crystallization system of an API with strict particle size requirements. Unlike the former case study, this case has a well-defined solvent system and crystallization technique, yet there are some variables needed to be further controlled in order to obtain the desired product. Therefore, statistical modeling was applied to assess the impact of mixing parameters such as suspension height to clearance ratio (H/C), percentage of filling volume in the reactor (%Volume), power per volume (PV) and tip speed (TS) on the particle size distribution. A statistical methodology was also proposed for the scale-up of anti-solvent crystallization processes by using models developed with data obtained in scale-down experiments, which predict the particle size and were validated with batches from the production scale. Furthermore, the models developed herein were used to estimate design spaces through Monte-Carlo simulations, indicating the operating conditions that lead to a higher probability of success, i.e., probability of obtaining API with particle size distribution parameters within specification.

Lastly, some guidelines were provided based on the actions taken in this work that allowed attaining the desired product properties and thus, can be helpful to follow in the development of similar crystallization systems.

Resumo

O *scale-up* de processos de cristalização é extremamente desafiante, dado que à medida que a escala aumenta, o rácio entre a área superficial e volume diminui, e os gradientes de temperatura e/ou concentração tornam-se significativos, o que por sua vez, poderá impactar determinadas propriedades dos cristais de API (ingrediente farmacêutico activo), como por exemplo a distribuição do tamanho de partícula, o hábito cristalino, entre outros. São reportados, no *scale-up*, desafios como a formação de finos e a consequente perda de rendimento e, como tal, é crítico compreender e controlar o processo de cristalização de forma a produzir um API com as propriedades desejadas.

O objetivo da presente tese consiste em adquirir conhecimento relativamente a processos de cristalização e desenvolver metodologias que facilitem a minimização da ocorrência de desafios no futuro. Por conseguinte, atentou-se particulamente na fase de desenvolvimento do processo (escala laboratorial). Com este intuito, consideraram-se dois casos de estudo da Hovione, que abrangem técnicas de cristalização exigentes: cristalização por evaporação seguida de arrefecimento e cristalização por anti-solvente.

O primeiro caso de estudo destaca os aspetos relevantes a serem considerados numa fase embrionária do desenvolvimento de processos de cristalização. Este reporta as tentativas de alterar o hábito cristalino e aumentar o tamanho da partícula de um API num processo de cristalização por evaporação seguida de arrefecimento, na escala laboratorial. Induziu-se o fenómeno de *Ostwald ripening* durante a monitorização da dimensão e população das partículas ao longo do processo por meio de uma ferramenta PAT (Tecnologia Analítica de Processo). Determinou-se a curva de solubilidade e curva de supersolubilidade do produto para estimar a zona metastável (MSZW) e posteriormente quantificar a sobressaturação atingida no processo. Adicionalmente, foram testadas experiências a baixa sobressaturação e com semente de forma a promover o crescimento dos cristais, no solvente de processo (etanol). Estudos relativos à avaliação da estabilidade polimórfica, hábito cristalino e tamanho de partícula foram executados usando um sistema distinto de solventes (heptano:1,2-dimetoxietano). Observou-se que operando a uma temperatura acima da temperatura de fusão do API leva à cristalização de produto na sua forma mais estável, com um hábito cristalino e tamanho diferentes e com uma pureza aceitável, tal como desejado.

O segundo caso de estudo, distintamente do caso de estudo anterior, possui um sistema de solventes e uma técnica de cristalização bem consolidada, porém, requer um estudo mais aprofundado de certas variáveis para se obter o produto desejado. Este, por sua vez, aborda uma técnica de cristalização por anti-solvente, em que é necessário obter um API cuja distribuição do tamanho de partícula cumpra uma especificação bastante restrita. Nesse sentido, recorreu-se à modelação estatística para avaliar o impacto de parâmetros de mistura como o rácio entre a altura da suspensão e *clearance* (H/C), percentagem de volume ocupado no reactor (%Volume), potência aplicada por unidade de volume (PV) e *tip speed* (TS) na distribuição do tamanho de partícula. Propôs-se uma metodologia estatística para o *scale-up* de processos de cristalização por anti-solvente, que prevê o

tamanho de partícula com base em modelos desenvolvidos com dados de experiências de *scale-down* e validados com dados de lotes na escala de produção.

Complementarmente, os modelos desenvolvidos ao longo do doutoramento foram utilizados para estimar janelas operacionais através de simulações *Monte-Carlo*, indicando as condições operatórias que levam a uma maior probabilidade de sucesso, isto é, maior probabilidade de produzir API com uma distribuição de tamanho de partícula que cumpra a especificação.

Para finalizar, sugeriram-se algumas linhas orientadoras, com base nas acções tomadas neste trabalho que levaram à obtenção de um produto com as propriedades físicas desejadas, e cuja aplicação poderá vir a ser útil em processos de cristalização similares.

Table of Contents

List of Figures

List of Tables

Chapter 1 Introduction

1.1. Motivation

Above 90% of all pharmaceutical products including tablets, aerosols, capsules, suspensions, and suppositories contain the drug in particulate form, generally crystalline [1]. Therefore, it is critical to master and control the crystallization process to produce an API (Active Pharmaceutical Ingredient) or drug product with the desired solid-state characteristics: purity, crystal morphology and particle size distribution (PSD) [2].

The difficulty in capturing the detailed mixing and heat transfer of an industrial scale vessel using a geometrically similar laboratory vessel leads to several problems during the scale-up of crystallization processes. Furthermore, particle size does not scale with the vessel dimensions, nor do the transport properties associated with the particles and suspension. At last but not the least, it is tempting to maintain the specific power input of the agitator in both scales, albeit the power required is often too large and may end up damaging the growing crystals and leading to unwanted secondary nucleation [2].

Challenges such as fines' formation, undesired crystal form and habit are the most common to befall during the scale-up. These modifications of the crystal properties have a high impact on the downstream unit operations such as filtration, where fine crystals can cause clogging of the porous membrane, which decreases the product yield and delays the process. Drying and milling operations can also be influenced [3]. Moreover, the physical and chemical properties, such as dissolution rate and solubility and consequently the bioavailability of the final drug product can also be affected by the aforementioned properties [4].

For instance, the desired particle size can be attained by controlling the nucleation and growth kinetics. Operating near the supersolubility curve favors spontaneous nucleation and thus, fines' formation, whereas, the growth of crystals is promoted in regions near the solubility curve. Supersaturation, the driving force of crystallization processes, can be achieved by temperature reduction (cooling), solvent evaporation, anti-solvent addition and precipitation [5]. The latter is commonly used in the pharmaceutical industry. Regularly, a seeding process is also combined with the aforementioned techniques to control the crystal size and form [6]. The zone between the supersolubility curve and the solubility curve is defined as the metastable zone, which is commonly used to understand when nucleation occurs and determine the operation window for crystallization processes. The metastable zone width (MSZW) can be influenced by several process parameters, as for instance, cooling, agitation and evaporation rates as well as the presence of impurities [7] which, in turn, are decisive in the scale-up process.

Consequently, the main goal of this work is to understand two challenging crystallization processes at Hovione and develop methodologies that can help avoid or minimize their occurrence in the future.

Moreover, tackling these hindrances can also aid in reducing the financial loss caused by having out of specification batches.

1.2. Thesis contributions

The work developed during this Ph.D. resulted in several scientific contributions.

Publications

- A. Tulcidas, N. M. T. Lourenço, R. Antunes, B. Santos, S. Pawlowski and F. Rocha, “Crystal habit modification and polymorphic stability assessment of a long-acting, β_2-adrenergic agonist”, CrystEngComm, vol. 21, pp. 3460 - 3470, 2019.

- A. Tulcidas, S. Nascimento, B. Santos, C. Alvarez, S. Pawlowski and F. Rocha, “Statistical methodology for scale-up of an anti-solvent crystallization process in the pharmaceutical industry”, Separation and Purification Technology, vol. 213, pp. 56 - 62, 2019.

- A. Tulcidas, B. Santos, S. Pawlowski and F. Rocha, “Quality by statistical control in crystallization - Assessment of mixing conditions and probability of obtaining the desired particle size”, Industrial & Engineering Chemistry Research, vol. 58, pp. 20162 - 20172, 2019.

Oral communications

- "Development of scale-up methodologies for pharmaceutical crystallization processes" at 2nd Doctoral Congress in Engineering; FEUP; Porto; 8th - 9th June 2017.

- "Impact of mixing conditions on the nucleation rate and particle size of an API in an anti-solvent crystallization" at 13th International Chemical and Biological Engineering Conference (ChemPor 2018); Aveiro; 2nd - 4th October 2018.

- "QbD in pharmaceutical anti-solvent crystallization: probability of obtaining the desired particle size" at 3rd International Congress of Chemical Engineering; Santander, Spain; 19th - 21st June 2019.

- "Crystal habit modification and polymorphic stability assessment of a drug substance" at 3rd Doctoral Congress in Engineering; FEUP; Porto; 27th - 28th June 2019.

1.3. Thesis outline

The work developed in this thesis is described in seven chapters.

Chapters 1 and 2 provide the motivation and goals of this thesis, as well as the theoretical background regarding crystallization principles.

Chapter 3 presents the relevant aspects to be considered in the early stages of the development of crystallization processes. For that purpose, this chapter addresses a case study, where an API with different crystal habit, size and specific polymorphic form was desired, in order to ease the downstream processes. The crystallization process consisted of an evaporation step followed by cooling, leading to needle-shaped crystals, which are not suitable for further processing steps. This chapter describes the attempts performed until achieving the desired physical properties, from using Process Analytical Technology (PAT) tool to monitor the particle counts and dimensions *in-situ*, MSZW (Metastable Zone Width) determination for supersaturation quantification, execution of experiments with low supersaturation, to slurry tests with a different mixture of solvents at different operational conditions.

Chapters 4, 5 and 6 are based on a case study of an API obtained through an anti-solvent crystallization process that requires meeting very strict particle size specifications. Unlike the first case study, the latter has a well-defined solvent system and crystallization technique. Nevertheless, some variables needed to be explored further to assess their impact on the particle size of the product. Therefore, Chapter 4 provides an insight into the impact of the clearance and agitation applied during an anti-solvent crystallization on the particle size distribution parameters of the product. Additionally, Chapter 5 focuses on building a statistical methodology that can predict the particle size parameters at an industrial scale using data from scale-down anti-solvent crystallization experiments performed at the laboratory scale. Chapter 6 quantifies the risk, i.e., the probability of obtaining the product within specification when working at certain conditions. Thus, a methodology was developed using the models found in chapters 4 and 5, to build a design space that quantifies the probability of the product meeting the particle size specification, which can be helpful in the development of crystallization processes to avoid operating at conditions that can lead to out-of-specification batches.

Chapter 7 summarizes the main conclusions. Furthermore, some guidelines are provided based on the actions taken in this work that allowed attaining the desired product properties, which can be helpful to follow during the development of similar crystallization systems. Lastly, suggestions for future research are presented.

References

[1] P. Shekunov, B. Y.; York, “Crystallization process in pharmaceutical technology and drug delivery design.,” *J. Cryst. Growth*, vol. 211, no. 1–4, pp. 122–136, 2000.

[2] A. S. Myerson, *Handbook of Industrial Crystallization*, 2nd ed., no. October. Elsevier Science & Technology Books, 2001.

[3] J. Chen, B. Sarma, J. M. B. Evans, and A. S. Myerson, “Pharmaceutical Crystallization Published as part of the Crystal Growth & Design 10th Anniversary Perspective,” *Cryst. Growth Des.*, vol. 11, pp. 887–895, 2011.

[4] C. Schaefer, C. Lecomte, D. Clicq, A. Merschaert, E. Norrant, and F. Fotiadu, “On-line near infrared spectroscopy as a Process Analytical Technology (PAT) tool to control an industrial seeded API crystallization,” *J. Pharm. Biomed. Anal.*, vol. 83, pp. 194–201, 2013.

[5] W. L. McCabe, J. C. Smith, and P. Harriott, *Unit Operations of Chemical Engineering*, 5th ed. USA: McGraw-Hill, 1993.

[6] R. Hilfiker, *Polymorphism in the Pharmaceutical Industry*. Germany: Wiley-VCH, 2006.

[7] G. Zeng, H. Li, S. Huang, X. Wang, and J. Chen, “Determination of metastable zone width and the primary nucleation kinetics of sodium sulfate,” *Theor. Found. Chem. Eng.*, vol. 49, no. 6, pp. 869–876, 2015.

Chapter 2 State-of-the-art

This chapter introduces the theoretical principles of the crystallization process, such as the crystalline state, applications, kinetics, batch crystallizers and scale-up challenges.

2.1. Crystallization – crystalline state and applications

2.1.1. Crystallization definition and crystalline state

Crystallization is a separation process, which forms pure accurately organized solid structures (crystals) from a liquid homogeneous solution. It is the most preferable operation used when producing heat-sensitive particulate products, requiring less energy consumption and being consequently more economical than, for instance, a distillation process [1].

In a crystalline solid, the motion of molecules, atoms or ions is restricted to oscillations about fixed positions arranged in a regular or lattice pattern. Crystals are rarely spherical in shape. When crystals grow, they form polyhedrons with flat sides and sharp corners if ungoverned by other surfaces such as container walls and other crystals.

Crystals consist of many units, each shaped like the larger crystal. This led to the concept of a space lattice as a regular arrangement of points (molecules, atoms, or ions) such that if a line is drawn between any two points and then extended in both directions, the line will pass through other lattice points with identical spacing. In 1848, Bravais showed that only fourteen space lattices are possible. Based on the symmetry of the three mutually perpendicular axes with respect to their relative lengths (a, b, c) and the angles (α, β, γ) between the axes, these fourteen lattices can be classified into the seven crystal systems (Table 2.1).

Table 2.1 - The seven crystal systems (from [2]*).*

Crystal system	Space Lattices	Length of axes	Angles between axes
Cubic (regular)	Simple cubic Body-centered cubic Face-centered cubic	a = b = c	α = β = γ = 90º
Tetragonal	Square prism Body-centered square prism	a = b < c	α = β = γ = 90º
Orthorhombic	Simple orthorhombic Body-centered orthorhombic Base-centered orthorhombic Face-centered orthorhombic	a ≠ b ≠ c	α = β = γ = 90º

Table 2.1 (Cont.) - The seven crystal systems (from [2]*).*

Crystal system	Space Lattices	Length of axes	Angles between axes
Cubic (regular)	Simple cubic Body-centered cubic Face-centered cubic	a = b = c	α = β = γ = 90º
Tetragonal	Square prism Body-centered square prism	a = b < c	α = β = γ = 90º
Orthorhombic	Simple orthorhombic Body-centered orthorhombic Base-centered orthorhombic Face-centered orthorhombic	a ≠ b ≠ c	α = β = γ = 90º
Monoclinic	Simple monoclinic Base-centered monoclinic	a ≠ b ≠ c	α = γ = 90º β ≠ 90º
Rhombohedral (trigonal)	Rhombohedral	a = b = c	α = β = γ ≠ 90º
Hexagonal	Hexagonal	a = b ≠ c	α = β = 90º γ ≠ 90º
Triclinic	Triclinic	a ≠ b ≠ c	α ≠ β ≠ γ ≠ 90º

2.1.2. Applications

Crystallization is a widely solid-liquid separation process employed in several industries, from agrochemicals, food, petrochemical to pharmaceuticals [2], [3].

Xu *et al.* [4] simultaneously recovered potassium and phosphorous, from synthetic and real urine, by crystallization of magnesium-potassium-phosphate-hexahydrate, for nutrient recycling which is imperatively necessary for countries that depend strongly on imported potassium fertilizers.

In the food industry, crystallization of sugars is controlled to give the desired textural properties of, for example, hard candies or fondant icing [5].

Curiously, crystallization is also researched in the petrochemical field to avoid the formation of n-paraffin wax crystals, which in turn, clog fuel filters and cease the fuel flow to the engine, leading diesel engines to operate ineffectively [6].

Regarding the pharmaceutical industry, crystallization is widely used during the intermediate and final stages of purification and separation, resulting in a solid intermediate or API.

Detailed information about the crystallization process in the pharmaceutical industry is described in the following section.

2.1.3. Crystallization in the Pharmaceutical Industry

Shekunov and York [7] stated that above 90% of all pharmaceutical products including tablets, aerosols, capsules, suspensions, and suppositories contain the drug in particulate form, generally crystalline.

Consequently, it is critical to master and control the crystallization process to produce an API or final product with the desired solid-state characteristics: purity, crystal form and morphology, particle size distribution (PSD), density and flowability [2]. These properties translate into a high impact on the downstream unit operations such as filtration, where fine crystals can cause clogging of the porous membrane, which decreases the product yield and delays the process. Drying and milling operations can also be influenced [8]. Moreover, the physical and chemical properties, such as dissolution rate, solubility and consequently the bioavailability of the final drug product can also be affected by the aforementioned properties [9]. Table 2.2 presents the most relevant solid-state parameters and their subsequent influence on the final drug product.

Table 2.2 - Crystal properties controlled by crystallization and their influence on the final drug product (based on [7]*).*

	Solid-state properties	**Effect on final drug product**
Structural	Crystallinity (amorphous or semi-crystalline form)	Physical and chemical stability
	Polymorphs	Hygroscopicity
	Solvates (hydrates)	Solubility profile and dissolution rate
	Salts	All aspects of processing (milling, wet granulation, oven drying, compaction)
	Crystal defects	
Dimensional	Particle size distribution	Processing behaviour: bulk density, agglomeration, flow/rheology, compaction
	Particle morphology	Particle permeability/adsorption
	Particle surface structure	Bioavailability (drug absorption)
		Consistency and uniformity of dosage
Chemical	Impurities, residual solvents, decomposition products	Toxicity
	Chiral forms and chiral separation	Chemical, physical and enantiomeric stability
Mechanical	Brittleness	Milling and tableting behaviour
	Fracture stress	
	Indentation hardness	
	Stress/strain relaxation	
Electrical	Electrostatic charge distribution	Agglomeration and flow properties

The physical and chemical stability of the drug product is linked to the polymorphism (internal structure of the crystal), as amorphous solids are less stable chemically. These are also more hygroscopic since the irregular shape of the powder creates a high surface area, which attracts water

molecules. The physical stability of hydrates and anhydrous forms strongly depends upon the relative humidity and/or temperature of the environment. Transitions from one form to another occur as a consequence of variations in storage conditions or technological treatments [10]. For instance, milling can impart a significant amount of energy on a solid, and could potentially lead to a full or partial polymorphic conversion or generation of an amorphous substance (or at least a degree of amorphous content). Amorphous forms, being metastable, can, in turn, reconvert to a crystalline state, which may differ from the originally desired product. Additionally, during wet granulation – a step that often precedes the production of tablets – the API is exposed to a solvent (water or an organic solvent with low toxicity, such as ethanol) and is once more prone to undergoing solvent-mediated transformations. Exposure to humidity can create similar conditions that can lead to hydrate formation. During compaction, unstable polymorphs can convert to the stable form, a fact that can be attributed to the energy applied in the process. The extent of transformation is dependent on the zone of the tablet, the pressure applied, the compression temperature and the particle size of the API powder [11].

The enantiomeric stability of the drug is related to the fact that one isomer may produce the desired therapeutic activities, whereas the other may be inactive or produce unwanted effects [12].

Most of the pharmaceutical powders are dielectric materials and are often unavoidably charged during the manufacturing process due to interparticle and particle-wall collisions. Electrostatic charges of both positive and negative polarities give rise to attractive or repulsive electrostatic forces between the individual particles. As a result, electrostatic charging may cause the agglomeration or segregation of particles during powder dispersion, transport, and other handling processes. Electrostatic charging also has a significant effect on powder blending performance. For example, it was found that the total adhesion forces between the API and excipients decreased with the charge decay during storage [13].

Furthermore, pharmaceutical industries deal with a fast-paced environment, resulting from the excessive pressure to improve process efficiency and reduce time to launch the drug product into the market. Improvements in the process efficiency are always necessary for the manufacture of generic drugs and when large quantities of drugs are needed to cure life-threatening diseases. Additionally, reducing time to market as soon as possible extends the period before patent expiration [14].

According to Myerson [2], several common hurdles are encountered in the crystallization process in the pharmaceutical field, such as:

- The control of supersaturation and particle size distribution in a batch crystallizer;

- The effective use of seed – Seeding can have two main goals such as, promoting the growth of crystals and controlling particle properties, particularly, polymorphism and particle size distribution. The selection and preparation of the seed, the point of addiction and the relation between the amount used (0.1 – 1 wt% of the solute) and the proceeding of the crystallization, play a determining role for the success of seeding [15];

- Identification and retention of the most stable polymorphic form - Polymorphs are essentially different crystalline forms of a solid resulting from different crystal packing of the same molecules or ions. Since polymorphs represent distinct solid phases, their physical properties

such as, for instance, solubility and dissolution rate, also differ [16]. Since the molecules are arranged differently in the different polymorphs, it is possible to have different portions or functional groups on the molecule exposed at the surfaces at the crystal. These differences, especially when involving hydrogen bonding groups, can cause the crystal to interact differently with solvents and therefore change the solubility of the drug [17]. Problems encountered range from sudden unexpected inability to produce reliably a form that has been used for pivotal clinical studies to variations in the drug product properties due to seemingly random changes of the solid form during processing or storage [18]. For instance, 2 years after the launch of the first Ritonavir product, a drug used to treat HIV-1 infections, several batches failed dissolution specifications due to the presence of a new thermodynamically stable form II having ~50% solubility of the reference form. This forced the manufacturer to withdraw the original formulation from the market and perform a new reformulation of the product [10].

One other important benefit of understanding the various polymorphs and methods of preparation of different polymorphs is that polymorphs are patentable. This knowledge may thus provide commercial benefits for the organization [17].

- Efficient measurement of solubility in multiple solvent systems to maximize purification and yield;

Therefore, to comprehend the aforementioned hindrances, the solubility and supersaturation degree, nucleation and growth kinetics, batch crystallizers and factors governing crystal purity, habit and morphology are under the main scrutiny to achieve the optimal process and the desired specifications. It is necessary to comprehend the complex process that is crystallization.

2.2. Crystallization principles and techniques

To promote crystallization, two primary particle formation processes are necessary: nucleation - the birth of new crystals and their growth [19]. The relation between the nucleation rate and crystal growth rate influences relevant product properties, for instance, product crystal size and size distribution (fast nucleation translates into small-sized crystals). The growth conditions affect the crystal shape, regarding the solvent used or the presence of impurities. The growth rate also has a strong influence in the purity of the crystals, for example, a fast growth promotes the formation of liquid inclusions in the crystal [20].

To meet the desired crystal properties, crystallization thermodynamics including solubility and metastable zone width should be understood.

Supersaturation is the driving force of the crystallization process. According to Myerson [2], a supersaturated solution is defined as a solution in which the solute concentration exceeds the equilibrium (saturation) solute concentration, at a given temperature. Supersaturation, is often expressed, for an ideal solution, as a concentration difference Δc:

$$\Delta c = c - c^* \tag{2.1}$$

and as a ratio of concentrations, S:

$$S = \frac{c}{c^*} \tag{2.2}$$

where c is the concentration and c^* is the saturation concentration, respectively.

A saturated solution is a solution in which the solute and solvent are in equilibrium at a given temperature [21]. Saturation can be represented by a curve plotting concentration versus temperature (solubility or saturation curve) since it is mainly dependent on the latter [3].

Between the supersolubility and solubility curves, there is a metastable zone, which provides a region of driving force: supersaturation [22]. The solubility curve can be determined accurately experimentally. On the other hand, the position of the supersolubility curve is uncertain, due to its dependence on factors such as the rate of supersaturation generation, the degree of agitation and the presence of crystals or impurities. In the stable unsaturated zone, crystallization is impossible to occur, whereas in the metastable zone, the nucleation is unlikely but growth is possible. Above the supersolubility curve, nucleation of small nuclei, invisible to the naked eye, occurs spontaneously [21], [23].

According to Myerson [2] the effect of size on particle solubility can be expressed by Gibbs-Thomson (Ostwald-Freudlinch) (Equation 2.3):

$$r = \frac{\beta\, V \sigma_s}{k_B\, T\, ln(S)} \tag{2.3}$$

Where r is the particle radius, β is the shape factor available in the literature, V is the volume of the crystals (m^3), σ_s is the specific surface energy of solid particles (J/m^2), k_B is the Boltzmann constant (1.346×10^{-23} J/K), T is the temperature (K) and S is the supersaturation ratio given by Equation 2.2.

Particles have different dissolution rates based on their size when present in a suspension of particles with a size distribution. This difference in solubility results in the small particles dissolving and depositing on the larger particles and therefore increase the average crystal size. This process is called Ostwald ripening and it is important in processes where crystallization is rapid and crystal sizes are small [2].

Supersaturation can be achieved by the following methods [24]: cooling, evaporation, anti-solvent and precipitation (reactive crystallization).

- Temperature reduction (cooling)

  Cooling is applied when the solubility of the solute increases strongly with the temperature, which is the case of inorganic salts and organic substances. This technique turns a saturated solution into a supersaturated by simple cooling. Normally, the cooling method complements other techniques such as evaporation or anti-solvent addition, in order to achieve higher yields [16].

- Solvent evaporation or evaporative crystallization

This method is used when the solute solubility is relatively independent of temperature, as is the case of common salt. Supersaturation is attained by evaporating a portion of the solvent [2].

Normally, in pharmaceutical applications, this technique is often combined with cooling crystallization to increase the yield of the product, usually applying a partial vacuum to promote evaporation. In evaporative crystallization, crystals are sometimes observed to form preferentially near the surface of the solution, due to a higher local concentration of solute. The meniscus of a solution can also have geometry favoring higher evaporation rates, with crystals then forming at the contact line with the crystallization vessel [11].

- Anti-solvent addition (salting out)

This technique is employed when the solubility of the solute is intensely high in a certain solvent and neither cooling nor evaporation is desirable. It consists of adding a third component, which may form a mixed solvent with the original solvent, reducing significantly the solubility of the solute. The solubility decreases with anti-solvent addition and the metastable zone width will depend primarily on the anti-solvent addition rate [16].

New approaches include, for instance, using gas anti-solvent such as supercritical carbon dioxide to produce high purity anthracene from a highly contaminated feed. The solubility of the impurities was significantly reduced and therefore salted out by the introduction of the supercritical fluid. Similar gas anti-solvent procedures seem to be advantageous in the separation of isomers from solution. Supercritical carbon dioxide has also been used to separate essentially pure β-carotene from carotene oxidation products [25].

- Precipitation (reactive crystallization)

Reactive crystallization occurs where two compounds react in solution to give a product that is less soluble than the reactants from which it is formed. Supersaturation is generated by the formation of the new product, and the rate at which it develops is determined by the rate of reaction and the solubility of the product species relative to the reactants and the conditions employed. Reactive crystallizations are employed quite often in the pharmaceutical industry, in particular, when in the final synthesis step a product is less soluble than the reactants and any by-products such that isolation can follow through simply by crystallization or precipitation from the solution in which the reaction has been carried out. Furthermore, it is also important to take into account the heating or cooling applied when the reaction is either exothermic or endothermic, due to its influence on supersaturation [16].

Another common method of reactive crystallization in the pharmaceutical industry is via pH modification. Many drug substances are slightly soluble weak acids or bases, whose anionic or cationic salt forms are much more soluble in water. Adjustment of the pH can thus lead to the crystallization or precipitation of the free acid or base, and this can be used to purify and consolidate the final product. Proton transfer reactions associated with pH shifts are generally rapid, and supersaturation is achieved rapidly [16].

The combination of rapid reaction and delayed nucleation usually results in conditions analogous to a very wide metastable zone, promoting the formation of amorphous materials, unstable and metastable polymorphs or crystals of poor quality [16].

As aforementioned, in the majority of crystallizations, either nucleation or growth contribute to the final properties and therefore it is critical to have maximum control and robustness over the crystallization kinetics. The next section discusses the nucleation and growth mechanisms.

2.3. Kinetic parameters

As mentioned in section 2.2, the rates of nucleation and growth play an important role in crystallization processes, due to their influence on the crystal size and size distribution [23].

2.3.1. Nucleation

Nucleation may be primary if the supersaturated solution is free of crystalline surfaces or secondary when it contains crystals. A high level of supersaturation is required for the primary nucleation to occur, being the main mechanism for precipitation. On the other hand, secondary nucleation is the principal mechanism when large crystals are desired. It involves the presence of crystals and their interaction with the environment, such as crystallizer walls or impellers [2], [23].

Primary Nucleation

Primary nucleation occurs in the absence of any foreign matter (neither crystals nor dust) and can be categorized into homogeneous or heterogeneous.

Homogeneous nucleation

The process is initiated when the molecules, present in the supersaturated solution, associate to form a cluster, which can either dissociate or grow. If a cluster grows to an appearance of a lattice structure, it develops into an embryo. Advanced embryo growth can result into a stable crystalline nucleus. The classical theory of nucleation postulates that clusters are created through an addition mechanism which continues until a critical size is attained [2], [23].

The rate of nucleus formation (B^0, number of nuclei/cm^3.s) by this mechanism is described by an expression similar to Arrhenius expression (Equation 2.4).

$$B^0 = A\ exp\left(\frac{-\Delta G_{cr}}{k_B T}\right) \tag{2.4}$$

Where A is the frequency factor, theoretically equal to 10^{30} nuclei/cm^3.s, ΔG_{cr} is the critical free energy for nucleation (J), k_B is the Boltzman's constant in J/K and T is the temperature in K.

The free energy change for the formation of this new solid phase (ΔG) is the sum of the free energy change for the formation of the nucleus surface (a positive quantity, ΔG_s) and the free energy

change for the phase transformation (a negative quantity, ΔG_v). For spherical nuclei, the free energy change is given by Equation 2.5:

$$\Delta G = \Delta G_S + \Delta G_v = 4\pi r^2 \sigma_{s,L} + \frac{4}{3}\pi r^3 \Delta G_v \quad (2.5)$$

Where $\sigma_{s,L}$ is the interfacial tension (J/m^2) and r the nucleus' radius (m).

The critical size (or critical nucleus radius, r_c in m) can be found by minimizing Equation 2.5:

$$\frac{d(\Delta G)}{dr} = 8\pi\, r_c\, \sigma_{s,L} + 4\pi\, r_c^2 \Delta G_v = 0 \quad (2.6)$$

Or

$$r_c = -\frac{2\,\sigma_{s,L}}{\Delta G_v} \quad (2.7)$$

Substituting for ΔG_v from Equation 2.5 and 2.7, it is obtained the critical free energy for nucleation ΔG_{cr} in Equation 2.8.

$$\Delta G_{cr} = \frac{4\pi\, r_c^2\, \sigma_{s,L}}{3} \quad (2.8)$$

The growth of the clusters is expressed by the Gibbs-Thomson equation.

$$\ln\left(\frac{c}{c^*}\right) = \ln(S) = \frac{2\,\sigma_{s,L}\, V_m}{k_B\, T\, r} \quad (2.9)$$

Where c is the concentration of clusters of size r and V_m is the molar volume (m^3/mol). Thus, smaller clusters dissolve (Ostwald ripening as mentioned in the previous subchapter), whereas larger clusters grow until they reach a critical size r_c, and a new phase is created. Substituting for r_c in Equation 2.8 from Equation 2.9, it is obtained:

$$\Delta G_{cr} = \frac{16\pi\ V_m^2\, \sigma_{s,L}^3}{3(k_B\, T \ln(S))^2} \quad (2.10)$$

Substituting in Equation 2.4, the nucleation rate is given by [23]:

$$B^0 = A\, exp\left[\frac{-16\,\pi\ V_m^2\, {\sigma_{s,L}}^3\, N_a}{3v^2\ (RT)^3\ [ln(S)]^2}\right] \quad (2.11)$$

Where v is the number of ions/molecule of solute, R is the gas constant (8.314 J/K.mol) and N_a is the Avogadro number (6.022 x 10^{23} molecules/mol).

Heterogeneous nucleation

Heterogeneous nucleation is more likely to occur, since it is extremely difficult to prepare solutions without incorporating any foreign particles like dust or colloidal. The presence of foreign substances in a supersaturated solution generally reduces the energy required for nucleation [26]. Since the free energy barrier is lower in the case of a heterogeneous system, nucleation occurs at a lower supersaturation. The decrease in the free energy (φ) depends on the wetting angle (θ) of the solid phase (Equation 2.13) [2].

$$\Delta G_{homogeneous} = \varphi \Delta G_{heterogeneous} \tag{2.12}$$

$$\varphi = \frac{1}{4}(2 + \cos\theta)(1 - \cos\theta)^2 \tag{2.13}$$

Spontaneous nucleation would occur for a system with zero contact angle, nevertheless, no such systems occur in practice [2].

Secondary Nucleation

As mentioned previously, secondary nucleation occurs by the presence of crystals in the supersaturated solution [23]. This type of nucleation can be promoted by the following mechanisms [2]:

- Initial breeding, which occurs when dry crystals are first introduced into a solution. Small crystalline fragments present on the crystal surface are washed from the surface by the solution and form new nuclei;
- Polycrystalline breeding, where the fragmentation of irregular polycrystalline aggregates, formed at high supersaturation, serves as nucleation centers;
- Abrasion of crystals, caused at high stirring speeds, which results into fragments which serve as nucleation sites;
- Fluid shear forces are enough to produce secondary nuclei from an existing crystal surface [27]. For example, when at high supersaturation, dendritic growth takes place at the crystal surface that can break due to the shear flow around it or due to the dendrite coarsening mechanism, being the source of crystal nuclei. Additionally, the shearing action of the fluid is enough to detach a layer of the crystals [2];

Contact nucleation (collision breeding or collision nucleation), the most important mechanism of secondary nucleation in industrial crystallizers, is promoted by the contact between a growing crystal and the walls of the vessel, stirrer or other crystals, resulting into the genesis of contact nuclei. It is the most common type, since it occurs at lower supersaturation values [2].

The following function is widely used, to obtain the rate of secondary nucleation, which correlates much of the experimental data:

$$B^0 = k_N (S - 1)^b M_T^j N^r \tag{2.14}$$

Where M_T is the mass of crystals per volume of suspension and *N* is the agitation rate (rpm of an impeller). The constants k_N, *b*, *j* and *r* are obtained from experimental data, on the respective system [23].

Factors that influence secondary nucleation

Supersaturation, degree of agitation and the presence of impurities are the factors that affect secondary nucleation. At a higher supersaturation degree, the adsorbed layer is thicker, resulting in a higher number of nuclei. On the other hand, increasing the agitation degree translates into an increase in the contact between the crystals themselves, crystals and crystallizer walls and crystal-impeller, and hence favor contact nucleation. Furthermore, the agitation also induces flow shear, aiding the secondary nucleation mechanism [28]. The effect of impurities is complex and unpredictable [2]. According to Denk and Botsaris [29], trace amounts of certain dissolved impurities can diminish the nucleation rate of crystals or even hinder their formation. The impurity uptake by the growing seed crystal may lead to an impurity concentration gradient in the boundary layer surrounding the seed crystal. Due to this gradient, the impurity concentration near the crystal surface may be considerably lower than the bulk concentration. The Impurity Concentration Gradient (ICG) nucleation model states that if the conditions were such that the only reason that spontaneous nucleation did not occur in the bulk solution was because of the high impurity concentration that existed there, and if the impurity concentration near the crystal surface was reduced to a low enough level, nucleation could occur in the boundary layer near the crystal surface [29].

As aforementioned, nucleation refers to the birth of new nuclei and once it has been achieved, nuclei growth dominates by the addition of solute molecules from the supersaturated solution (crystal growth).

2.3.2. Crystal growth

Crystal growth is a layer by layer process, where the deposition of the layers is dependent on the crystal packing of the unit cell, which means, how the elements of a specific molecular species are three-dimensionally assembled in a crystalline state [23].

Growth takes place when the rate of integration of single molecules or aggregates into an existing lattice structure transcends the rate of release of these entities from the surface, a process also driven by local concentration variation [30].

The growth of crystals can be described by three mechanisms: continuous growth mechanism, two-dimensional nucleation and spiral growth.

Continuous growth mechanism

According to this growth mechanism, high roughness crystalline material, containing kink and step sites on the surface, accommodates easily any approaching growth unit (Figure 2.1). This might be explained by the fact that molecules tend to bond at the location where they have the maximum number of nearest neighbors.

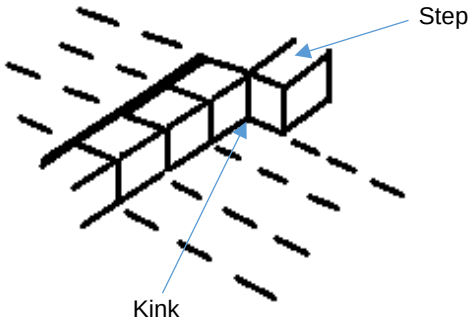

Figure 2.1. Surface structure of a growing crystal.

Growth by two-dimensional nucleation mechanism

Many crystallized materials do not have enough roughness to promote continuous growth, hence it is necessary to create steps to accommodate the incoming growth units. The two-dimensional nucleation is a mechanistic explanation for the conception of these steps, through the formation of nucleated circles on the flat surface of the crystal, where the molecules are being adsorbed onto, desorbed from and diffusing to the surface (Figure 2.2).

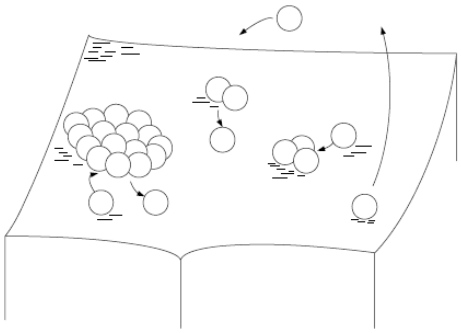

Figure 2.2. Two-dimensional nucleus formation on a crystal surface [30].

Spiral growth mechanism (screw dislocation)

The spiral growth or screw dislocation mechanism was proposed by Burton, Cabrera and Frank (BCF theory). This mechanism postulates that once the screw dislocation is created, the crystal growth at the edge of the dislocation is energetically favorable, resulting in a spiral growth of the crystal [31].

Dislocation can occur within crystals as a result of stresses in crystal growth on seeds and around surface nuclei and inclusions [30]. Spiral can promote different growth rates on different crystals of the same material, due to the fact that each crystal is responding to the structure of its own unique dislocation (Figure 2.3).

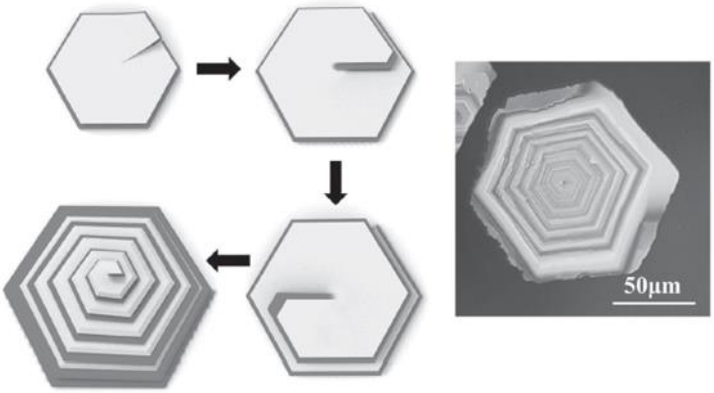

Figure 2.3. Development of a spiral growth from a screw dislocation of a Tin (IV) sulphide crystal [31].

Mass transfer principles

The mass transfer in crystal growth can be described by the two-step theory. In the first step, the mass transfer of the solute occurs from the bulk of the solution to crystal-solution interface and is expressed by Equation 2.15:

$$\frac{dm}{dt} = k_c\, A\, (c - c_i) \tag{2.15}$$

Where $\frac{dm}{dt}$ is the rate of mass deposited on the crystal surface, k_c is the mass transfer coefficient (m/s), A is the surface area of the crystal (m^2), c is the mass solute concentration in the bulk supersaturated solution (kg/m^3) and c_i is the supersaturated concentration in the interface (kg/m^3). Since the molecular diffusion of the solute occurs through a thin stagnant film of solution adjacent to the crystal surface: $k_c = D/\delta$, where D is the diffusion coefficient (m^2/s) and δ is the film thickness (m) which depends on the velocity of the solution past the crystal, which is defined by the degree of agitation [23]. Regarding the second step, a first-order reaction is assumed to occur at the crystal-solution interface, in which solute molecules are integrated into the crystal-lattice structure, being this kinetic step expressed by Equation 2.16:

$$\frac{dm}{dt} = k_i\, A\, (c_i - c^*) \tag{2.16}$$

Where k_i (m/s) is the kinetic coefficient.

Combining both equations 2.15 and 2.16, equation 2.17 is obtained:

$$\frac{dm}{dt} = \frac{A\,(c - c^*)}{\frac{1}{k_c} + \frac{1}{k_i}} \tag{2.17}$$

At low solution agitation velocities, the growth rate may be controlled by the first step. The second step can be important, especially when the solution velocity surrounding the crystal surface is high, such that k_c is large compared to k_i. The former is independent of the crystallization process and can be estimated from general fluid-solid particle mass-transfer coefficient correlations, whereas k_i is peculiar to the crystallization process. Diverse theories have been advanced for the kinetic step, for instance the one by Burton, Cabrera and Frank (BFC) where their theory indicates that the crystal growth starts from

a screw dislocation (imperfection in the crystal structure), confirmed by experiments using scanning-electron microscopy, as aforementioned. The kinetic coefficient k_i, is back-calculated from experimental data [23].

Although crystals do not grow as spheres, the equation for the rate of increase of the diameter of a spherical particle can be deduced from Equation 2.17, considering an overall coefficient K_c .

$$\frac{dm}{dt} = K_c\, A\, (c - c^*) \tag{2.18}$$

Where $A = \pi D_p^2$ and $m = \frac{\pi\, D_p^3}{6}\rho$, D_p is the particle (crystal) diameter in m, and ρ is the crystal density (kg/m^3). Therefore, substituting in Equation 2.18:

$$\frac{dD_p}{dt} = \frac{2K_c\,(c - c^*)}{\rho} = \frac{2K_c\,\Delta c}{\rho} \tag{2.19}$$

If the rate of growth is controlled by k_i , which is assumed to be independent of D_p:

$$\frac{\Delta D_p}{\Delta t} = \frac{2k_i\,\Delta c}{\rho} \tag{2.20}$$

And the rate of crystal size is linear in time for a constant supersaturation. If the growth rate is controlled by k_c at a low velocity, then from the convective mass transfer using Fick's law of diffusion:

$$K_c = k_c = \frac{2D}{D_p} \tag{2.21}$$

Substituting Equation 2.21 into Equation 2.19:

$$\frac{dD_p}{dt} = \frac{4D\,\Delta c}{D_p\,\rho} \tag{2.22}$$

Integrating from D_{p0} to D_p:

$$\frac{D_p^2 - D_{p0}^2}{2} = \frac{4D\,\Delta c}{\rho}\, t \tag{2.23}$$

If D_{p0} << D_p:

$$D_p = \sqrt{\frac{8D\,\Delta c\, t}{\rho}} \tag{2.24}$$

In this case, the increase in crystal diameter slows with time. It is common to assume that the rate of crystal growth is controlled by k_i and that it is not dependent on crystal size and is invariant with time [23].

The following chapter mentions the concerns that must be taken into account regarding the scale-up stage.

2.4. Scale-up of pharmaceutical crystallization processes

Conventionally, pharmaceutical crystallization processes are operated in batch mode to allow flexibility to produce diverse products and respond to changing market demands [32]. Nevertheless, much effort has been put to transit to continuous operating mode, to achieve homogeneity in the production process and therefore obtain more consistent product specifications [22].

This section will be focused on batch crystallizers since it was the operation mode studied throughout this thesis.

Batch crystallizers are classified according to the method used to generate supersaturation: cooling, evaporation, anti-solvent addition and reaction [33]. Moreover, they are also simple and flexible in operations, involving less investment and less process development than those for a continuous mode [34]. Batch crystallization may also include the semi-batch system in which one or more feed solutions are continuously added to the crystallizer, as for instance in the anti-solvent and reaction methods [2].

2.4.1. Batch crystallizers

Laboratory batch crystallizers have been successfully used during the crystallization process development phase, in order to estimate and measure the effects of the operating conditions on the kinetics, metastable zone width and help decide what crystallization method to use. Additionally, it also aids in the determination of the design features which will lead to the desired yield and crystal properties [2].

According to the literature [35]–[40], the laboratory crystallizers (Figure 2.4) usually consist of agitated jacketed glass vessels with temperature control using a thermo-stated bath, since these emulate the ones employed in the pharmaceutical industrial scale (Figure 2.5).

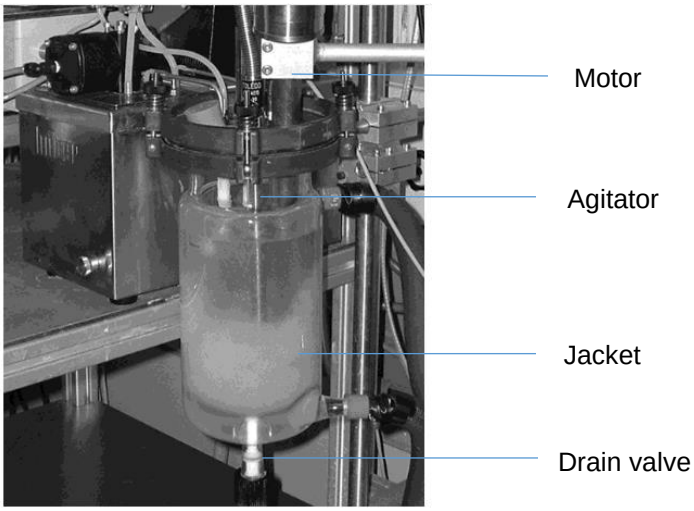

Figure 2.4. Batch laboratorial scale crystallizer [44].

The agitation is generally promoted by a bladed impeller. The vessel is also equipped with a condenser to prevent loss of solvent by evaporation.

The agitation keeps the solution at a uniform temperature and the fine crystals in suspension, which can grow uniformly without forming too large crystals or aggregates. The limitations relay on the heat transfer efficiency, since the solubility is lower near the surface of the cooling coils, resulting in a rapid build-up of crystals on that area [33].

Figure 2.5. Agitated batch pilot plant crystallizer [41].

However, there are two requisites that must be accomplished by any crystallizer: the crystals must be maintained in suspension using the agitator and there should exist a proper circulation inside the crystallizer, in order to promote the homogenization of the suspension for an adequate mass transfer process. The latter requisite decreases the possibility of occurring local supersaturation peaks that can lead to an excessive formation of fine crystals. The critical zones where these phenomena might occur are the feed and the heat transfer zones [28].

2.4.2. Scale-up foresight

Scale-up of crystallization processes is very challenging and therefore several points must be considered to obtain product within specification.

Process time/rate of crystallization

During the scale-up of a crystallization process, each process time, rate of cooling or rate of addition of anti-solvent or reactant, should be kept constant [30].

Regarding the scale-up of cooling processes with a given cooling rate, in larger scales much lower jacket temperatures are needed to obtain the same overall cooling rate as on laboratory scale. This

lower wall temperature can lead to incrustations or increased nucleation rates near or on the wall. Alternatively, cooling rates can be decreased, although the resulting longer processing times may then be critical to the product obtained or the longer stirring may lead to increased abrasion of the final product [30].

In case the crystallization is induced by spontaneous nucleation, it is advisable to keep the cooling rate constant so that the supersaturation at which nucleation occurs is kept constant [30].

During the scale-up of seeding processes, it is advisable to use the same type of seed, for example, polymorph, size, and type of preparation. In this case, the weight percentage of seed should also be kept constant [30].

Stirring

Stirring is typically the most critical parameter in the scale-up of crystallization processes. Two aspects must be considered: homogenization of the batch and mixing during the addition of anti-solvent or reactants and suspension of the crystals [30].

Regarding the mixing during the addition of anti-solvent, it is important to have a good understanding as to how sensitive the process is toward stirring effects. It pays off if the process is designed in a way that is independent of addition rates, addition mode (spray ball or pipe), and position of addition (under or above liquid level) or turbulence. All these may be very critical if mixing (micro or mesomixing) plays a decisive role, for example, in precipitations or sometimes also in crystallizations with anti-solvent addition, if local supersaturation leads to additional nucleation.

Keeping the crystals well suspended by stirring is the other important aspect in scale-up, namely, for large crystals that are fast settling. Whereas it may be easy to keep these particles suspended on small scale, especially if high stirring rates and stirrers with a good axial flow are used, it can be difficult to keep these suspended in a large industrial reactor [30].

A higher tip speed can lead to increased particle attrition or even breakage. If specific power input is reduced, the crystals will settle and maybe clog the bottom outlet or fuse to large aggregates while sitting on the bottom of the crystallizer. In such cases, it may be necessary to change the stirrer type during scale-up. In this case, it is recommended to turn to a stirrer that generates higher axial flow [30].

Zeng *et al*. [35] verified that with the increase of agitation rate, the agglomeration phenomenon was reduced due to broken crystals, as showcased in Figure 2.6. However, the cooling and agitation rate have no influence on the crystal shape, which is spherical.

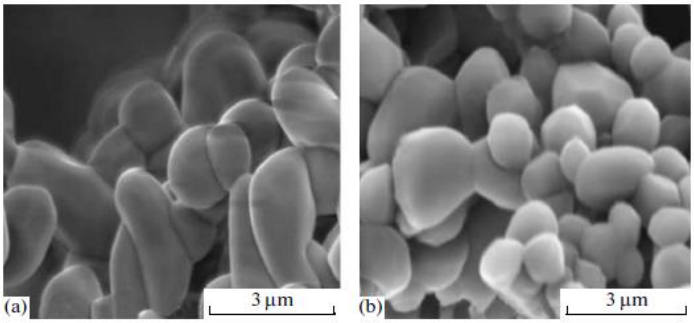

Figure 2.6. The SEM of sodium sulphate crystals under different cooling rate and agitation rate (a) 300 rpm and (b) 900 rpm [35].

Manipulating Particle Shape

As stated previously, crystals usually grow in a preferred orientation. Occasionally, the “natural” shape is not favored in downstream processing and formulation. For instance, plate crystals tend to filter poorly and needles can break easily during handling or they can be bulky and hence require too large volumes in handling and formulation. Employment of different solvents and processing conditions may modify the polymorphic state (internal structure) and the habit of the purified drug, consequently altering its final properties. Properties such as particle orientation, flowability, packing, compaction, syringability, suspension stability, and dissolution are the most influenced by changes in the crystal habit of a drug substance. For instance, a suspension of plate-shaped crystals may be injected through a small needle with greater ease than one with needle-shaped crystals of identical dimensions [42].

Different habits may be produced when the environment of a growing crystal affects its external shape without changing its internal structure. Surface theories suggest that the equilibrium form should be such that the crystal has a minimum total surface free energy per unit volume [43]. The crystals may grow rapidly, or be stunted, in one direction, thus an elongated growth of a prismatic habit gives a needle shaped crystal (acicular habit) and a stunted growth gives a flat plate-like crystal (tabular, platy or flaky habit). The relative growths of the faces of a crystal can be altered and often controlled by a number of factors. Rapid crystallization, produced by the sudden cooling or seeding of a supersaturated solution, may result in the formation of needle crystals. The growth of a crystal may be stunted in certain directions due to the presence of impurities in the crystallizing solution. A change of solvent often changes the crystal habit [43].

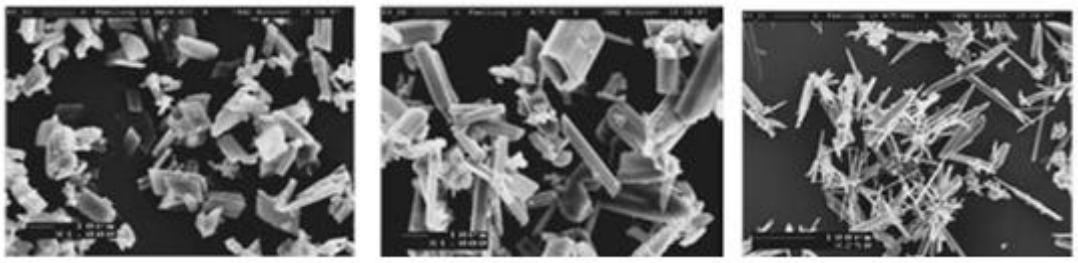

Figure 2.7. The effect of the polarity of the solvents on the crystal habit [30].

Therefore, it may become necessary to modify the natural shape in a way that it becomes more advantageous for the following steps. In an example shown in Figure 2.7, the crystal structure reveals that polar groups are most pronounced at the tips of the elongated plate crystals. Polar solvents interacting preferentially with this crystal face can hinder the growth of this face and the crystal becomes more compact, while non-polar solvents, such as hexane, inhibit lateral growth so that the crystals become more needle-like [30].

Due to the unpredictability of the crystallization process, it is necessary to understand which variables influence the most and therefore study their impact on the final product properties.

References

[1] R. W. Rousseau, *Handbook of Separation Process Technology*. Canada: John Wiley & Sons, 1987.

[2] A. S. Myerson, *Handbook of Industrial Crystallization*, 2nd ed., no. October. Elsevier Science & Technology Books, 2001.

[3] C. J. Geankoplis, *Transport Properties and Unit Operations*, 3rd ed. USA: Prentice-Hall, 1993.

[4] K. Xu, C. Wang, X. Wang, and Y. Qian, “Laboratory experiments on simultaneous removal of K and P from synthetic and real urine for nutrient recycle by crystallization of magnesium-potassium-phosphate-hexahydrate in a draft tube and baffle reactor,” *Chemosphere*, vol. 88, no. 2, pp. 219–223, 2012.

[5] R. W. Hartel and A. V. Shastry, “Sugar Crystallization in Food Products,” *Crit. Rev. Food Sci. Nutr.*, vol. 30, no. 1, pp. 49–112, 1991.

[6] S. R. Reddy, “A thermodynamic model for predicting n-paraffin crystallization in diesel fuels,” *Fuel*, vol. 65, no. 12, pp. 1647–1652, 1986.

[7] P. SHEKUNOV, B. Y.; YORK, “Crystallization process in pharmaceutical technology and drug delivery design.,” *J. Cryst. Growth*, vol. 211, no. 1–4, pp. 122–136, 2000.

[8] J. Chen, B. Sarma, J. M. B. Evans, and A. S. Myerson, “Pharmaceutical Crystallization Published as part of the Crystal Growth & Design 10th Anniversary Perspective,” *Cryst. Growth Des.*, vol. 11, pp. 887–895, 2011.

[9] C. Schaefer, C. Lecomte, D. Clicq, A. Merschaert, E. Norrant, and F. Fotiadu, “On-line near infrared spectroscopy as a Process Analytical Technology (PAT) tool to control an industrial seeded API crystallization,” *J. Pharm. Biomed. Anal.*, vol. 83, pp. 194–201, 2013.

[10] R. Censi and P. Di Martino, “Polymorph impact on the bioavailability and stability of poorly soluble drugs,” *Molecules*, vol. 20, no. 10, pp. 18759–18776, 2015.

[11] N. Stieger and W. Liebenberg, “Recrystallization of Active Pharmaceutical Ingredients,” *Cryst. - Sci. Technol.*, vol. 7, pp. 183–204, 2012.

[12] J. McConathy and M. J. Owens, “Stereochemistry in Drug Action,” *Prim. Care Companion J. Clin. Psychiatry*, vol. 5, no. 2, pp. 70–73, 2003.

[13] Y. Pu, M. Mazumder, and C. Cooney, “Effects of Electrostatic Charging on Pharmaceutical Powder Blending Homogeneity,” *J. Pharm. Sci.*, vol. 98, no. 7, pp. 2412–2421, 2009.

[14] M. Fujiwara, Z. K. Nagy, J. W. Chew, and R. D. Braatz, “First-principles and direct design approaches for the control of pharmaceutical crystallization,” *J. Process Control*, vol. 15, no. 5, pp. 493–504, 2005.

[15] W. Beckmann, *Crystallization: Basic Concepts and Industrial Applications*. Weinheim; Germany: Wiley-VCH, 2013.

[16] H. G. Brittain, *Polymorphism in pharmaceutical solids*, 2nd ed., vol. 192. USA: Informa Healthcare, 2009.

[17] J. F. Bauer, “Polymorphism - A Critical Consideration in Pharmaceutical Development, Manufacturing and Stability,” *J. Valid. Technol.*, pp. 15–23, 2008.

[18] R. Hilfiker, *Polymorphism in the Pharmaceutical Industry*. Germany: Wiley-VCH, 2006.

[19] A. G. Jones, *Crystallization Process Systems*. USA: Butterworth Heinemann, 2002.

[20] S. Al-Jibbouri, C. Strege, and J. Ulrich, “Crystallization kinetics of epsomite influenced by pH-value and impurities,” *J. Cryst. Growth*, vol. 236, no. 1–3, pp. 400–406, 2002.

[21] J. F. Richardson and J. H. Harker, *Coulson and Richardson’s Chemical Engineering – Particle Technology and Separation Process - Vol II*, 5th ed. Butterworth Heinemann, 2002.

[22] S. Lawton, G. Steele, P. Shering, L. Zhao, I. Laird, and X. W. Ni, “Continuous crystallization of pharmaceuticals using a continuous oscillatory baffled crystallizer,” *Org. Process Res. Dev.*, vol. 13, no. 6, pp. 1357–1363, 2009.

[23] D. Seader and E. J. Henley, *Separation Process Principles*, 2nd ed. USA: John Wiley & Sons, 2006.

[24] W. L. McCabe, J. C. Smith, and P. Harriott, *Unit Operations of Chemical Engineering*, 5th ed. USA: McGraw-Hill, 1993.

[25] J. C. Givand, A. S. Teja, and R. W. Rousseau, “Manipulating crystallization variables to enhance crystal purity,” *J. Cryst. Growth*, vol. 198–199, no. pt 2, pp. 1340–1344, 1999.

[26] J. Nývlt, “Nucleation and growth rate in mass crystallization,” *Prog. Cryst. Growth Charact.*, vol. 9, no. 3–4, pp. 335–370, 1984.

[27] J. Garside and R. J. Davey, “Secondary contact nucleation: Kinetics, growth and scale-up,” *Chem. Eng. Commun.*, vol. 4, no. 4–5, pp. 393–424, 1980.

[28] M. J. da C. G. Meireles, “Modelização e Simulação Computacional de Uma Unidade Industrial de Cristalização de Açúcar,” FEUP, 1996.

[29] E. G. Denk and G. D. Botsaris, “Fundamental Studies in Secondary Nucleation,” *J. Cryst. Growth*, vol. 13/14, pp. 493–499, 1972.

[30] H. H. Tung, E. L. Paul, M. Midler, and J. A. McCauley, *Crystallization of Organic Compounds: An Industrial Perspective*. USA: John Wiley & Sons, 2009.

[31] J. Xia, D. Zhu, L. Wang, B. Huang, X. Huang, and X. M. Meng, “Large-Scale Growth of Two-Dimensional SnS2 Crystals Driven by Screw Dislocations and Application to Photodetectors,” *Adv. Funct. Mater.*, vol. 25, no. 27, pp. 4255–4261, 2015.

[32] Q. Su, Z. K. Nagy, and C. D. Rielly, “Pharmaceutical crystallisation processes from batch to continuous operation using MSMPR stages: Modelling, design, and control,” *Chem. Eng. Process. Process Intensif.*, vol. 89, pp. 41–53, 2015.

[33] K. Sambamurthy, *Pharmaceutical Engineering*. Delhi: New Age International, 1998.

[34] N. S. Tavare, *INDUSTRIAL CRYSTALLIZATION Process Simulation, Analysis and Design*. USA: Springer Science + Business Media, LCC, 1995.

[35] G. Zeng, H. Li, S. Huang, X. Wang, and J. Chen, “Determination of metastable zone width and the primary nucleation kinetics of sodium sulfate,” *Theor. Found. Chem. Eng.*, vol. 49, no. 6, pp. 869–876, 2015.

[36] M. Tao, J. K. Wang, and Y. Wang, “Solubilities of pioglitazone hydrochloride in different solvents,” *J. Chem. Eng. Data*, vol. 56, no. 5, pp. 2710–2713, 2011.

[37] P. Barrett and B. Glennon, “Characterizing the Metastable Zone Width and Solubility Curve Using Lasentec FBRM and PVM,” *IC*, vol. 80, no. October, pp. 799–805, 2002.

[38] M. Barrett, D. O’Grady, E. Casey, and B. Glennon, “The role of meso-mixing in anti-solvent

crystallization processes," *Chem. Eng. Sci.*, vol. 66, no. 12, pp. 2523–2534, 2011.

[39] D. O'Grady, M. Barrett, E. Casey, and B. Glennon, "The Effect of Mixing on the Metastable Zone Width and Nucleation Kinetics in the Anti-Solvent Crystallization of Benzoic Acid," *Chem. Eng. Res. Des.*, vol. 85, no. 7, pp. 945–952, 2007.

[40] Q. Chen, Y. Wang, X. Wu, and J. Wang, "Solubility of 11beta-Hydroxypregna-1,4,16-triene-3,20-dione in Different Solvents," *J. Chem. Eng. Data*, vol. 53, pp. 1414–1416, 2008.

[41] Pfaudler, "Reatores de Escala Piloto." [Online]. Available: https://www.pfaudler.com/pt/produtos/Reatores-de-escala-piloto#lightbox. [Accessed: 25-Aug-2017].

[42] A. K. Tiwary, "Modification of Crystal Habit and Its Role in Dosage Form Performance," *Drug Dev. Ind. Pharm.*, vol. 27, no. 7, pp. 699–709, 2001.

[43] S. S. Joshi, "Crystal habit modification using habit modifiers," in *Modern Aspects of Bulk Crystal and Thin Film Preparation*, 2012, pp. 413–436.

[44] J. Worlitschek and M. Mazzotti, "Model-Based Optimization of Particle Size Distribution in Batch-Cooling Crystallization of Paracetamol Model-Based Optimization of Particle Size Distribution in Batch-Cooling Crystallization of Paracetamol," *Cryst. Growth Des.*, vol. 4, no. 5, pp. 891–903, 2004.

Chapter 3 Characterization at lab-scale of crystal habit, size and polymorphic stability of an API[1]

[1] Part of this work was published in:
A. Tulcidas, N. M. T. Lourenço, R. Antunes, B. Santos, S. Pawlowski and F. Rocha, "Crystal habit modification and polymorphic stability assessment of a long-acting, β_2-adrenergic agonist", CrystEngComm, vol. 21, pp. 3460 - 3470, 2019.

3.1. Scope

Properties such as particle orientation, flowability, packing, compaction, syringeability, suspension stability and dissolution are the most influenced by changes in the crystal habit and polymorphic form of an API. Therefore, the main goal of this chapter is to gain knowledge about crystallization principles and understand how crystal habit, size and polymorphic form of an API can be affected and then, improved. For this purpose, an industrial case study was addressed, where a different crystal habit, size, and a specific polymorphic form were desired, in order to ease the downstream processes. The crystallization process consisted of solvent evaporation step followed by cooling in ethanol, leading to needle-shaped crystals, which are not suitable for further processing steps.

To overcome this challenge, firstly, the crystallization process was monitored with a Focused Beam Reflectance Measurement (FBRM) Lasentec probe and minor changes in the process were performed, such as Ostwald ripening induction and slow cooling, to seek improvements in the crystal habit and size, without the need to change the whole process. Secondly, in order to gain a thorough understanding of the supersaturation attained during the crystallization process, the solubility curve of the API in ethanol (process solvent) and MSZW were determined at different cooling rates, using turbidity. Subsequently, cooling crystallization experiments were conducted, at low supersaturation, without and with seed, to check for improvements in the crystal habit and dimensions.

Lastly, since the previous studies in ethanol did not lead to a product with the desired characteristics, a new solvent system was used where the crystal habit and size modifications, as well as the purity, were researched while performing polymorphic stability tests. The polymorphic stability of the drug was studied by performing slurry tests with 1,2-dimethoxyethane:heptane solution at 50 ºC. These slurry tests consist of a process where the product is kept suspended rather than dissolved, with agitation, for polymorphic conversion evaluation. Since no significant modifications were observed in the crystal shape and dimensions at 50 °C, a new slurry test was performed at a temperature above the melting point of the starting material (80 °C). In the latter test, it was possible to obtain crystals with increased dimensions by 480% compared with the starting material. Additionally, the desired polymorphic form (form I) was obtained as well as an acceptable purity of approximately 99%. These are promising results, not only for downstream purposes but also concerning the bioavailability of the API. This study shows

that working at a temperature higher than the melting point of the compound seems to modify the crystal habit, size and form of the product.

3.2. Introduction

Crystals usually grow in a preferred orientation and, occasionally, the “natural” shape is not favored in downstream processing and formulation [1]. For instance, plate crystals tend to filter poorly, while needles can break easily during handling. Properties such as particle orientation, flowability, packing, compaction, syringeability, suspension stability and dissolution are the most influenced by changes in the crystal habit of a drug substance [2], [3]. Linezolid, a drug that acts as an antibacterial agent for the treatment of skin infections and pneumonia presents both needles and irregular plate crystals. The latter shape is desired since it presents a higher flowability than needle-shaped crystals and thus, a suspension of plate-shaped crystals may be administered easily to the patients than one with needle-shaped crystals of identical dimensions [4].

Different habits may be produced when the environment of a growing crystal affects its external shape without changing its internal structure [5]. The crystals may grow rapidly, or be stunted, in one direction, thus an elongated growth of a prismatic habit gives a needle-shaped crystal (acicular habit) and a stunted growth gives a flat plate-like crystal (tabular, platy or flaky habit) [5]. The relative growth of the faces of a crystal can be altered and often controlled by a number of factors [5]. Rapid crystallization, produced by the sudden cooling or seeding of a supersaturated solution, may result in the formation of needle crystals. The growth of a crystal may be tricked in certain directions due to the presence of impurities in the crystallizing solution [5].

The polarity of the solvent also exerts effects on the crystal habit [3], [6]. Different crystal faces exhibit different surface chemistry and hence interact differently with solvents, process impurities and excipients [7]. For instance, Stoica *et al*. found that the habit modification of the stable form of a steroid is caused by surface-solvent interactions, which affect the growth rate of the polar faces differently [8]. Additionally, Chen *et al*. assessed the effect of different solvents (methanol, pyridine, acetone, dichloromethane and isopropanol) on the crystal structure or habit of hydrocortisone. It was observed that the hydrocortisone crystals grew into different habits (plate, bladelike, prism to parallelepiped morphology) depending on the solvent that entered the inner crystal lattice as well as the external crystallization conditions employed (Figure 3.1) [9].

Furthermore, employing different solvents and processing conditions besides modifying the habit, it may also influence the polymorphic state (internal structure) of the purified drug, consequently altering its final properties [5], [10], [11]. Regarding the polymorphism, obtaining an undesired form can lead to bioavailability issues as occurred to ritonavir, a drug used to treat HIV and AIDS [10]. The problem was caused by a change in the solubility of ritonavir that caused the drug to precipitate with a different internal structure, from the capsule formulation, which reduced its bioavailability to less than 5% [10].

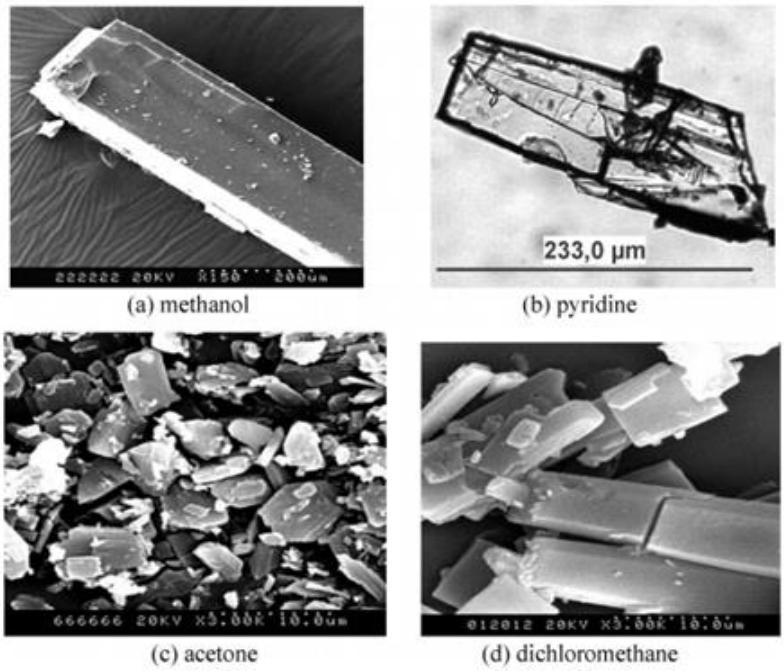

Figure 3.1. The effect of polarity of solvents on the crystal habit of hydrocortisone [9].

Therefore, it may be necessary to modify the natural shape of the crystals and assess the internal structure in order to avoid hindrances in the processing steps and obtain a product with the desired properties.

Consequently, this work reports the attempts performed to modify the crystal habit, size and polymorphic form of an API. Firstly, the crystallization process was monitored with a FBRM probe and minor changes in the process were performed, such as heating/cooling cycles to induce Ostwald ripening and slow cooling to seek improvements in the crystal habit and size, without the need to change the whole process. Secondly, in order to gain a thorough understanding of the supersaturation attained during the crystallization process, the solubility curve of the API in ethanol (process solvent) and MSZW were determined. Subsequently, cooling crystallization experiments were conducted, at low supersaturation, without and with seed, to check for improvements in the crystal habit and dimensions. Lastly, a new solvent system was used where the crystal habit and size modifications, as well as the purity, were researched while performing polymorphic stability tests.

3.3. Experimental methods and materials

3.3.1. Particle size monitoring with FBRM probe

An evaporative crystallization process (evaporation followed by cooling) was repeated and simultaneously monitored with the FBRM probe (model D600L, Lasentec Inc., USA) where additional steps such as Ostwald ripening phenomenon and slow cooling were induced to assess their impact on the size of the crystals.

FBRM probe working principle

FBRM measures a chord length distribution (CLD), which tracks the dimension and population of the particles under investigation. FBRM uses an infrared focused beam of laser light with a wavelength of 785 nm, which scans in a circular path, with a speed from 2 to 8 m/s. As this light scans across a particle or particle structure passing in front of the probe window, light is scattered in all directions. The light scattered back towards the probe is used to measure a chord length of the given particle. Typically, many thousands of chords are measured per second, providing a robust measurement that is sensitive to the change in the size or number of particles. Unlike, for example, optical turbidity or laser diffraction, FBRM does not depend on the presence of a limit nuclei concentration before a nucleation event is detected — as soon as one particle is in the detectable size range it will be detected. FBRM has been used by previous researchers to help characterize the metastable zone width and is widely used as a tool for both batch and continuous crystallization development and scale-up crystallization control, and for troubleshooting and optimization of downstream processing problems [12], [13]. Figure 3.2 depicts the FBRM probe's components and summarizes the aforementioned working principle.

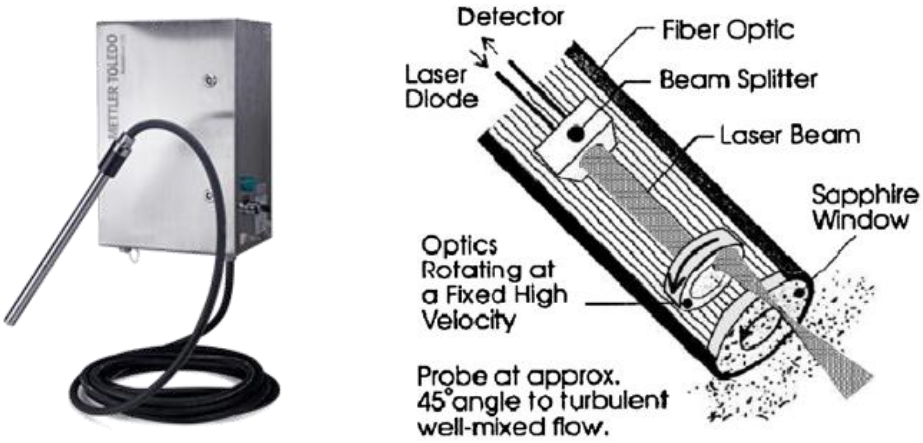

Figure 3.2. FBRM probe's components and features [13].

Experimental procedure

The FBRM Lasentec probe was used to observe any changes in the crystal dimensions when employing heating/cooling cycles (Ostwald ripening induction) and slow cooling in a vacuum evaporative crystallization. The crystallization process performed is schematized in Figure 3.3.

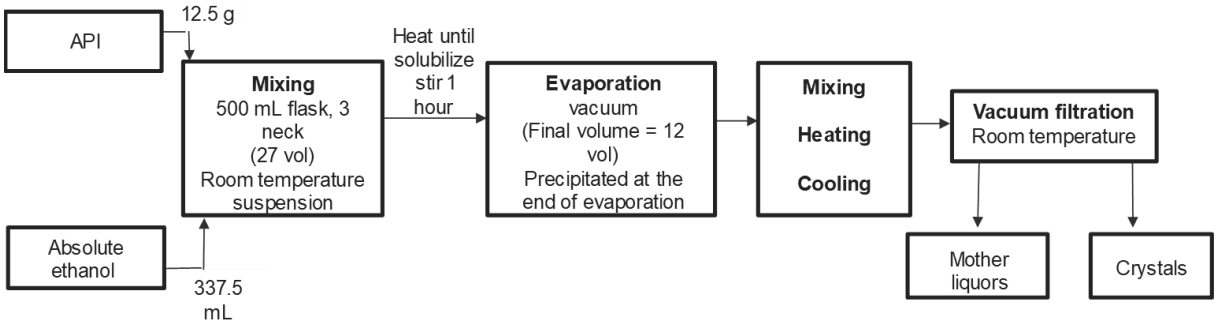

Figure 3.3. Process block flow diagram.

Firstly, the API was suspended in ethanol, with a concentration of 27 volumes at room temperature and heated until complete dissolution, in a three-neck round flask with temperature controlled externally by a water bath. Ethanol was the solvent of choice since it was the solvent used in the synthesis step before crystallization. Subsequently, the API solution was filtered, transferred into a glass jacketed reactor equipped with the FBRM probe, stirring and temperature controlled by Huber cryostat. The three-neck flask was washed with three volumes of ethanol and transferred into the reactor. The resulting API solution (30 volumes) was distilled under vacuum until a concentration of 12 volumes. The suspension formed in the previous step was then submitted to heating and cooling cycles in order to promote the Ostwald ripening phenomenon, followed by a cooling step. The resulting suspension was then filtered under vacuum, isolating the crystals from the mother liquors.

3.3.2. Solubility and metastable zone width determination of the API in ethanol

As previously mentioned, supersaturation can affect the size of the crystals and thus, it is necessary to quantify it. For that purpose, the solubility of the API in ethanol and the supersolubility curve were determined. Additionally, the influence of the cooling rate on the metastable zone width (the zone between the solubility curve and the supersolubility curve) was assessed. In order to perform these tests easily, a reactor system with four 50 mL reactors coupled with turbidity probes was used.

The system consisted of four jacketed reactors with temperature and turbidity probes installed in each reactor. The temperature and turbidity results were recorded throughout the time by the WinISO data acquisition software. The turbidity probe was immersed in the medium and changes in the quantity of reflected light were monitored as the experiment progressed. Thus, the probe can be used to detect changes in turbidity, which is a measure of the clarity of the solution. The light is transmitted via a bundle of six fibers to the probe end where it crosses the gap to the reflector. The back-reflected light returns into a seventh “reading” fiber. The amount of reflected light is converted to a voltage signal and recorded by the WinISO data acquisition software. When the light beam passes through a clear solution, the light passes through relatively unobstructed to the probe reflector and is reflected back into the “reading” fiber of the probe. In the presence of suspended particles, the light is scattered in all directions and the intensity of the light beam is reduced. This alteration in intensity and hence voltage signal is also detected and recorded in the software.

The solubility was determined by heating up suspensions of the API in ethanol until complete dissolution. Therefore, the solubility curve is occasionally labeled the clear point curve, which is the temperature when the solution becomes clear (decrease in the turbidity). On the other hand, the supersolubility curve was obtained by cooling the solution and detecting the first appearance of solid, which translates into an increase in the turbidity [14].

The heating and cooling rates were controlled by a Huber cryostat with Syltherm oil. A four-bladed PTFE retreat curve impeller ensured the agitation of the mixture.

The system used is presented in Figure 3.4.

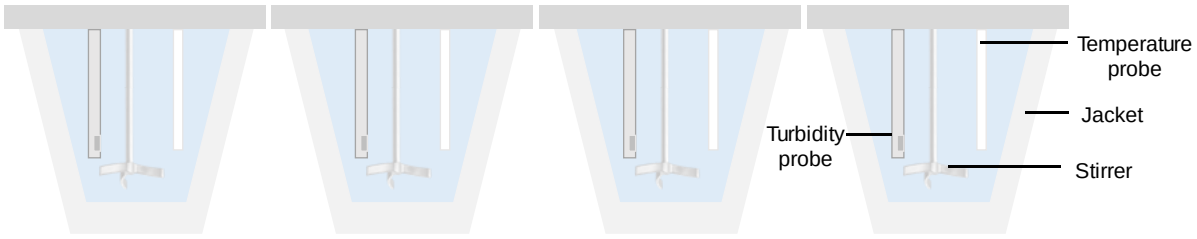

Figure 3.4. System of 50 mL reactors coupled with turbidity and temperature probes and impeller.

The solubility and metastable zone width determination procedure is described below.

Firstly, the turbidity probe was calibrated using the pure solvent (ethanol) as blank. Concentrated solutions of the API were prepared and the stirring was started at room temperature, except the less concentrated solution, whose stirring was started at -15 ºC to avoid dissolution of the drug. The suspension was heated nearly until the boiling point of the solvent with a temperature increase rate of 0.5 ºC/min. After total dissolution, the solution was cooled with a rate of 0.25 ºC/min to the temperature at which precipitation occurs and the procedure was repeated once more in order to obtain two measurements of cloud point and clear point for each concentration. The suspension was then heated until complete dissolution and cooled with a rate of 1 ºC/min, and the procedure was repeated to have double measurements.

The necessary amount of solvent was added into the previous suspensions to obtain the next less concentrated solutions and the aforementioned procedure was repeated.

Solutions with a concentration of 100 g/L, 50 g/L, 25 g/L, 12.5 g/L and 6.3 g/L were tested. This study was not performed for solutions with a saturation temperature above 50 ºC since it was previously known from a study executed out of the scope of this thesis that higher temperatures promote the formation of impurity.

3.3.3. Cooling crystallization – Lower supersaturation

An attempt with a low supersaturation ratio of about 2.0 (below a supersaturation of 2.6 used in section 3.3.1) and a slow cooling rate of 2 ºC per hour and smooth agitation was performed, in order to check any improvement on the final crystal habit and size.

Firstly, about 0.45 g of API were suspended in 40 volumes of ethanol, at room temperature and heated until dissolution (38 ºC), in a three-neck round flask with temperature controlled externally by a water bath and stirred with a magnetic bar at low agitation of 100 rpm. The solution was remained under agitation at 38 ºC for 30 minutes to ensure complete dissolution. Subsequently, the solution was slowly cooled with a rate of 2 ºC per hour until the nucleation was detected visually. The first crystals were detected at 21 ºC and the solution was maintained under agitation overnight at a constant temperature (supersaturation ratio of 2.0). After the twelve-hour agitation, the product seemed to have fully precipitated into a thick paste. The agitation was set off and the product was remained to sit for about two hours. Forwardly, the suspension was filtered under vacuum at room temperature and the cake was washed twice with three volumes of ethanol at 5 ºC. The crystals were dried under vacuum at 40 ºC until constant weight.

Figure 3.5 depicts the aforementioned experimental setup.

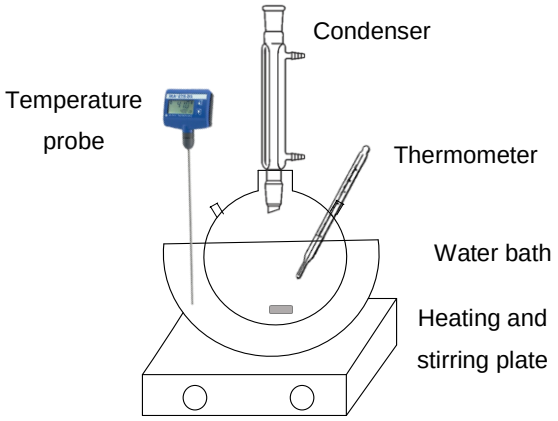

Figure 3.5. Experimental setup for the cooling crystallization experiment.

3.3.4. Cooling crystallization – Seeding experiment

In an attempt to decrease spontaneous nucleation and thus, avoid the formation of fine particles, a new experiment was performed by adding seed at a supersaturation of 1.6. A cooling rate of 1 ºC per minute was applied, as from the previous experiments it was observed that fast cooling rates widen the metastable zone width.

For this purpose, about 0.50 g of API were suspended in 20 volumes of ethanol at room temperature and heated until dissolution (50 ºC), in a three-neck round flask with temperature-controlled externally by a water bath and stirred with a magnetic bar at low agitation of 100 rpm. The solution was remained under agitation at 50 ºC for 30 minutes to ensure complete dissolution. Subsequently, the solution was cooled with a rate of 1 ºC per minute until 40 ºC and 0.5% wt. of the initial solute mass was added into the solution and the cooling proceeded until -10 ºC. The first crystals were detected at 30 ºC. The product fully precipitated into a thick white paste and the suspension was maintained under agitation

for four hours. The crystals were filtered under vacuum at room temperature and the cake was washed twice with ethanol at -10 ºC. The crystals were dried under vacuum at 40 ºC until constant weight. The experimental setup is similar to the one used in Figure 3.5.

3.3.5. New solvents' system approach and polymorphic stability studies

Due to commercial purposes and intellectual property, the chemical structure of the compound of interest cannot be presented. In a study out of the scope of this paper, slurry tests were performed in other solvents, both single and binary mixtures. However, the product obtained in such solvent systems did not show promising results concerning the crystal habit. Growth was observed only when using 1,2-dimethoxyethane:heptane system, therefore this study was focused on performing the slurry tests only in this system of solvents. Since this system enabled the production of the targeted form, a few attempts were performed in order to test the stability of the polymorphic form when using starting materials of different forms. Simultaneously, besides analyzing the final form, purity, melting point and morphology of the crystals were also assessed in order to check if there was any impact on these properties. For this purpose, analytical methods such as XRPD (X-Ray Powder Diffraction), HPLC (High Performance Liquid Chromatography), DSC (Differential Scanning Calorimetry) and SEM (Scanning Electron Microscopy) were used.

Slurry test procedure

The process flow followed to evaluate the polymorphic stability of the API is presented in Figure 3.6. This test aims to maintain a product suspended in a solvent and not dissolved, with agitation, for polymorphic conversion evaluation. The experimental setup is identical to the one shown in Figure 3.5.

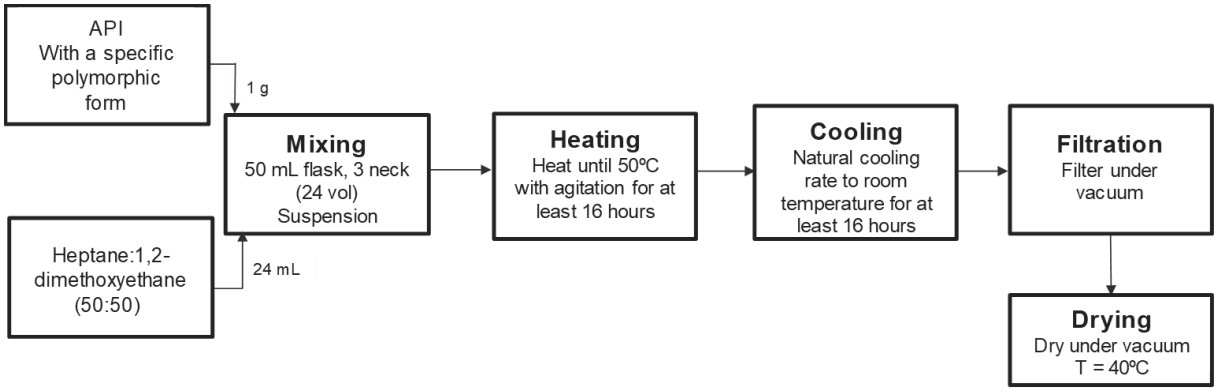

Figure 3.6. Experimental process flow for polymorphic stability tests.

Firstly, the API with a specific polymorphic form was stirred in 24 volumes of a mixture of heptane:1,2-dimethoxyethane, in a 3-neck round glass 50 mL flask. The suspension was heated to 50 ºC during at least 16 hours, followed by cooling during the same period (0.075 ºC/min). The slurry was filtered under vacuum and the cake was remained in vacuum for approximately 10 minutes and

dried under vacuum at 40 ºC until constant weight. The operating conditions used in each of the six slurry tests performed are described in the following table (Table 3.1):

Table 3.1 - Operating conditions employed in the polymorphic stability tests.

Test	Starting material's form	Temperature (°C)	Observations
1	II	50	Performed for reproducibility purpose
2	II	50	
3	I	50	For final form analysis
4	III	50	
5	II	50	Smooth agitation
6	II	80	Higher temperature attempt

Six experiments were performed, as shown in Table 3.1, where tests 1 and 2 were performed for reproducibility purposes when starting from form II. Tests 3 and 4 were accomplished to check the final polymorphic form when using a starting material of forms I and III, respectively. Lastly, test 5 was performed starting with form II and smooth agitation, whereas test 6 was executed at a higher temperature (80 °C) and from form II. Since the work was carried out at a considerable scale (gram) and the variability of the results is significant in smaller scales (milligram), it was assumed that the inherent variability of the remaining tests is similar to the variability existent in tests 1 and 2.

The starting material used in each test and the wet and dry solids obtained were characterized by XRPD (X-Ray Powder Diffraction), DSC (Differential Scanning Calorimetry) and SEM (Scanning Electron Microscopy). The purity of the resulting crystals was assessed by HPLC (High Performance Liquid Chromatography). The analytical procedures are described below.

Analytical procedure

Polymorphic form identification by XRPD

For the XRPD total scans, the sample was measured over a 2θ interval from 4° to 40° with a step size of 0.017° and a step time of 60 s. A Kapton film was also used throughout the test for safety purposes.

Melting point determination by DSC

The procedure consisted of weighing 3 to 4 mg of sample into a 40 µL aluminum pan with pinhole lid and sealed using a manual compressor. The sealed pan with the sample was placed in the DSC Q200 equipment, the sample was equilibrated at 25ºC, and a ramp of 10ºC per min to 350ºC was applied.

Purity by HPLC

A Waters Alliance HPLC system, equipped with a Waters 2690 separation module and Waters 2487 Dual Absorbance Detector was used to perform the analysis. The chromatographic separation was performed using a Symmetry Shield RP-18 column (150 x 4.6 mm, 3.5 µm) at 30 °C. The mobile phases consisted of acetonitrile 0.1%(v/v) trifluoroacetic acid and water 0.1%(v/v) trifluoroacetic acid, filtered through a 0.2 µm membrane filter and degassed in an ultrasonic bath prior to use. The mobile phase was delivered at a flow rate of 0.8 mL/min in gradient mode. Identification of the API was performed by injecting 10 µL volume of 0.5 mg/mL of the sample with the UV detector set at 220 nm.

The LC-MS grade water, gradient grade acetonitrile, and trifluoroacetic acid were purchased in Merck.

Crystal habit analysis by SEM

For the SEM test, the sample was attached to adhesive carbon tape, previously fixed to an aluminum stub.

3.4. Results and discussion

3.4.1. Particle size monitoring with FBRM probe

The particle count and size were followed throughout the time during the entire process in ethanol and the results are shown in Figure 3.7, using the FBRM Lasentec probe.

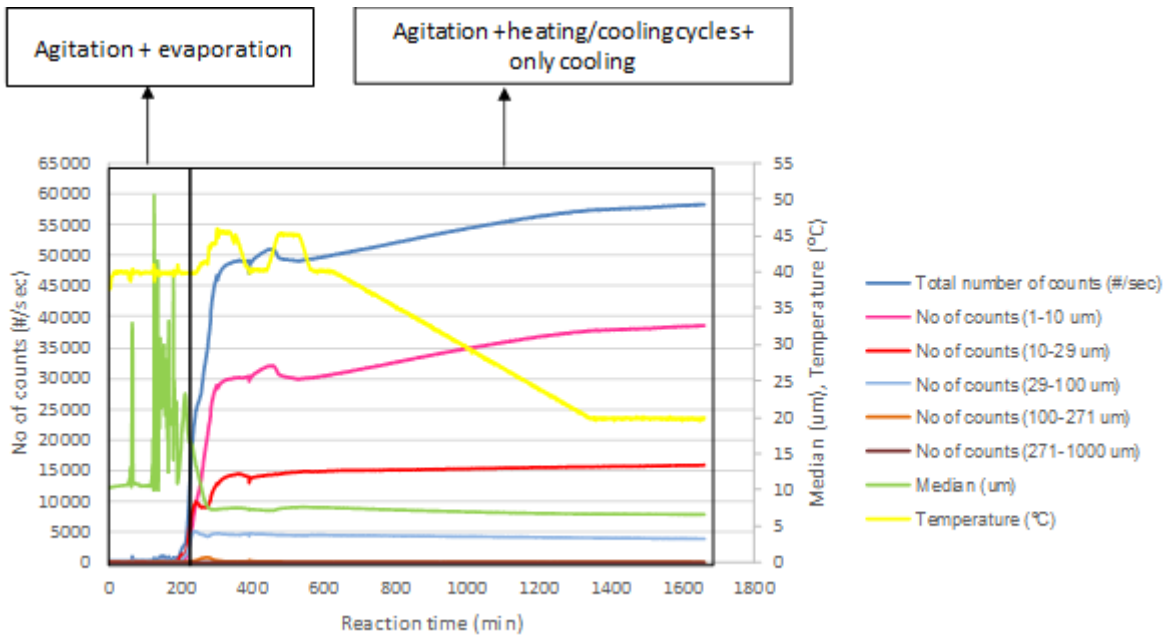

Figure 3.7. FBRM data acquired throughout the time during evaporation and subsequent cooling.

From the data gathered (Figure 3.7), it is possible to observe the increase of the total number of particle counts near the end of the evaporation step. This corresponds to the nucleation phenomenon due to the higher supersaturation achieved, caused by the solvent evaporation. To quantify the supersaturation at the end of the evaporation process, the ratio between the final concentration and the saturation concentration was considered, for which a supersaturation value of 2.6 was obtained. Additionally, heating and cooling cycles were applied in order to induce the Ostwald ripening phenomenon, which translates into dissolving smaller particles to produce larger crystals, as explained in Chapter 2. This occurs since fine particles have a high surface area in comparison with larger particles, having a tendency to dissolve before the larger ones. As detected by the FBRM probe, and as expected, the fine particles' count (chord length range of 1-10 µm) slightly decreases when the temperature increases, due to the dissolution of these smaller particles, while the remaining particles' count maintains constant. However, there is no evident sign of growth or production of larger particles visible in Figure 3.7, being necessary to analyze the chord length distribution obtained in these steps.

The probe allows identifying these peculiar phenomena, which cannot be easily detected by other optical devices. Moreover, it is also possible to observe that, when applying cooling ramps, only the number of fine particles increases, which justifies the low chord length median values obtained (≈ 8 µm). This increase in the number of counts of small particles can be either due to the supersaturation attained during cooling or due to the stirring speed applied which might additionally induce secondary nucleation. Finally, it was possible to observe that during the agitation at a constant temperature, the number of smaller particles increases, which can be interpreted as the existence of secondary nucleation caused by the stirrer (particle-particle collision, particle-baffle-impeller-reactor walls collision).

In order to better understand the evolution of the particle dimension of the product in each step of the process, the chord length distribution was plotted with the raw data given (Figure 3.8).

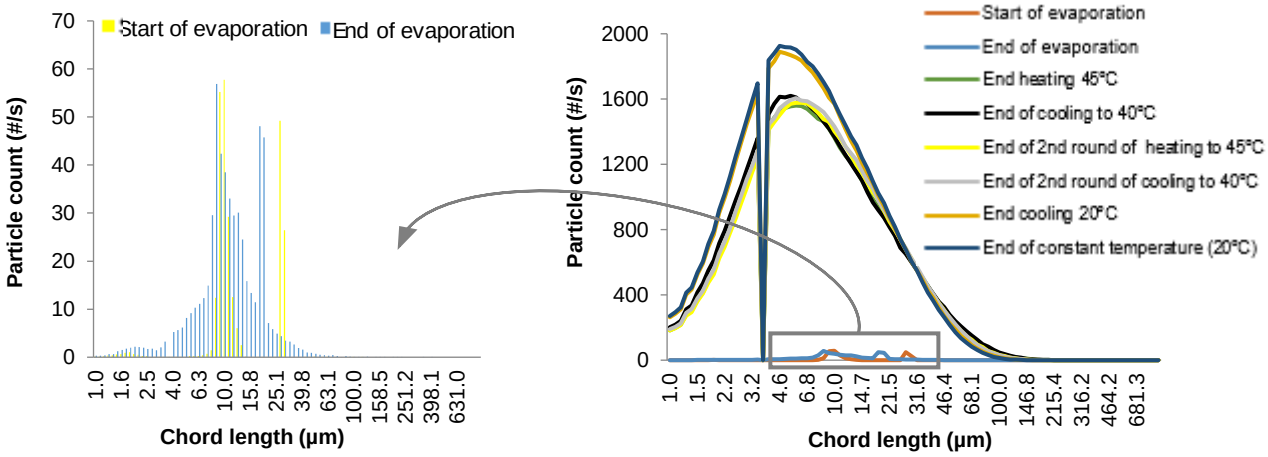

Figure 3.8. Chord length distribution obtained from raw data of FBRM in each step of the process.

As depicted in Figure 3.8, the chord length distribution obtained at the start and end of the evaporation process confirms that the nucleation process occurred near the end of this step. Moreover,

the chord length distribution, obtained for each of the evaporation and subsequent heating and cooling steps, indicates the increase of the number of particles and the displacement of the curve to the left, due to the decrease in the size of the particles, expressed by the chord length. This effect was clearly enhanced after cooling the slurry to 20 ºC and maintaining the same temperature, due to the increase of supersaturation at lower temperatures, as aforementioned. It is also visible the decrease in the particle size on the steps after the evaporation process due to the supersaturation generation. Comparing the curves obtained during the Ostwald ripening attempt (two cycles of heating to 45 ºC and cooling to 40 ºC), it is possible to observe that the crystals' chord length seems to slightly increase at the end of the second cooling to 40 ºC (visible shift of the curve to the right). This indicates that the cooling and heating cycles applied might have not been enough to induce a significant growth and a further number of cycles should have been used. For instance, Pfizer achieved the desired crystal size of the API applying five cycles of Ostwald ripening [15].

Nevertheless, it should be noted that the FBRM technique does not provide a particle size distribution (PSD) but a chord length distribution, although this data can show a trend of the alterations of the size of the product during the process. An informative wet solid sample was taken to analyze its crystal habit by SEM (Scanning Electron Microscopy), as depicted in Figure 3.9.

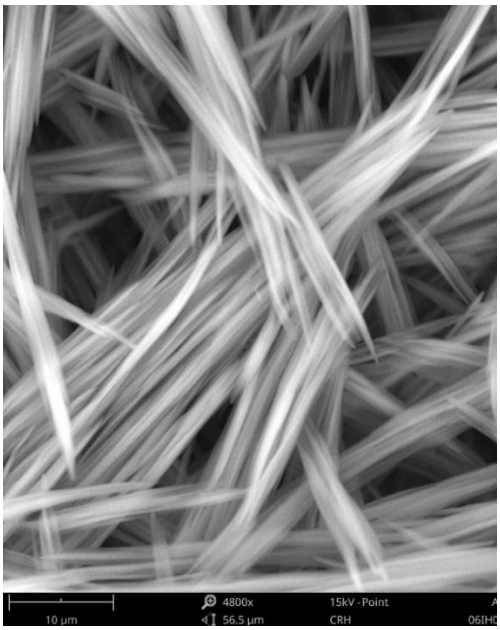

Figure 3.9. Needles of API obtained after evaporation and cooling, observed using the SEM technique (Zoom x4800).

Analyzing Figure 3.9, it was possible to observe that the formation of fine crystals persists.

As concluding observations, it can be stated that following a crystallization process with a FBRM probe, allowed gaining knowledge regarding the impact of the temperature on the supersaturation generation and the consequent nucleation induction. Apart from identifying the dissolution and nucleation phenomena, it also enabled to monitor the alterations on the particle size of the API, by

means of a chord length distribution, throughout the process. This knowledge acquisition is relevant during the development phase of a crystallization process, to define the operating conditions. For instance, in this specific case, it was observed that supersaturation of 2.6 led to the formation of fines and therefore for future references, lower supersaturation levels should be tested in order to check the impact on the particle size.

However, the solubility and the metastable zone width of the product on ethanol are unknown and these should be determined in order to understand if the operating conditions are above the supersolubility curve.

3.4.2. Solubility and metastable zone width determination of the API in ethanol

The metastable zone width was calculated as the difference between the clear point and the cloud point. The solubility curve and the cloud point obtained for the two different cooling rates (0.25ºC per min and 1ºC per min) are plotted in Figure 3.10.

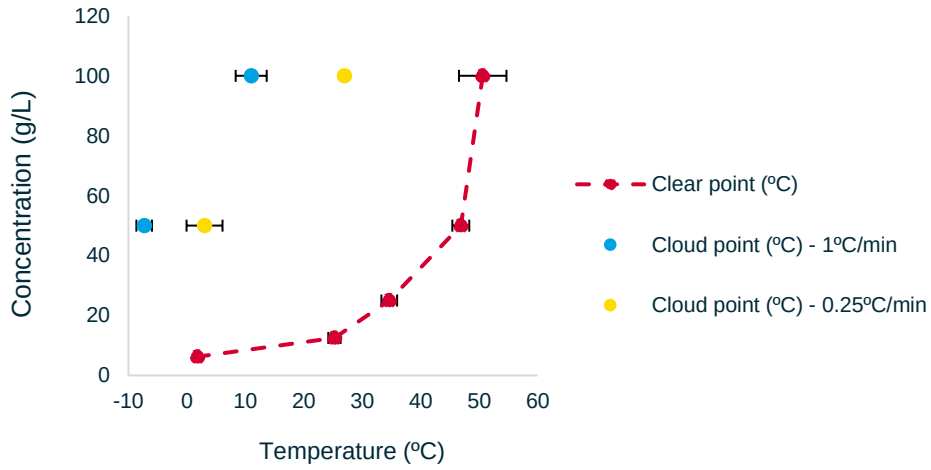

Figure 3.10. Measured solubility curve (clear points) and cloud points obtained at a cooling rate of 0.25ºC per min and 1ºC per min of the API in ethanol.

The cloud point for the less concentrated solutions was not obtained, although the solution was cooled to negative temperatures such as -15ºC. However, it is predictable that the cloud points of these solutions are below this temperature since these decrease with lower concentrations.

From the data obtained (Figure 3.10), it is possible to observe that the metastable zone is wider using high cooling rates. Additionally, it is also detected that the metastable zone widens as the saturation temperature decreases. Barret & Glennon and Ulrich also verified a similar tendency for potash alum and citric acid, respectively [12], [16].

After knowing the solubility curve, an additional experiment was performed in order to operate at lower supersaturation (less nucleation), as it will be described in the following section.

3.4.3. Cooling crystallization – Lower supersaturation

The cloud point detected visually in this experiment was plotted among the ones obtained with the aid of turbidity probes (section 3.3.2) for comparison purposes (Figure 3.11).

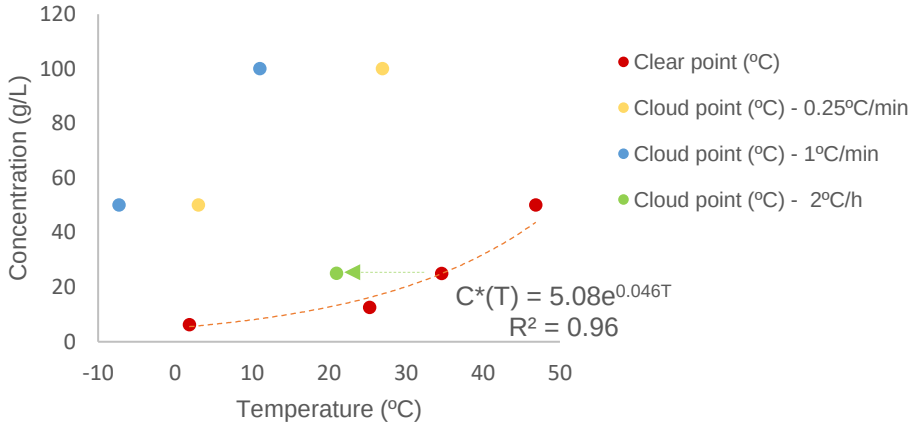

Figure 3.11. Solubility curve (clear points) and cloud points detected at different cooling rates for each concentration.

The data gathered in Figure 3.11 supports the hypothesis mentioned in section 3.4.2, where it was concluded that the metastable zone width decreases with slow cooling rates. This observation is reinforced since in the current experiment, where the cooling was performed at a rate of 2 ºC/hour (≈ 0.03 ºC/min), the cloud point was visually detected at 21 ºC. On the other hand, in section 3.3.2., where the cooling procedure was executed with a rate of 0.25 ºC/min and 1ºC/min, no cloud point was recorded even at negative temperatures of -15 ºC, for a similar API concentration (25 g/L).

The crystals obtained after drying were analyzed by SEM and the results are shown in Figure 3.12.

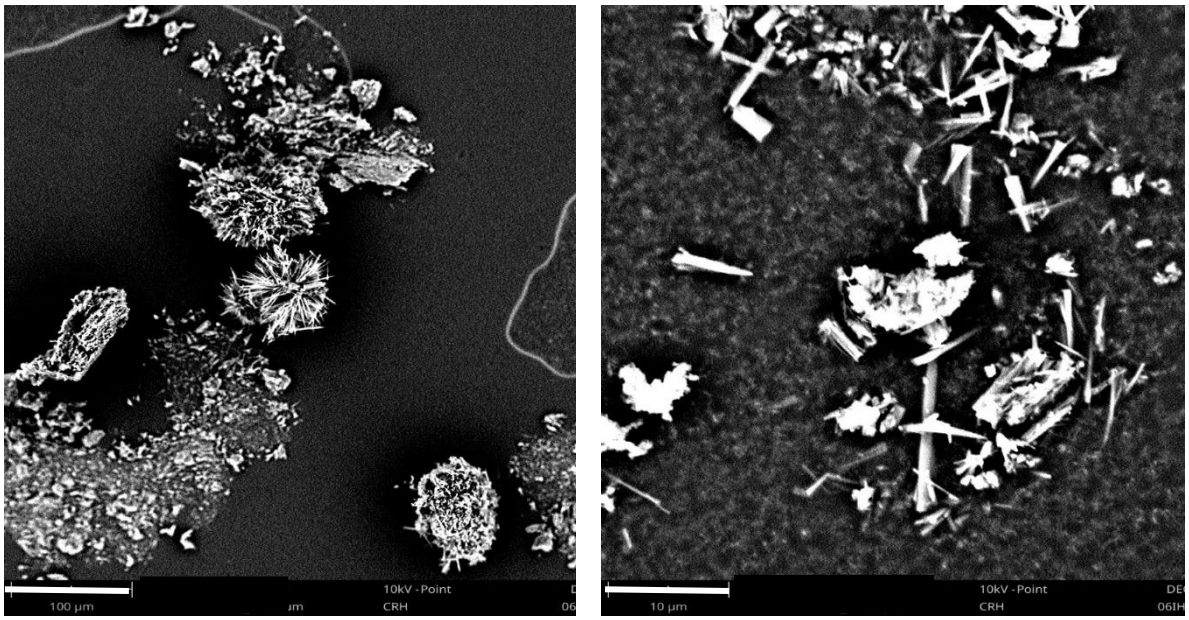

Figure 3.12. Morphology of the crystals obtained during cooling crystallization (supersaturation ratio of 2.0) by SEM analysis (zoom of 480x and 4800x respectively).

Analyzing Figure 3.12, no significant modification is detected in the crystal dimensions, since aggregates of needles with an average needle length of 6.5 µm ± 0.7 µm and an average width of 0.8 µm ± 0.2 µm, were observed and measured by SEM.

Since the low cooling rate and the used supersaturation did not enable any significant growth of the crystals, a new attempt was performed, using seeding to reduce spontaneous nucleation and hence, promote growth.

3.4.4. Cooling crystallization – Seeding experiment

Figure 3.13 depicts the metastable zone width when the drug is cooled at 1 ºC per minute and the seeding point.

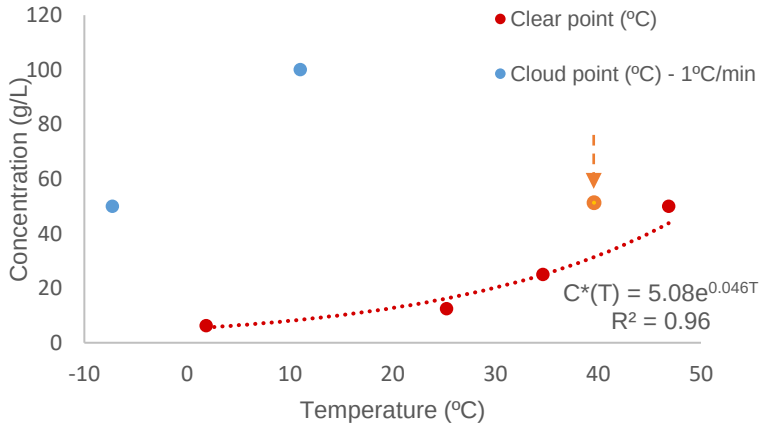

Figure 3.13. Metastable zone width obtained when using a cooling rate of 1 ºC per minute and the seeding point (orange spot).

The habit of the crystals obtained after drying was analyzed by SEM and the results are shown in Figure 3.14.

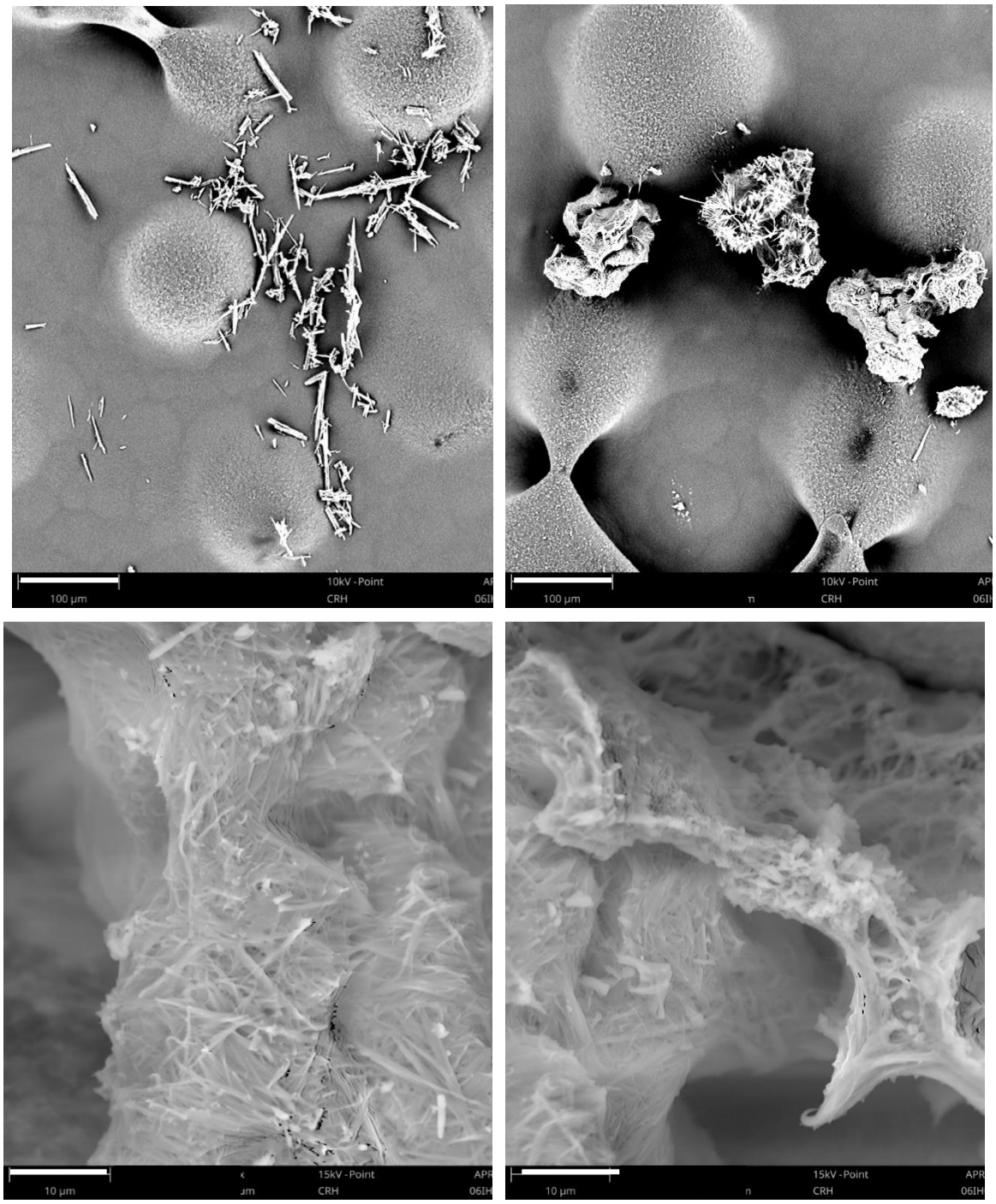

Figure 3.14. Morphology of the crystals obtained after the seeding experiment (top - zoom 480x; bottom – zoom 4800x) by SEM analysis.

Analyzing Figure 3.14, it was possible to observe that the seeding procedure led to compact agglomerates of needles and not aggregates as in the previous experiments. In the agglomeration phenomenon, firstly, individual crystals collide due to fluid motion in agitated systems, followed by

stabilization of these adhered or aggregated particles due to attractive forces. Finally, molecular growth forms solid bridges that transform the aggregates into agglomerates, which in this particular case, might have been induced by the seed. The agglomeration can be influenced by the degree of supersaturation, particle concentration, particle size and agitation. Since the supersaturation level at which the seed was added was lower than in the previous experiments and the stirring speed used was the same, these parameters do not seem to justify the agglomerates obtained. On the other hand, the concentration used was high compared to the previous experiment, which might have increased the collision rate among the particles and hence cause agglomerates. Figure 3.14 also depicts that the agglomerates seem to be composed by very small and narrow needles and Gielen *et al*. [17] state that in general, smaller particles exhibit a higher degree of agglomeration. Agglomerates of an average length of 132 µm ± 6 µm and an average width of 73 µm ± 3 µm were observed and measured by SEM.

As a final remark, the seeding did seem to promote growth and agglomeration of the crystals, which in turn resulted in more robust particles.

However, a new system of solvents should be tested in order to decrease the formation and agglomeration of fine needles and obtain the desired polymorphic form of the API in order to preserve its bioavailability properties.

3.4.5. New solvents' system approach and polymorphic stability studies

The results obtained regarding the analytical characterization of the API by XRPD, DSC, HPLC and SEM are presented below.

Polymorphic form identification by XRPD

The wet and dry solids obtained in each of the slurry tests were submitted to XRPD analysis in order to check which polymorphic form was obtained at the end. Analyzing the diffractograms, a halo is visible due to the Kapton film used during the measurements.

Figure 3.15 presents the XRPD diffractograms obtained for the wet and dry solids of tests 1 and 2.

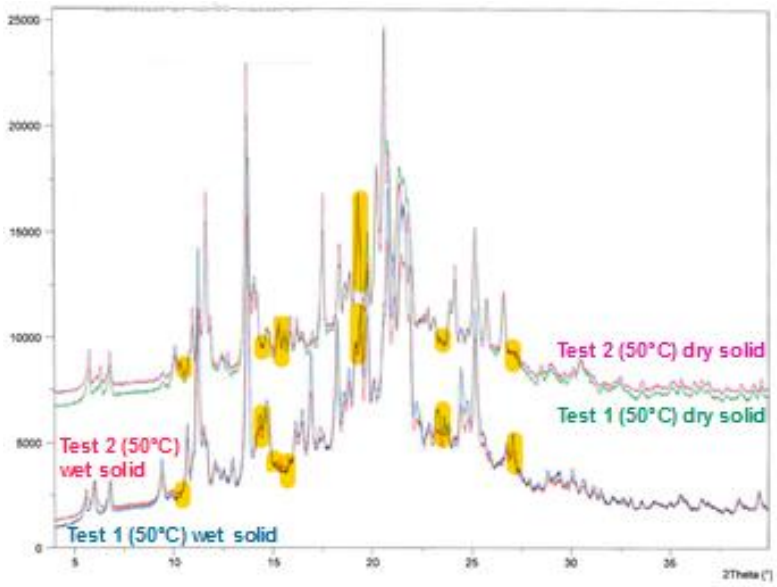

Figure 3.15. XRPD diffractograms of wet and dry solids of tests 1 and 2.

Tests 1 and 2 were both executed using a starting material of form II of different batches and, therefore, the diffractograms obtained for the wet and dry solids for both experiments were similar (Figure 3.15). This indicates that starting from a material of form II, regardless of the batch, leads to the same results. The diffractograms of the wet solids were compared with the dry ones for both tests and it was possible to detect some differences (marked in yellow in Figure 3.15). The diffractograms of the wet solids were overlaid afterwards with standard diffractograms of form I (desired form), II (starting materials' form) and XII (form obtained externally) in order to identify the odd peaks. Form XII was obtained by an external source by following the procedure described in the slurry experiments' section along with a rigorous heating and cooling ramps, as follows. The heat from 10 °C to 50 °C at 20 °C/h and stir for 3 hours at 50 °C; cool from 50 °C to 10 °C at -20 °C/h and stir for 3 hours at 10 °C. Repeat both heating and cooling steps with a ramp of 10 °C/h and then repeat with a ramp of 5 °C/h, maintaining the stirring steps in-between for 3 hours and in the end heat from 10 °C to 25 °C at 10 °C/h and stir for 24 hours at 25 °C.

Figure 3.16 presents the overlaying of the diffractogram of the wet solid from test 1 with the diffractogram of form XII.

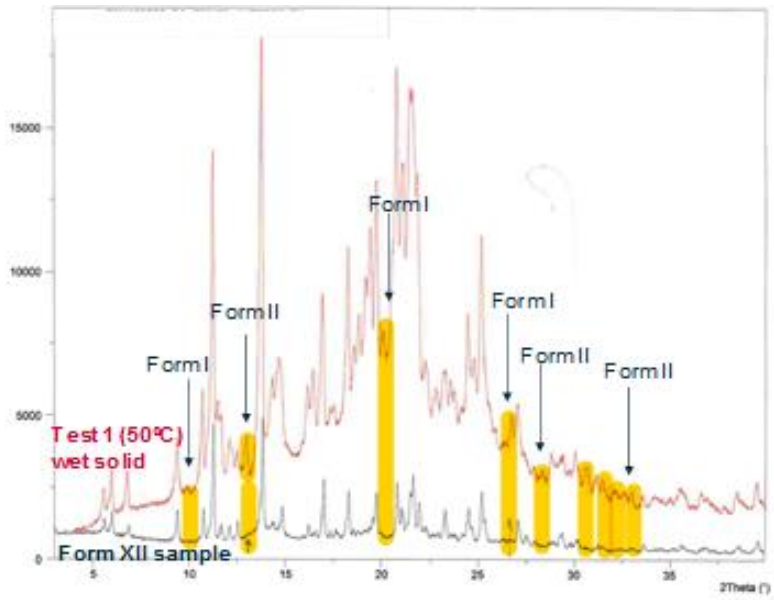

Figure 3.16. XRPD diffractograms' overlay of wet solid from test 1 and form XII obtained externally.

The overlaying presented in Figure 3.16 led to the conclusion that the wet solids were mainly of form XII with traces of the starting material's form II and stable form I.

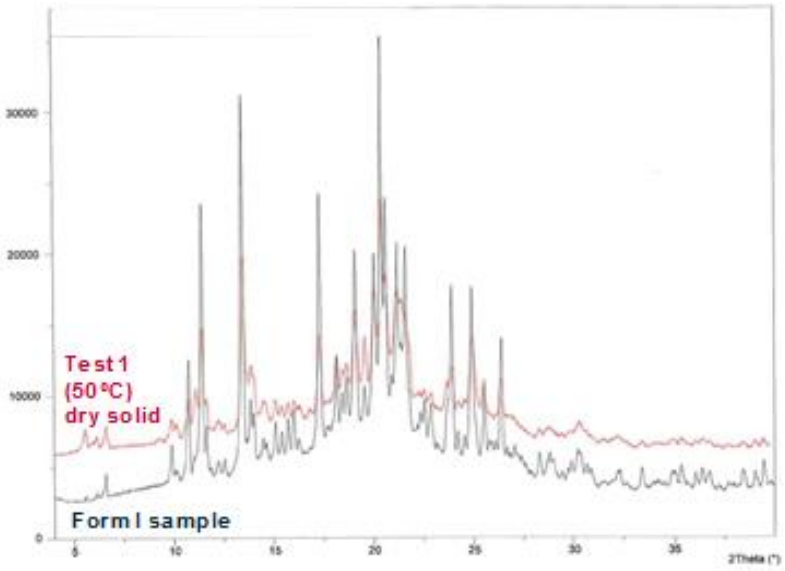

Figure 3.17 shows the overlay of the diffractogram of the dry solids of test 1 with a diffractogram of form I obtained.

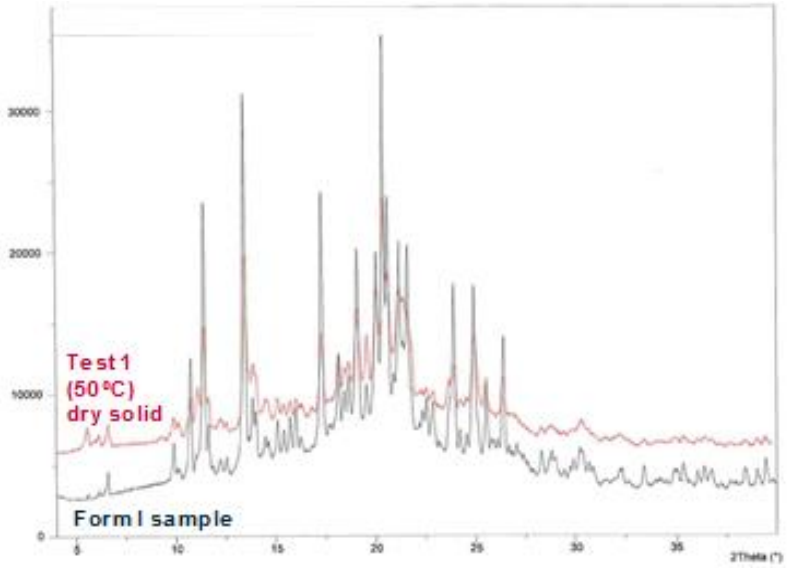

Figure 3.17. XRPD diffractograms' overlay of dry solid from test 1 and form I.

Regarding the diffractograms of the dry solids of both experiments, overlaying with a form I diffractogram, these indicate that after the drying procedure, the solids fully convert to the desired stable form I (Figure 3.17).

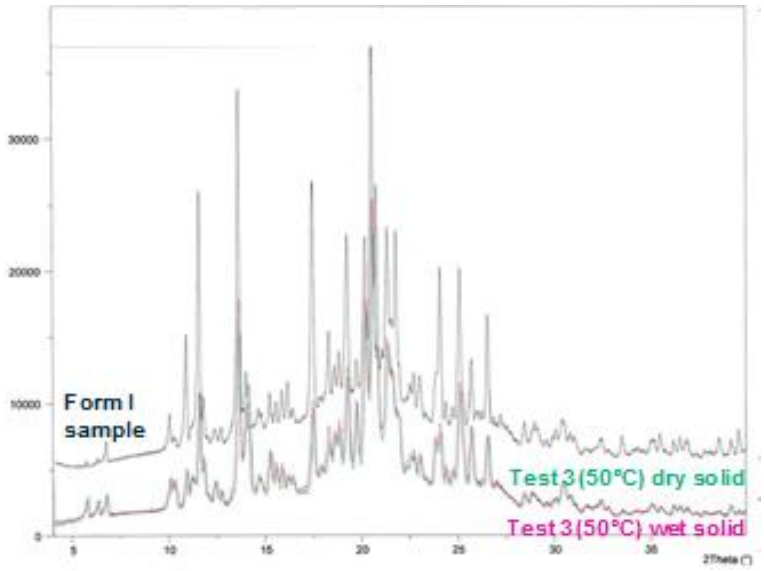

Figure 3.18. Overlay of the diffractograms of wet and dry solids of test 3 and form I.

Analyzing the diffractograms of Figure 3.18, it was possible to conclude that, when using a starting material of form I, both wet and dry solids of form I are formed and no transformation to form XII after the slurry test was observed.

Figure 3.19 represents the overlay of the diffractograms of the wet and dry solids from test 4 with a diffractogram of form XII obtained externally.

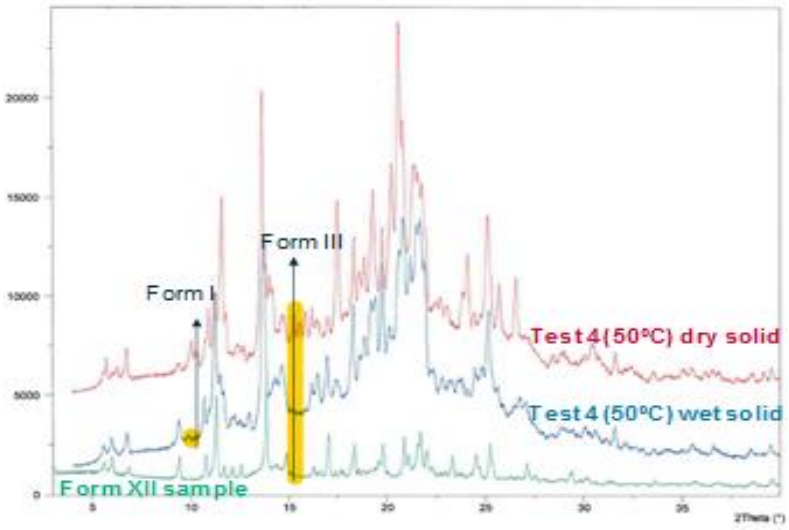

Figure 3.19. Overlay of the diffractograms of the wet and dry solids from test 4 with form XII obtained externally.

When performing the slurry test with a starting material of form III (test 4), the wet solid formed seems to be of form XII with traces of form III and I (Figure 3.19).

The diffractogram of the dry solid was subsequently overlaid with a form I's diffractogram (Figure 3.20) and it was possible to conclude that after the drying procedure the product was fully converted to the desired form I.

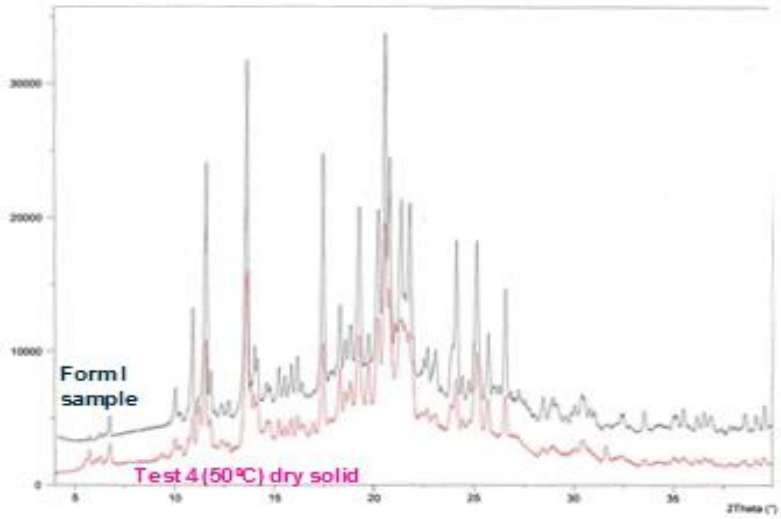

Figure 3.20. Overlay of the diffractograms of the dry solids from test 4 with one of form I.

Regarding the results obtained when using the starting material of form II and performing the slurry test at low agitation rates (test 5), Figure 3.21 was obtained by overlaying the wet solid diffractogram with the form XII.

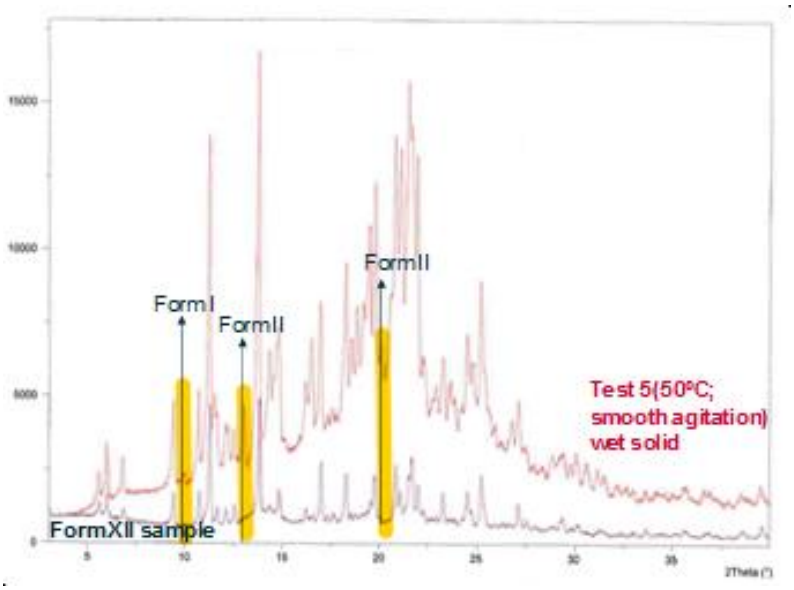

Figure 3.21.Overlay of the diffractogram of wet solids of test 5 with the form XII obtained externally.

The overlay of the diffractogram of wet solids obtained in test 5 with form XII (Figure 3.21) was analyzed and the odd peaks marked in yellow were compared with diffractograms of forms I and II. It was possible to conclude that the wet solids obtained are mainly of form XII with traces of form I and II, as expected from the previous tests 1 and 2. Additionally, in this specific case, the slow agitation rate did not seem to exert any impact on the final form of the wet solid. Concerning the dry solids, no overlay was available, however, the diffractogram was visually compared with a diffractogram of form I and it confirmed the full conversion of the solids into the required form I after the drying step. Comparing the results with the ones obtained in tests 1 and 2, performed at high stirring speeds, it is possible to conclude that, in this case, the stirring speed does not seem to affect the final form of the crystals, as the desired form was obtained in the end.

Regarding test 6, where the slurry experiment was performed at 80 °C, a different scenario was observed for the wet solids (Figure 3.22).

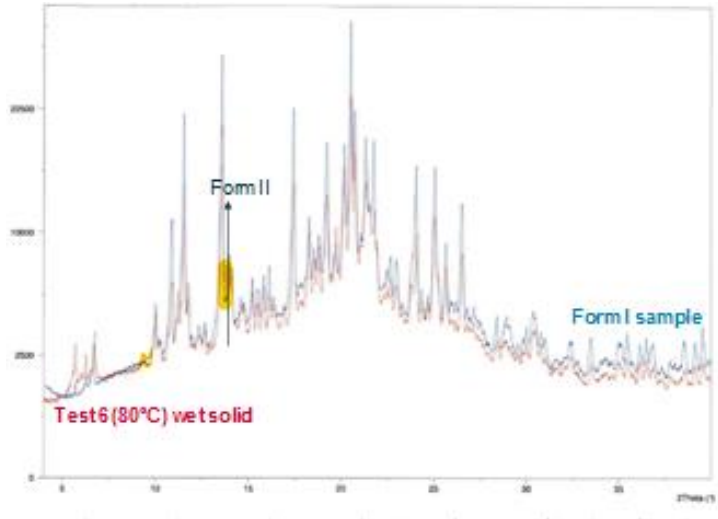

Figure 3.22. Overlay of the diffractogram of wet solids of test 6 with a standard diffractogram of form I.

Analyzing Figure 3.22, it was verified that performing slurry tests at high temperatures, promotes the formation of wet solids of form I with a few traces of the form of the starting material (form II), skipping the transformation into the metastable form XII observed in the wet solids of previous tests 1, 2, 4 and 5.

Figure 3.23 depicts the overlay of the dry solids' diffractogram with the form I standard.

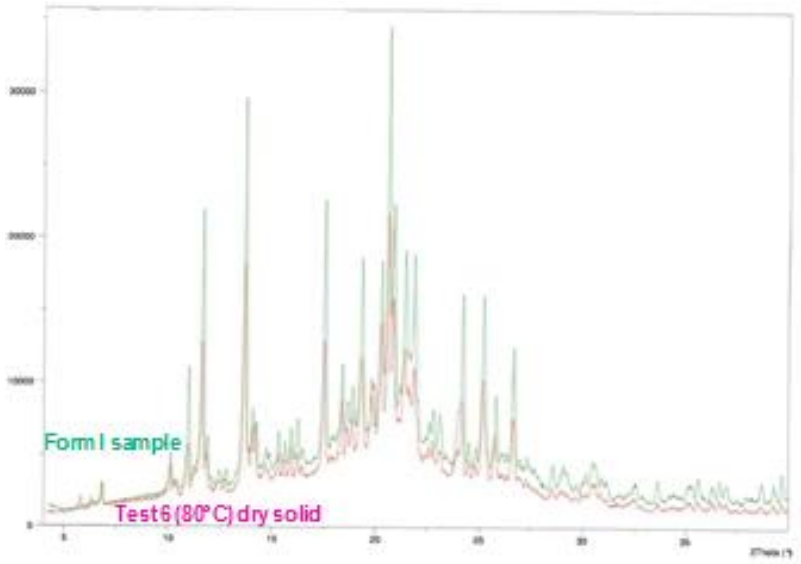

Figure 3.23. Overlay of test 6 dry solids' diffractogram with form I.

Comparing the overlay of the diffractograms of the dry solids with the form I (Figure 3.23), it was possible to confirm that the final solids were fully converted to form I, without any evident traces of form II.

Table 3.2 summarizes the aforementioned XRPD data obtained in each of the slurry tests.

Table 3.2 - Summary of the XRPD data obtained in each of the slurry tests.

	Polymorphic form					
Sample	Test 1	Test 2	Test 3	Test 4	Test 5	Test 6
Starting material	II	II	I	III	II	II
Wet product	XII+II+I	XII+II+I	I	XII+III+I	XII+II+I	I+II
Dry product	I	I	I	I	I	I

As concluding remarks and observing Table 3.2, the XRPD data confirmed that the stable form of the present API is form I, since at the end of the process only form I is obtained, regardless of the form of the starting material used. Moreover, employing high temperatures during the heating step in the slurry experiments starting from form II seems to favor the formation of form I, since no traces of form XII were detected in the wet solid. These observations were supported by the wet and dry solid diffractograms obtained in slurry test 6, where the test was performed using a starting material of form

II and was heated up to 80 °C and held at that temperature. In the experiment conducted at 80 °C (test 6), it was observed that the two liquids mixed together, showing a milky appearance. On the other hand, this milky appearance was not observed in the experiments performed at 50 °C, since at this temperature the API was in the solid state. Therefore, these observations suggest that, when working at 80 °C, the crystallization occurred from the melt phase. The transformation from one polymorph to another is determined by the system being monotropic or enantiotropic. In a monotropic system, the free energy of a polymorph remains below that of the other until the polymorph melts. In this way, one stable polymorph exists through heating [18]. This can explain why when working at a temperature above the melting point of form II, it converted into the most stable form I and no presence of metastable form XII was detected. On the other hand, when starting from a material of form II or III (tests 1, 2, 4 and 5) and executing the heating step at 50 °C, a metastable form XII is formed (Figure 3.16, Figure 3.19 and Figure 3.21) and is further converted to form I during the drying step. Thermogravimetry analysis (data not shown due to confidentiality purposes) showed solvent loss of 61.6% (w/w) in form XII product, which indicates that form XII is a solvate and therefore the heating applied during drying step might lead to solvent evaporation, converting into form I when the product is dry.

Melting point determination by DSC

The wet and dry solids obtained in each of the slurry tests, were submitted to DSC analysis in order to determine the melting point of the crystals. Table 3.3 summarizes the data regarding the melting point of the solids obtained in each slurry tests.

Table 3.3 – Melting point, heat of fusion and degradation temperature obtained for the starting material, wet and dry solids for each test, by DSC.

Experiment	Sample	Form by XRPD	Melting point (ºC)	Heat of fusion (J/g)	Degradation temperature (ºC)
Test 1	Starting material	II	68.18	83.61	190.98
	Wet solid	I, II, XII	135.58	72.83	191.26
	Dry solid	I	135.81	73.84	191.34
Test 2	Starting material	II	69.38	87.65	190.87
	Wet solid	I, II, XII	135.83	89.51	190.72
	Dry solid	I	136.15	76.76	191.19
Test 3	Starting material	I	Not available	Not available	Not available
	Wet solid	I	134.79	93.58	190.64
	Dry solid	I	135.18	53.38	191.75
Test 4	Starting material	III	78.63	89.1	191.21
	Wet solid	I, III, XII	134.45	89.43	191.03
	Dry solid	I	135.54	93.96	191.4

Table 3.3 (Cont.) – Melting point, heat of fusion and degradation temperature obtained for the starting material, wet and dry solids for each test, by DSC.

Experiment	Sample	Form by XRPD	Melting point (ºC)	Heat of fusion (J/g)	Degradation temperature (ºC)
Test 5	Starting material	II	71.12	84.59	191.04
	Wet solid	I, II, XII	135.44	87.74	190.7
	Dry solid	I	135.20	93.95	190.66
Test 6	Starting material	II	71.9	75.46	190.76
	Wet solid	I, II	135.67	68.68	190.74
	Dry solid	I	135.57	70.08	190.73

The melting point data summarized in Table 3.3, indicate that the wet solid's polymorphic form is similar to the dry solids' (form I) since the melting point is similar (approximately 135 °C) in all tests. Although the XRPD data (Table 3.2) identified the wet solids as a mixture of metastable forms (either II or III with XII), the DSC data only accused the presence of the stable form I. This might be due to the presence of minimum traces of the metastable forms in the wet solids, which were not sufficient to be identified in the DSC conditions employed and thus, detecting only the melt of the most predominant and stable form (form I in all cases).

Purity by HPLC

The purity data was acquired by HPLC method and the data obtained is presented in Table 3.4.

Table 3.4 - Purity results of the starting material, wet and dry product analyzed by HPLC.

	Purity by HPLC (%Area)					
Sample	Test 1	Test 2	Test 3	Test 4	Test 5	Test 6
Starting material	99.4	99.8	99.6	99.8	99.9	99.0
Wet product	98.6	99.8	99.5	97.7	99.9	98.6
Dry product	99.6	99.5	99.4	99.8	99.9	98.6

Analyzing the HPLC data presented in Table 3.4, it was possible to observe that the purity remains high, even starting from a material of a different polymorphic form. For instance, comparing the results of the tests with a starting material of form II (tests 1, 2, 5 and 6), it is visible the high purity obtained, although for test 6 the purity content was slightly lower. This might be given to the fact that, in this test, the slurry was heated to 80 °C whereas the remaining slurries were heated to 50 °C, which led to the increase of an unknown impurity. Additionally, test 5, performed at slow agitation rates, preserves the highest purity of 99.9% of the starting material. Regarding the purity results of the tests 3 and 4, with a

starting material of form I and III, respectively, these are also desirable. However, the slurry test seems to slightly decrease the purity of the product when working with a starting material of form I (test 3), since it presented a purity of 99.6%, ending with a purity of 99.4%.

Overall, the purity of the dry product is higher than 98.6% when working until 50 °C in the heating step. In this particular case, the solvents used do not absorb at 220 nm, which is the wavelength used in the HPLC detector. Additionally, the HPLC analysis was performed for purity determination and not assay, therefore it was expectable for the solvent peak to not show up in the analysis of the wet solid (form XII). The purity was obtained based on the percentage of the main peak in comparison to other impurities' peaks and not assay. This is an important aspect since it gives confidence that the crystallization process can affect the quality of the final product by promoting impurities' growth.

Crystal habit analysis by SEM

The SEM images of the crystal habit of the starting materials and dry solids obtained after the drying process for each of the tests are presented in Figure 3.24 to Figure 3.28. The morphology of the wet and dry crystals was identical and therefore only the SEM analysis of the starting material and dry solids were compared, since these depicted promising differences in the crystal habit.

Comparing the crystal habit of starting material of form II (tests 1 and 2), these are identical and also lead to similar results after the slurry test, appearing to depict less aggregation (Figure 3.24).

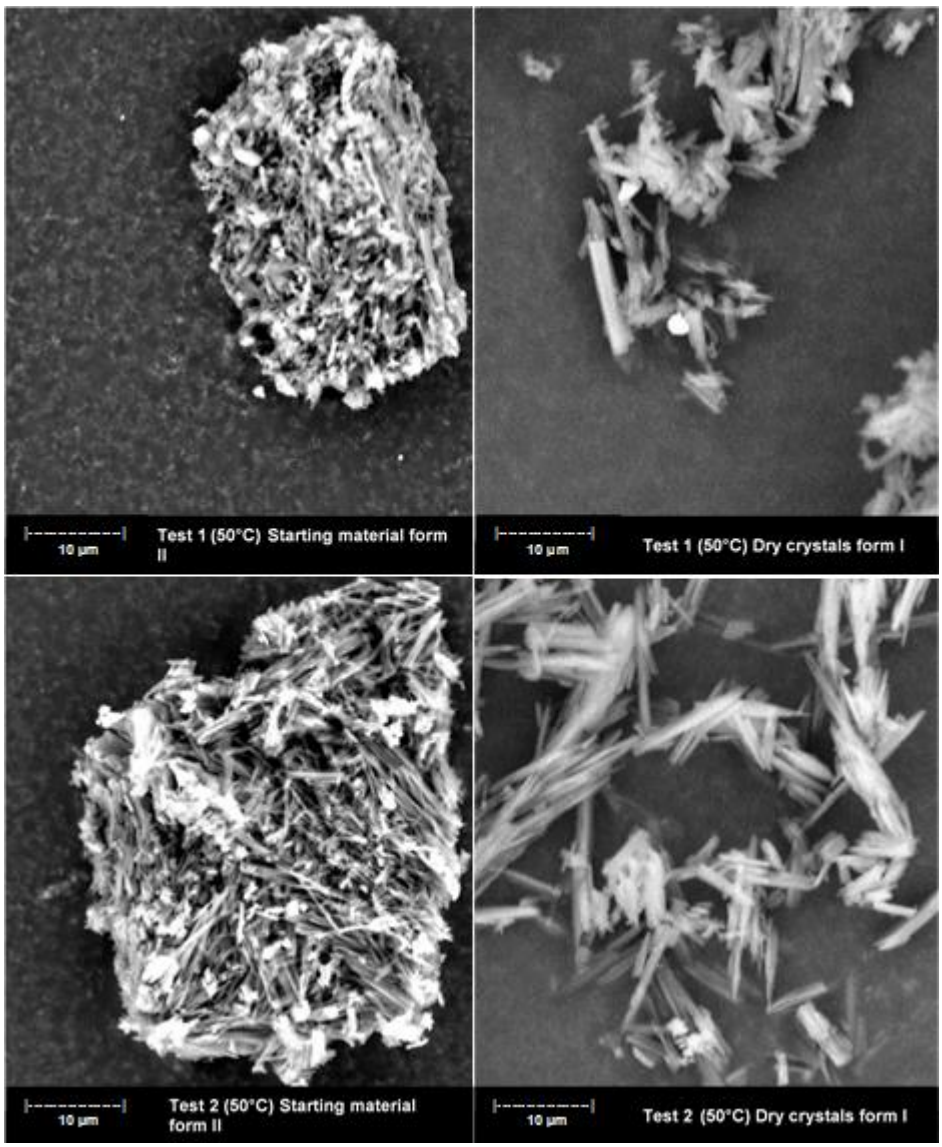

Figure 3.24. Comparison of the morphology of the crystals before and after the slurry tests 1 and 2 by SEM (Zoom 4800x).

Regarding Figure 3.25 and Figure 3.26, no significant differences are evident in the crystal habit when performing the slurry tests from forms I and III, respectively.

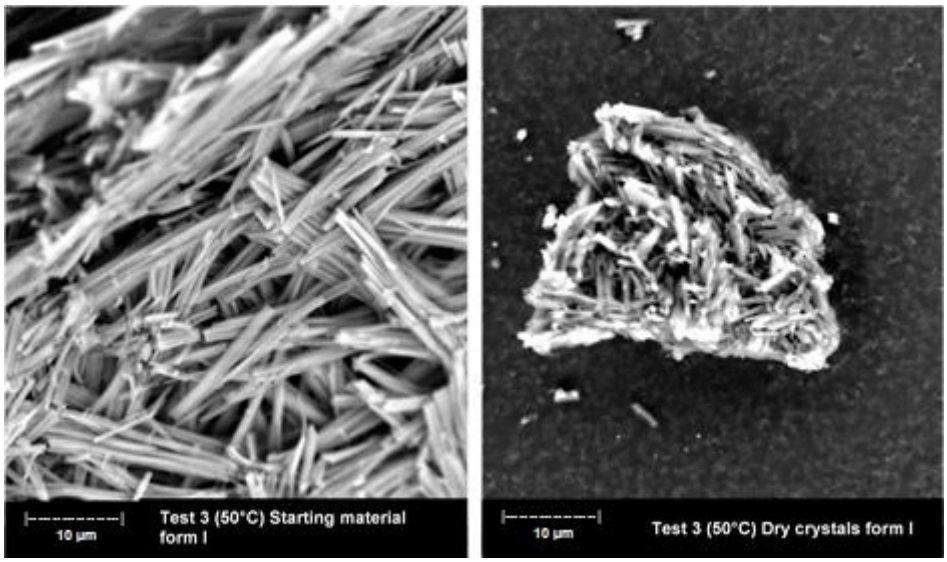

Figure 3.25. Comparison of the morphology of the crystals before and after the slurry test 3 by SEM (Zoom 4800x).

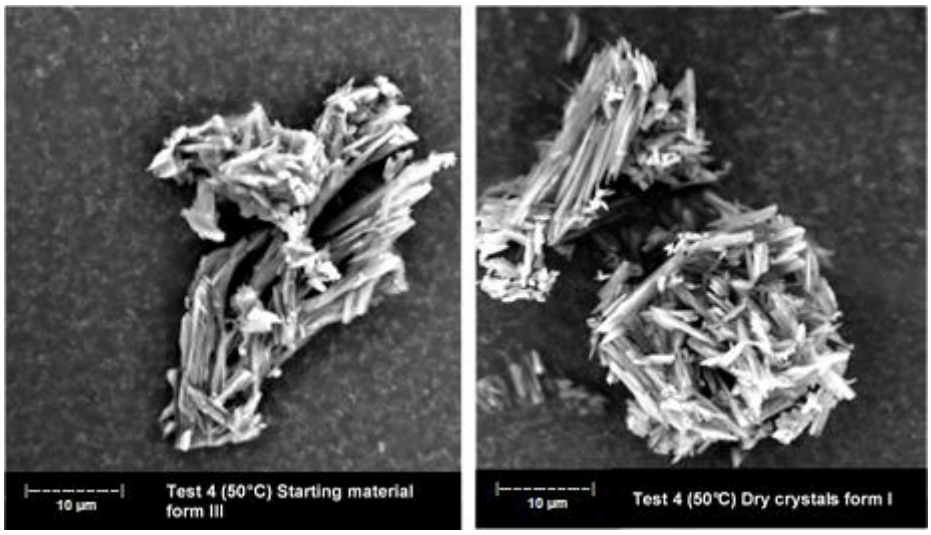

Figure 3.26. Comparison of the morphology of the crystals before and after the slurry test 4 by SEM (Zoom 4800x).

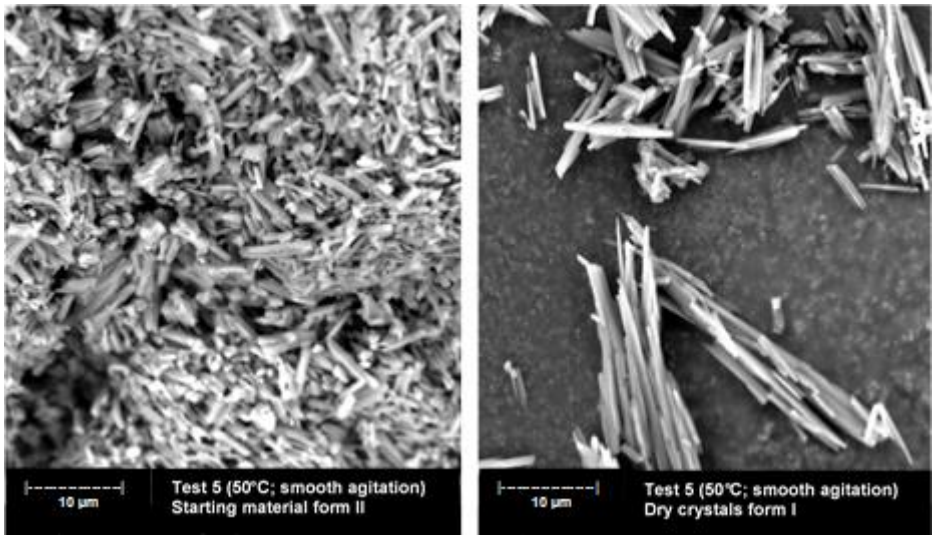

Figure 3.27. Comparison of the morphology of the crystals before and after the slurry test 5 by SEM (Zoom 4800x).

Test 5 was performed in order to check if a smooth agitation had any visible impact on the crystal habit of the API. Comparing the crystal habit resulting from test 5 (Figure 3.27) with the results of tests 1 and 2 performed at higher speed (Figure 3.24) it can be observed that the needles formed at lower stirring speed, seem to be longer than the ones obtained at a higher speed. This can be due to the less breakage caused by the presence of low fluid shear at smooth agitation.

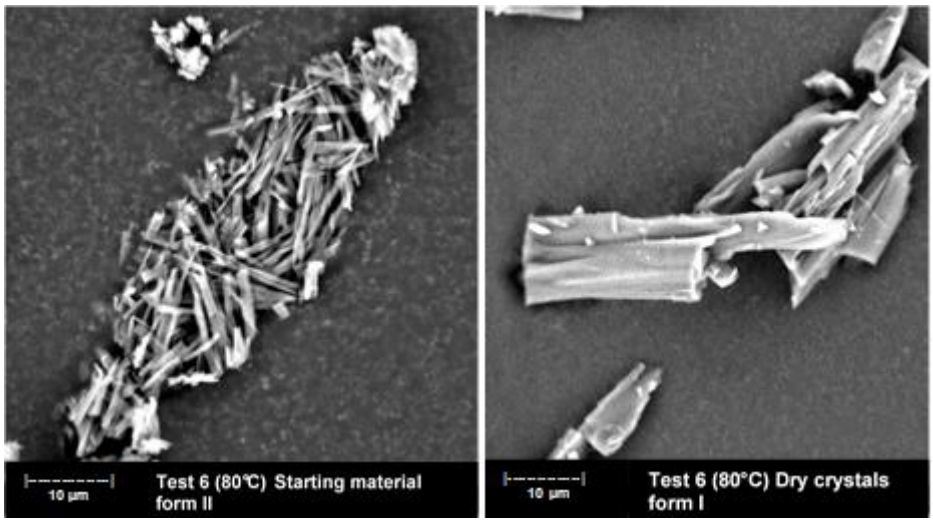

Figure 3.28. Comparison of the morphology of the crystals before and after the slurry test 6 by SEM (Zoom 4800x).

From Figure 3.28, it can be observed that for test 6 where the heating step was performed at 80°C, irregular rectangular shaped crystals (similar to form I which is the desired one) were obtained from fine needle-shaped material (form II). This behavior might be linked to the fact that, in test 6, the heating step at 80°C is above the melting point of form II starting material (71.9°C).

Figure 3.29 shows additional images of the dry solid resulting from test 6, where a mixture of irregular shapes and rectangular crystals is observed.

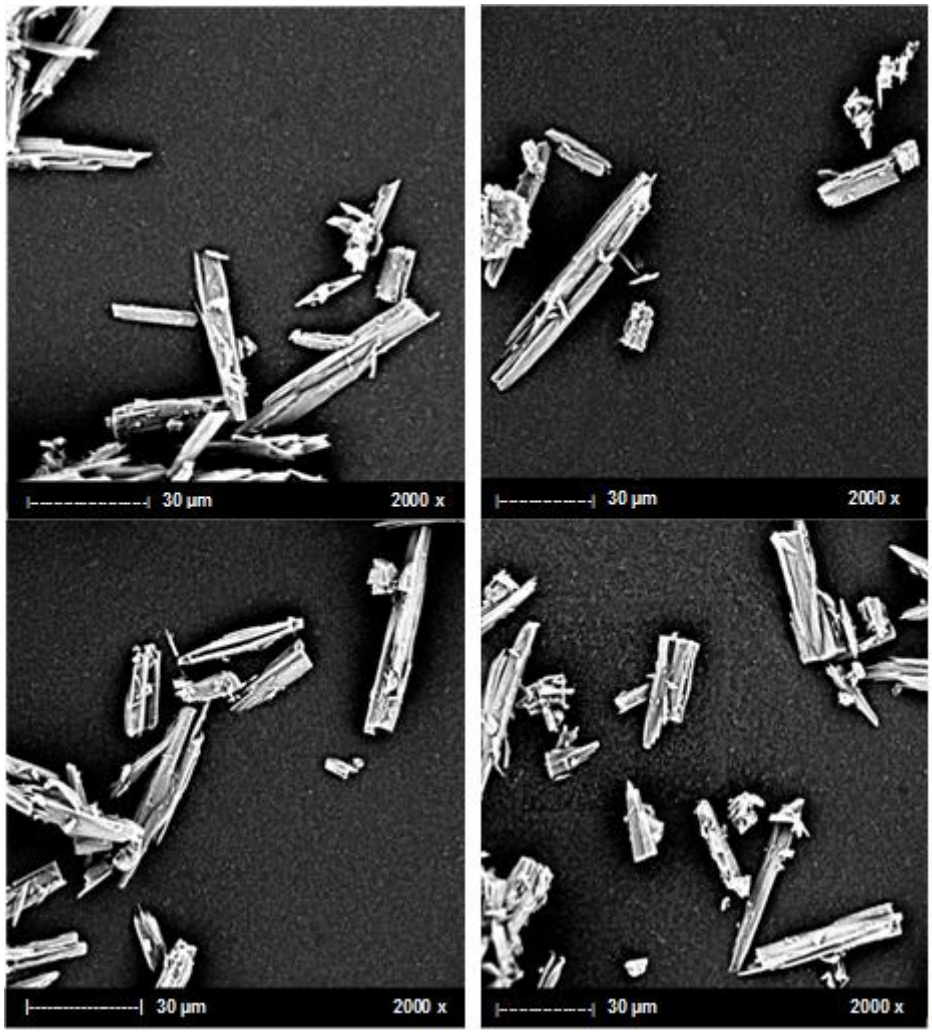

Figure 3.29. Thicker crystals obtained when performing the heating step at 80ºC in the slurry test 6 (Zoom 2000x).

Overall, although it is known that each polymorph of an API can exhibit multiple crystal habits [19], in the current case it does not seem to occur, since forms I, II or III present similar shapes.
Furthermore, the results obtained for test 6 (Table 3.2 and Figure 3.28 and Figure 3.29) suggest that, when working at a temperature above the melting point of the product, the crystallization seems to occur from the melt phase, leading straightforwardly to the most stable form and morphology change. On the other hand, it seems that in the remaining tests, the solid-solid polymorphic transformation seems to occur during the drying process, maintaining the morphology.

In order to analyze the size of the crystals before and after the experiment in detail, the length and width of the crystals of the starting material and the ones obtained at the end of each slurry test were also quantified by SEM analysis and the results are presented in Table 3.5.

Table 3.5 – Measurements of length and width of the crystals obtained in each slurry test, using the SEM technique; SM – starting material; DS – dry solid obtained after the slurry test.

	Test 1		**Test 2**		**Test 3**		**Test 4**		**Test 5**		**Test 6**	
	SM	DS	SM	DS	SM	DS	SM	DS	SM	DS	SM	DS
Length (μm)	6.3	12.2	6.1	14.0	5.2	7.1	6.0	12.6	7.8	13.7	5.0	29.4
Width (μm)	0.1	2.1	0.6	1.4	0.8	1.1	0.7	0.7	1.3	1.1	0.7	6.4

From the data summarized in Table 3.5, it is possible to observe that the length and width of the needle-shaped crystals of the starting materials used in all tests are similar, regardless of the polymorphic form. Generally, it can also be noted that, when performing the heating step at 50°C (tests 1-5), regardless of the polymorphic form of the starting material, there is a slight increase in the final dimensions of the crystals. Furthermore, the final dimensions of the crystals obtained in tests 1 to 5 are similar and might be characteristic of the stable form I. Nevertheless, in test 3, where a starting material of form I was used and crystals of form I were obtained in the slurry test (as depicted in Table 3.2), the resulting crystals show values of length and width similar to dimensions of the starting material used (Table 3.5). This might indicate that for this API, starting the slurry test with the stable form I, besides maintaining the internal structure of the crystals, also seems to preserve their external structure (dimensions). Regarding the dimensions of the crystals obtained in test 5 (starting material of form II, heating step at 50°C and slow stirring), these do not seem to differ significantly from the ones obtained at the same conditions and higher stirring speed (tests 1 and 2). Comparing the dimensions of the crystals that resulted from test 6 (heating at 80°C) with the ones obtained in the remaining tests, it is visible a significant increase in the size of the particles. In addition, comparing the crystal dimensions with the ones of the starting material, these are six times higher (an increase of 480%). This effect might have been exerted by working at a temperature higher than the melting point of the API.

Figure 3.30 depicts the comparison of the crystal habit obtained when performing the evaporative crystallization in ethanol (section 3.4.1) and test 6 in 1,2-dimethoxyethane:heptane.

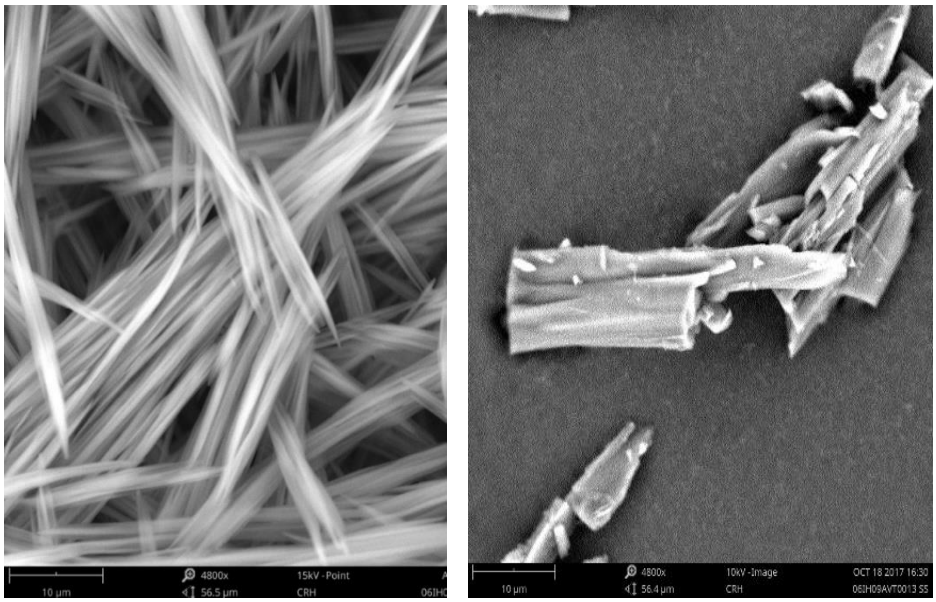

Figure 3.30. Comparison of the crystal habit obtained in the ethanol evaporative crystallization and test 6 performed with 1,2-dimethoxyethane (Zoom x4800).

Analyzing Figure 3.30 it is visible the modification of the crystal habit, where the needle-shaped crystals obtained when performing the evaporative process have no similarity in the habit of the crystals obtained in test 6 with 1,2-dimethoxyethane:heptane. Therefore, performing a slurry test with the operating conditions of test 6 is a promising process to obtain a product with the desired polymorphic form and a suitable size for further particle design operations.

3.5. Conclusions

This chapter aimed to obtain an API with a different crystal habit and size with a specific polymorphic form, in order to ease the downstream processes. To overcome this challenge, two approaches were tested. The first attempt reports the tests performed to achieve the goal, without modifying the solvent (ethanol), whereas the second describes the tests executed to find an alternative process using a mixture of solvents (heptane: 1,2-dimethoxyethane).

Regarding the first approach, the original evaporative crystallization process was repeated and simultaneously monitored with the FBRM Lasentec probe, where additional steps such as Ostwald ripening phenomenon and slow cooling were induced to assess their impact on the size of the crystals. As detected by the FBRM probe, and as expected, the fine particles' count slightly decreased when the temperature increased, due to the dissolution of these smaller particles, while the remaining particles' count maintained constant. This was only detected when applying the second heating cycle, which implies that inducing more cycles could result in better results. However, there was no evident sign of growth or production of larger particles visible. Moreover, it was also possible to observe that, when applying cooling ramps, only the number of fine particles increases, which justifies the low chord length median values obtained (≈ 8 µm). This increase in the number of counts of small particles can be either due to the supersaturation attained during cooling or due to the stirring speed applied which might

additionally induce secondary nucleation. At last but not least, it was possible to observe that during the agitation at constant temperature (20 ºC), the number of smaller particles also increased, which can be interpreted as the existence of secondary nucleation caused by the stirrer (particle-particle collision, particle-baffle-impeller-reactor walls collision).

In order to quantify the supersaturation during the crystallization step, the solubility curve of the API in ethanol was determined using turbidity probes. With the data from the solubility curve, it was possible to obtain a value of a supersaturation ratio of 2.6 at the end of the evaporation step. From the data obtained from the MSZW, it was possible to conclude that the metastable zone is wider using high cooling rates. Additionally, it was also detected that the metastable zone widens as the saturation temperature decreases. Next, a cooling crystallization experiment with a supersaturation ratio of 2.0 (lower than 2.6 of the evaporative method) and a slow cooling rate was performed in order to check the influence of the supersaturation on the shape and dimensions of the crystal. Since the crystals still presented needle shape, a new experiment at a lower supersaturation with seeding was performed. The seeding did seem to promote growth and agglomeration of the crystals, which in turn resulted in more robust particles. Nevertheless, this transformation was not sufficient and a new solvent system was tested (second approach).

Concerning the second approach, polymorphic stability studies of the API were executed in a slurry of the product in a mixture of 1,2-dimethoxyethane:heptane, with a heating step of 50 ºC and 80 ºC. The stirring speed did not seem to affect the final form, as in tests 1,2 and 5 a starting material of form II was used at high and low speed and at the end form I was obtained. The new system of solvents showed promising results when performing the heating step of the slurry experiment at higher temperatures (80 ºC). Comparing the dimensions of the crystals that resulted from heating the slurry of the API at 80 °C with the ones obtained in the remaining tests performed at 50 °C, it was visible a significant increase in the size of the particles. In addition, comparing the crystal dimensions with the ones of the starting material, these presented an increase of 480%. This effect seems to have been induced by the thermal treatment to which the API was subjected during the heating step of the slurry (80 °C), which was above its melting point (71.9 °C). The desired polymorphic form was attained as well as an acceptable purity. These experimental observations are highly promising, particularly in cases where the crystal habit cannot be easily attained by altering the solvent or the supersaturation, and in the future, these tests should be extended to other APIs to check if thermal treatment can be an alternative solution when modifications on the crystal habit are desired.

As concluding remarks, this chapter alerts to the importance of monitoring the crystallization process and how the used operating conditions affect the final properties of the product such as crystal habit, size, purity and polymorphic form.

References

[1] W. Beckmann, *Crystallization: Basic Concepts and Industrial Applications*. Weinheim; Germany: Wiley-VCH, 2013.

[2] A. K. Tiwary, "Modification of Crystal Habit and Its Role in Dosage Form Performance," *Drug Dev. Ind. Pharm.*, vol. 27, no. 7, pp. 699–709, 2001.

[3] Y. Wang and Z. Liang, "Solvent effects and its role in quantitatively manipulating the crystal growth: Benzoic acid as case study," *CrystEngComm*, vol. 19, no. 23, pp. 3198–3205, 2017.

[4] M. Sun, X. Hu, X. Zhou, and J. Gu, "Determination of minor quantities of linezolid polymorphs in a drug substance and tablet formulation by powder X-ray diffraction technique," *Powder Diffr.*, vol. 32, no. 2, pp. 78–85, 2017.

[5] S. S. Joshi, "Crystal habit modification using habit modifiers," in *Modern Aspects of Bulk Crystal and Thin Film Preparation*, 2012, pp. 413–436.

[6] H. H. Tung, E. L. Paul, M. Midler, and J. A. McCauley, *Crystallization of Organic Compounds: An Industrial Perspective*. USA: John Wiley & Sons, 2009.

[7] D. Hooper, F. C. Clarke, R. Docherty, J. C. Mitchell, and M. J. Snowden, "Effects of crystal habit on the sticking propensity of ibuprofen - A case study," *Int. J. Pharm.*, vol. 531, no. 1, pp. 266–275, 2017.

[8] C. Stoica, P. Verwer, H. Meekes, P. J. C. M. Van Hoof, F. M. Kaspersen, and E. Vlieg, "Understanding the effect of a solvent on the crystal habit," *Cryst. Growth Des.*, vol. 4, no. 4, pp. 765–768, 2004.

[9] J. Chen, J. Wang, J. Ulrich, Q. Yin, and L. Xue, "Effect of Solvent on the Crystal Structure and Habit of Hydrocortisone," *Cryst. Growth Des.*, vol. 8, no. 5, pp. 1490–1494, 2008.

[10] J. F. Bauer, "Polymorphism - A Critical Consideration in Pharmaceutical Development, Manufacturing and Stability," *J. Valid. Technol.*, pp. 15–23, 2008.

[11] D. Kumar, R. Thipparaboina, B. Sreedhar, and N. R. Shastri, "The role of surface chemistry in crystal morphology and its associated properties," *CrystEngComm*, vol. 17, no. 35, pp. 6646–6650, 2015.

[12] P. Barrett and B. Glennon, "Characterizing the Metastable Zone Width and Solubility Curve Using Lasentec FBRM and PVM," *IC*, vol. 80, no. October, pp. 799–805, 2002.

[13] H. Leba, A. Cameirao, J. M. Herri, M. Darbouret, J. L. Peytavy, and P. Glénat, "Chord length distributions measurements during crystallization and agglomeration of gas hydrate in a water-in-oil emulsion: Simulation and experimentation," *Chem. Eng. Sci.*, vol. 65, no. 3, pp. 1185–1200, 2010.

[14] R. C. A.R.Parsons, S. N. Black, "Automated Measurement of Metastable Zones for Pharmaceutical Compounds," *IChemE*, vol. 81, no. July, pp. 700–704, 2003.

[15] N. G. Anderson, *Practical Process Research and Development – A guide for Organic Chemists*, 2nd ed. Academic Press Elsevier, 2012.

[16] J. Ulrich and C. Strege, "Some aspects of the importance of metastable zone width and nucleation in industrial crystallizers," *J. Cryst. Growth*, vol. 237–239, no. 1-4 III, pp. 2130–2135, 2002.

[17] B. Gielen, J. Jordens, L. Thomassen, L. Braeken, and T. Van Gerven, “Agglomeration Control during Ultrasonic Crystallization of an Active Pharmaceutical Ingredient,” *Crystals*, vol. 7, no. 2, p. 40, 2017.

[18] D. Croker and B. K. Hodnett, “Mechanistic Features of Polymorphic Transformations: The Role of Surfaces,” *Cryst. Growth Des.*, vol. 10, pp. 2806–2816, 2010.

[19] N. Stieger and W. Lienenberg, “Recrystallization of Active Pharmaceutical Ingredients,” *Cryst. - Sci. Technol.*, pp. 183–204, 2007.

Chapter 4 Characterization at lab-scale of the influence of the mixing conditions on the particle size in anti-solvent crystallization of an API[2]

[2] Part of this work was published in:

A. Tulcidas, B. Santos, S. Pawlowski and F. Rocha, “Quality by statistical control in crystallization - Assessment of mixing conditions and probability of obtaining the desired particle size”, Industrial & Engineering Chemistry Research, vol. 58, pp. 20162 - 20172, 2019.

4.1. Scope

This chapter addresses part of a case study considering an anti-solvent technique that requires the crystallization of an API (Active Pharmaceutical Ingredient) that should meet considerably strict particle size specifications.

Usually, during the development of anti-solvent crystallization processes, parameters such as anti-solvent or solution addition rate and location are tested the most and no (or less) attention is given to the suspension height to clearance ratio (H/C). The latter can be an important factor to consider during tech transfer to a reactor with a different design or even during scale-up. Therefore, the current work was performed as a proof-of-concept, aiming to understand if varying clearance, along with power per volume (PV), could affect the particle size of an API obtained by anti-solvent crystallization. The impact of H/C and PV on the Particle Size Distribution (PSD) parameters Dv10, Dv50 and Dv90 were evaluated. Subsequently, Multiple Linear Regression (MLR) approach was used to disclose the existing correlations, in order to better understand the possible interactions among these parameters.

It was detected that Dv10 and Dv50 are proportional to the H/C, which implies that the particle size is higher when the ratio H/C increases (lower clearance, C). For instance, the results obtained for Dv50 indicate that, in order to obtain a larger Dv50, higher H/C (lower clearance) and lower PV should be applied during the crystallization. On the other hand, Dv90 seems to be only influenced by the PV applied. Regarding the morphology of the crystals obtained, no significant impact was detected. A relationship between the PSD parameters and the nucleation rate was also witnessed.

4.2. Introduction

Anti-solvent crystallization is a method extensively employed to produce crystals in the pharmaceutical field, due to lower energy consumption in comparison with cooling or evaporative techniques, as well as being preferred when heat-sensitive pharmaceutical compounds are involved [1]. The distribution of the supersaturation (driving-force of crystallization) can be affected by reactor hydrodynamics, in terms of micro- or meso-mixing [2]. In the case of anti-solvent crystallization, the mixing conditions can affect the blending of the anti-solvent into the solution and, as a consequence, the distribution of supersaturation inside the reactor. This, in turn, affects the nucleation and growth kinetics, and thus the particle size distribution (PSD) of the product [3]–[5]. Depending on the supersaturation present in the solution, either nucleation or growth may be predominant over the other, and as a result, crystals with different sizes and shapes are obtained [6], [7]. In order to reduce batch-to-batch variability at industrial scale, the impact of the hydrodynamics on the metastable zone width (MSZW) - which is the zone where no nucleation occurs, only crystal growth - must be better understood [8], [9].

Kaćunić *et al*. [10] studied the influence of the impeller clearance in a dual pitch blade turbine (PBT) impeller system on the crystal growth kinetics of Borax during a cooling crystallization and concluded that the clearance influences the crystal size over process time, since it was observed that lower clearances result into formation of larger but agglomerated crystals [10]. Shimizu *et al*. [11], studied the effect of the clearance of a turbine impeller on the crystal size distribution of aluminum potassium sulphate in a batch crystallizer by cooling with seed crystallization and observed that when increasing the clearance, the median diameter of the crystal increased [11]. Additionally, Jin Liu *et al*. [12], assessed the influence of agitation rate, impeller type and diameter and clearance, and the presence of baffles on the primary nucleation on cooling crystallization of butyl paraben in ethanol and m-hydroxybenzoic acid in 1-propanol [12]. They found that the induction time seems to decrease with increasing agitation rate and in presence of baffles and the induction time is shorter when using a Rushton turbine than with a marine propeller and a disk impeller [12]. Regarding the influence of impeller clearance on the average induction time of butyl paraben in ethanol at different agitation rates, with a disk impeller, no clear differences were observed [12]. However, most of the studies reporting the influence of the clearance on the induction time or nucleation rate only address cooling crystallization and thus, only a few references seem to report the impact of clearance on the particle size distribution during an anti-solvent crystallization of an API.

The H/C can be an important factor to consider in scale-up or during tech transfer for other equipment with a different design. Therefore, the current work was performed for a proof-of-concept, aiming to understand if varying clearance, along with power per volume, could influence the particle size parameters of an API obtained by anti-solvent crystallization. To minimize the experimental resources required to develop statistical-based models correlating all these variables, the design of experiments (DoE) might be an efficient way to maximize the gain of information [13]. This is particularly important in the pharmaceutical industry, where the costs of the ingredients are high and manufacturers have to deal with a fast-paced environment, resulting from excessive pressure to improve process efficiency and

reduce time to launch the drug product into the market [14]. For this purpose, a DoE approach was applied and the experimental data was analyzed by multiple linear regression, to investigate possible correlations among the aforementioned parameters.

4.3. Experimental methodology

The nature of the API, as well as used reagents, are not disclosed due to confidentiality limitations. Moreover, not revealing the chemical structure does not affect the purpose of this work, since the methodology presented herein is more mathematical than chemical and therefore it can be employed to other processes, regardless of the chemical compound involved.

4.3.1. Materials and experimental procedure

Anti-solvent crystallizations of an API were performed using a 500 mL glass reactor and a three-blade retreat curve impeller (RCI). The ratio between the impeller diameter and the reactor internal diameter was 0.66. The stirring speed to be used in the tests was calculated by Equation (4.1).

$$N = \sqrt[3]{\frac{PV \times V}{P_0 \, \rho \, D^5}} \tag{4.1}$$

where PV is the power per volume in W/m^3, V the volume of the solution in m^3, P_0 the power number which is dependent on the type of agitator [15], ρ is the density of the solution in kg·m^{-3}, N the stirring speed in s^{-1} and D the diameter of the impeller in m.

The suspension height (H) was approximately constant in all experiments, corresponding to about 50% of the total volume of the reactor. In these experiments, the height variation was minimal and it was considered negligible since no significant vortex was observed and the volume variation due to the API solution addition was also minimal, since the proportion API solution volume to anti-solvent volume was of 1:7. The height was defined based on the total volume (API solution + anti-solvent) inside the vessel. Although there is a linear relationship between height and volume, the clearance and power per volume could be adjusted independently. The clearance (C) was varied and the values used were H/2, H/6, and H/10. The API solution was added near the surface of the anti-solvent with a burette, at a constant rate of approximately 5 mL/min, instead of the conventional method (anti-solvent addition into the API solution) due to the small particle size requirements. In this approach, the higher ratio of anti-solvent to API solution will create a high local supersaturation ratio (concentration/ solubility concentration), which in turn, translates into the production of fine particles [16].

The working temperature range used was 25-30 ºC and was monitored with a Huber cryostat bath. Additionally, the nucleation rate was estimated throughout the experiments, with a FBRM (Focused

Beam Reflectance Measurement) Lasentec probe. The nucleation rate was calculated based on the number of crystals within a chord length distribution range of 1-10 µm, per second, obtained immediately after the API solution addition into the anti-solvent. The probes used were considered as baffles (Figure 4.1).

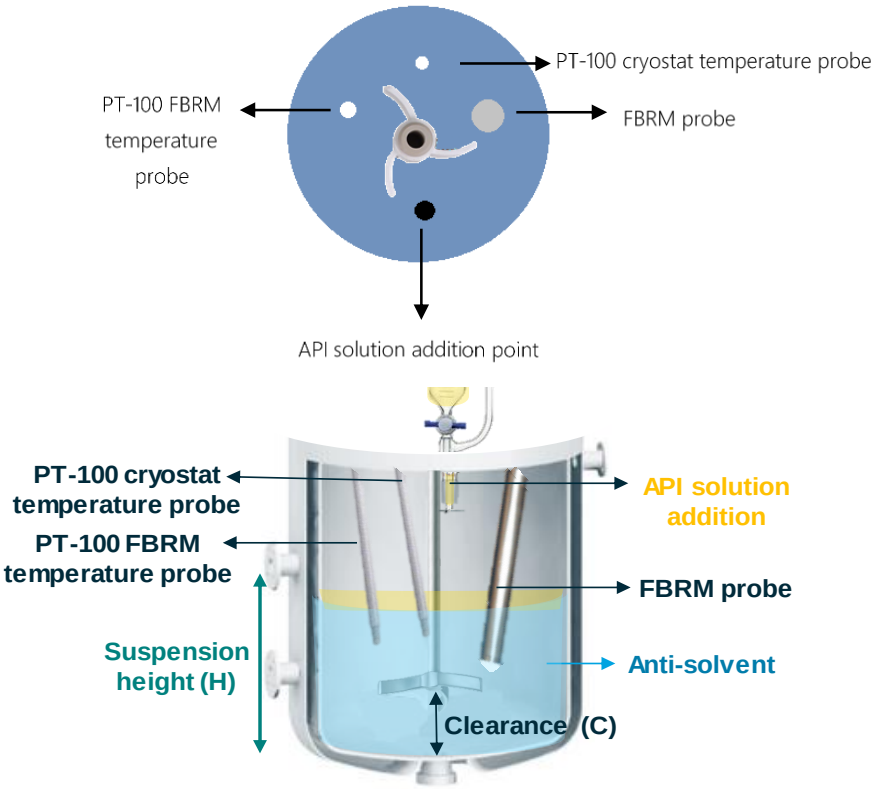

Figure 4.1. Top and vertical view of the reactor used in the experiments.

The experimental conditions tested are presented in Figure 4.2.

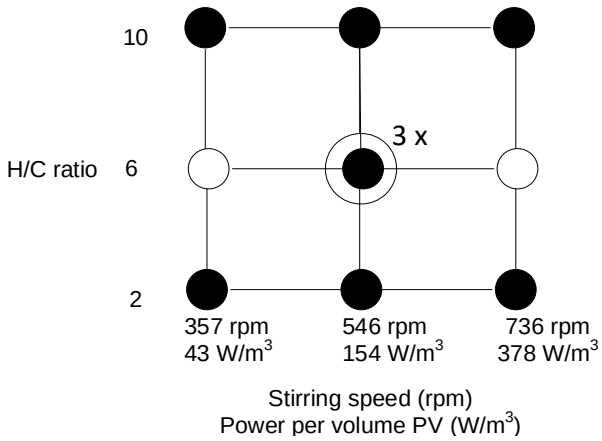

Figure 4.2. Experimental conditions of H/C, stirring speed (and the corresponding power per volume) used during the anti-solvent crystallization experiments at lab-scale. Filled dots represent the experiments performed.

Each of the experiments lasted approximately two hours. In the end, the resulting crystals were filtered under vacuum. The wet crystals were dried under vacuum at a temperature no greater than 60 ºC, until constant weight. The PSD of the dry crystals was measured using the Malvern Mastersizer 2000 particle size analyzer [17]. Additionally, the crystallization process was performed thrice at the center point conditions (speed = 546 rpm; H/C = 6).

4.3.2. Statistical analysis

The experimental data was normalized by subtracting the average and dividing by the standard deviation of the experimental points [18].

The least-squares method was used in Excel through the LINEST function, to obtain the correlation between uncorrelated predictors (X_1, X_2 ,X_3) and output (Y_i) variables, by adjusting the values of regression coefficients (β_1, β_2, …, β_0) of the following linear equation:

$$Y = \beta_1 X_1 + \beta_2 X_2 + \cdots + \beta_0 \quad (4.2)$$

Statistic parameters such as standard deviation of the regression coefficients and the coefficient of determination R^2 were also obtained. The latter coefficient enables the assessment of the fitting quality and assumes that every single variable explains the variation in the dependent variable. Thus, an adjusted R^2 (R^2_{adj}) was calculated from the values of R^2 as follows:

$$R^2_{adj} = 1 - \frac{n-1}{n-p-1}(1-R^2) \quad (4.3)$$

where n is the number of observations and p is the number of predictor variables used in the model. The R^2_{adj} penalizes the introduction of additional terms in the model, prevents overfitting and the use of predictors with less potential to explain the response's variability [19]. The value of the R^2_{adj} was the main criteria for the selection of the model. If needed, to improve models' prediction, quadratic, logarithmic and squared root terms of the H/C ratio and power per volume were additionally tested as input variables [20].

4.4. Results and discussion

4.4.1. Impact of H/C and PV on the PSD

The statistical models were developed using only simple linear combinations of the predictors at first. Then, to improve the values of the R^2_{adj} and thus, the variability explained by the models, the introduction of quadratic, logarithmic and squared root terms was evaluated. The models were further

optimized by eliminating the coefficients without statistical meaning. Models with simple interaction parameters such as H/C*PV were built but these results were not presented since the adjusted R^2 was low. Additionally, the interaction parameter (H/C*PV) was not statistically significant in this case, since the error obtained was higher than the parameter's value itself. Table 4.1 shows the R^2 and R^2_{adj} values of the simple and optimized models.

Table 4.1 – R^2 and adjusted R^2 of the simple linear and with interaction parameters (optimized) models.

	Model	R^2	R^2_{adj}
Linear	$D_{v10} = \beta_{1,Dv10}.H/C + \beta_{2,Dv10}.PV + \beta_{3,Dv10}$	0.63	0.45
	$D_{v50} = \beta_{1,Dv50}.H/C + \beta_{2,Dv50}.PV + \beta_{3,Dv50}$	0.79	0.68
	$D_{v90} = \beta_{1,Dv90}.PV + \beta_{2.Dv90}$	0.77	0.71
Interaction	$D_{v10} = \beta_{1,Dv10}.(H/C)^2 + \beta_{2,Dv10}.PV + \beta_{3,Dv10}$	0.72	0.58
	$D_{v50} = \beta_{1,Dv50}.(H/C)^2 + \beta_{2,Dv50}.PV + \beta_{3,Dv50}$	0.81	0.71
	$D_{v90} = \beta_{1,Dv90}.PV^2 + \beta_{2.Dv90}$	0.83	0.80

As shown in Table 4.1, the R^2 values obtained are between 0.63 and 0.83. Henseler *et al*. [21] classified values of 0.67, 0.33 and 0.19 of R^2 as substantial, moderate and weak, respectively, thus indicating that developed models adequately fit the experimental data. It was also observed that the introduction of quadratic terms allowed the improvement of the models, although these differences are small since the linear combinations already moderately described and captured the variance of experimental data. The different models that were obtained for Dv10, Dv50 and Dv90 can be explained by the following. As a first approach, the models of Dv10, Dv50 and Dv90 were developed using both H/C and PV as factors and, as aforementioned, the models were further optimized by eliminating the coefficients without statistical meaning (error of the estimated coefficient is higher than the value of the coefficient itself). Consequently, the obtained models for Dv10 and Dv50 both depend on H/C and PV, whereas, Dv90 model only depends on the PV since the coefficient estimated for H/C did not have statistical meaning.

Figure 4.3 shows the values of the predictors' regression coefficients of the optimized models. PSD parameters of the product were calculated and compared with the experimental values.

Regression coefficients	Experimental vs modelled
$D_{v10} = \beta_{1,Dv10}.(H/C)^2 + \beta_{2,Dv10}.PV + \beta_{3,Dv10}$	
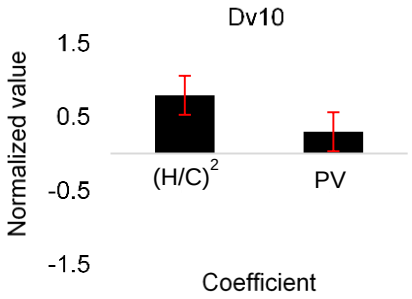	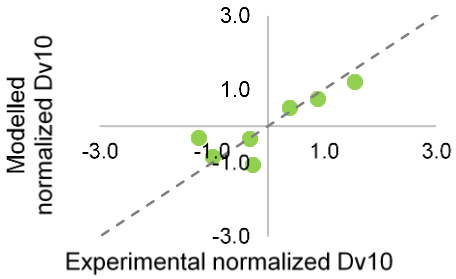
$D_{v50} = \beta_{1,Dv50}.(H/C)^2 + \beta_{2,Dv50}.PV + \beta_{3,Dv50}$	
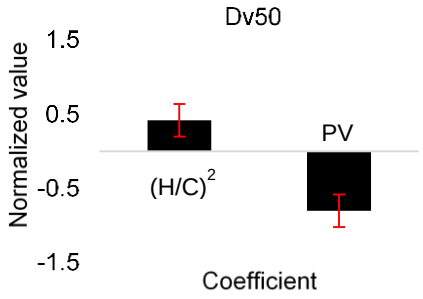	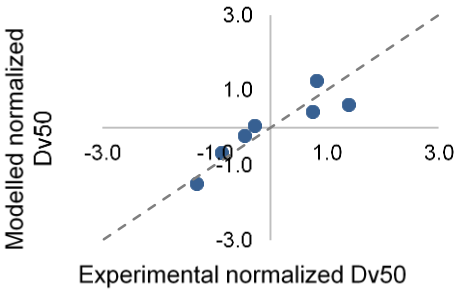
$D_{v90} = \beta_{1,Dv90}.(PV)^2 + \beta_{2,Dv90}$	
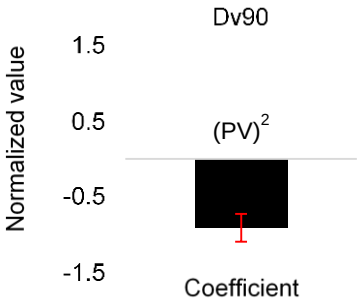	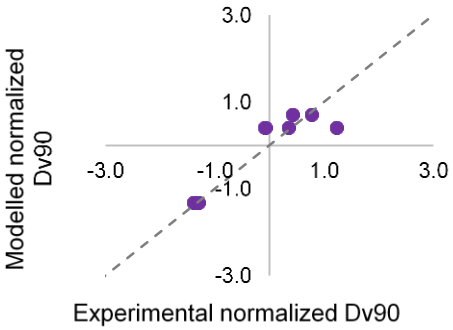

Figure 4.3. Regression coefficient values and respective standard deviation, for each output variable and the comparison between the modelled and experimental data.

Analyzing Figure 4.3, it can be observed that Dv10 and Dv50 are proportional to the H/C, which implies that the particle size is higher when the ratio H/C increases (narrow clearance, C). Since the API solution is added on the surface, supersaturation is higher on the surface of the anti-solvent solution (upper zone of the solution) and at high supersaturation, nucleation is more favored than growth and therefore, since growth is less dominant, the particles formed are smaller [22]. For instance, the results obtained for Dv50 indicate that, in order to obtain a larger Dv50, higher H/C (lower clearance) and lower PV should be applied during the crystallization. Experimentally, it was observed that at slower agitation and at narrow clearances, the product precipitated near the surface (upper region of the reactor), since

the supersaturation was not dissipated enough and therefore small-clustered particles seemed to be formed. As the laser diffraction method does not differentiate the clustered particles from the non-clustered ones, it can be assumed that higher Dv50 values were measured in these conditions. On the other hand, Dv90 seems to be only influenced by the PV applied. Dv90 is a parameter that represents large sized particles and thus, can be more sensitive to the agitation applied. As mentioned previously, higher agitation rates, besides narrowing the metastable zone width, promote collision among crystals, baffles and impeller, which therefore increases secondary nucleation and the formation of smaller particles [23]. At stronger agitation, larger particles have a higher chance to collide with the reactor's walls, probes and other particles, which can cause breakage and thus, a decrease in the Dv90. Therefore, PV seems to have more weight in the Dv90 than H/C, since high PV can promote high nucleation rates, which can lead to less formation of large particles, which translates into lower values of Dv90. Regarding the repeatability results performed for the center point conditions, coefficient of variation values of 15%, 12% and 11% were obtained for Dv10, Dv50 and Dv90 respectively, which indicate low variability among the experiments.

The leave-one-out method was used to study the predictability of the models, where a single experiment was successively left out and new models of Dv10, Dv50 and Dv90 were obtained from the remaining experimental points. The left out experimental point was used in the developed models to predict the value of Dv10, Dv50 and Dv90. These predicted values of Dv10, Dv50 and Dv90 were plotted against the experimental values in Figure 4.4.

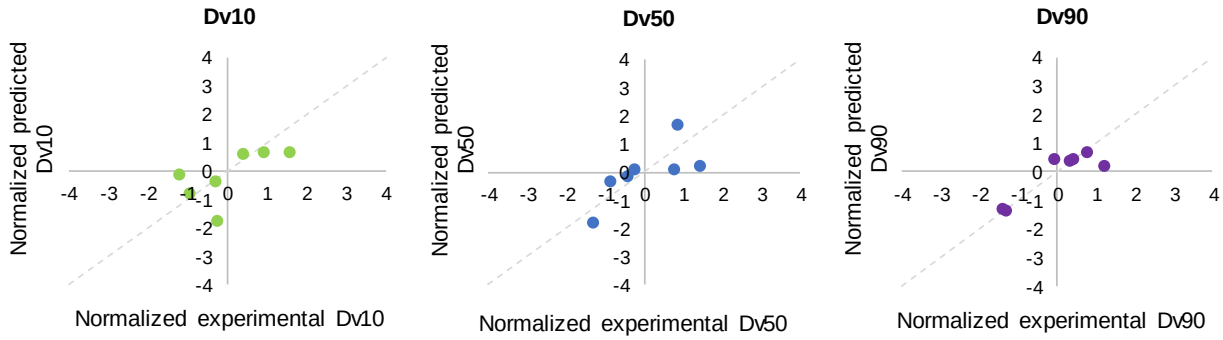

Figure 4.4. Comparison of the PSD parameters predicted by the leave-one-out method with the experimental PSD values.

The data presented in Figure 4.4 indicates that the Dv10, Dv50 and Dv90 values predicted by the leave-one-out method are quite similar to the experimental ones, since these show a linear tendency. This technique allows testing the model's ability to predict new data that was not used in the training set. Nevertheless, some variability can be observed in certain predictions since the chosen input variables do not fully predict the particle size. Additionally, the experimental variability found in the center point conditions might have also contributed to these observations.

4.4.2. Impact of nucleation rate on the PSD

The nucleation rate data obtained by the use of a FBRM probe was used to assess its impact on the particle size parameters (Figure 4.5).

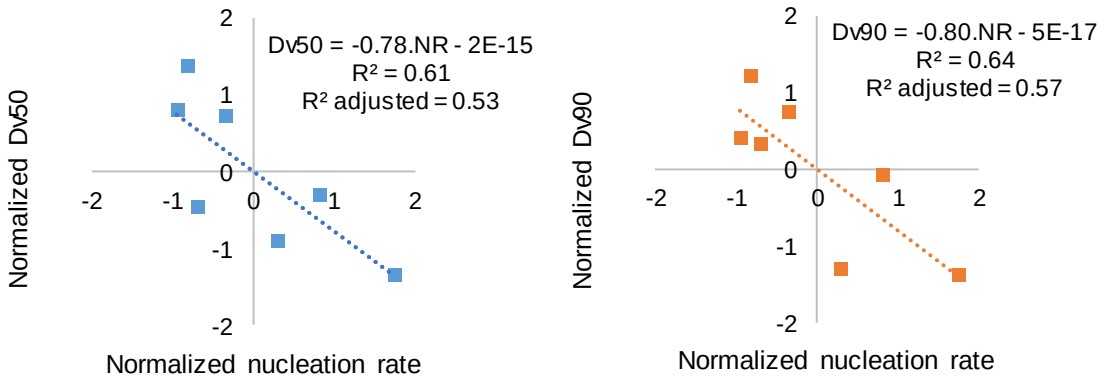

Figure 4.5. Relationship between normalized particle size parameters (Dv50 and Dv90) and normalized nucleation rate.

In Figure 4.5, the results regarding the impact of nucleation rate on the particle size parameter Dv10 were not presented, since no correlation was observed between the two variables, which implies that the nucleation rate does not seem to have any effect on fine particles (represented by Dv10) in this process. On the other hand, the nucleation rate seems to moderately influence the particle size parameters Dv50 and Dv90, since the fitting of the models to the experimental data, expressed by the R^2, were below 0.68 but higher than 0.33. The models indicate that the particle size parameters Dv50 and Dv90 decrease when the nucleation rate increases, as expected since higher nucleation rates indicate a low growth rate and as result, small-sized particles are formed. Moreover, collision among crystals, baffles and impeller occurs at high agitation, increasing secondary nucleation, which can lead to the formation of smaller crystals [23].

Microscope images of the dry API crystals were obtained by using Scanning Electron Microscopy (SEM) and are presented in Figure 4.6.

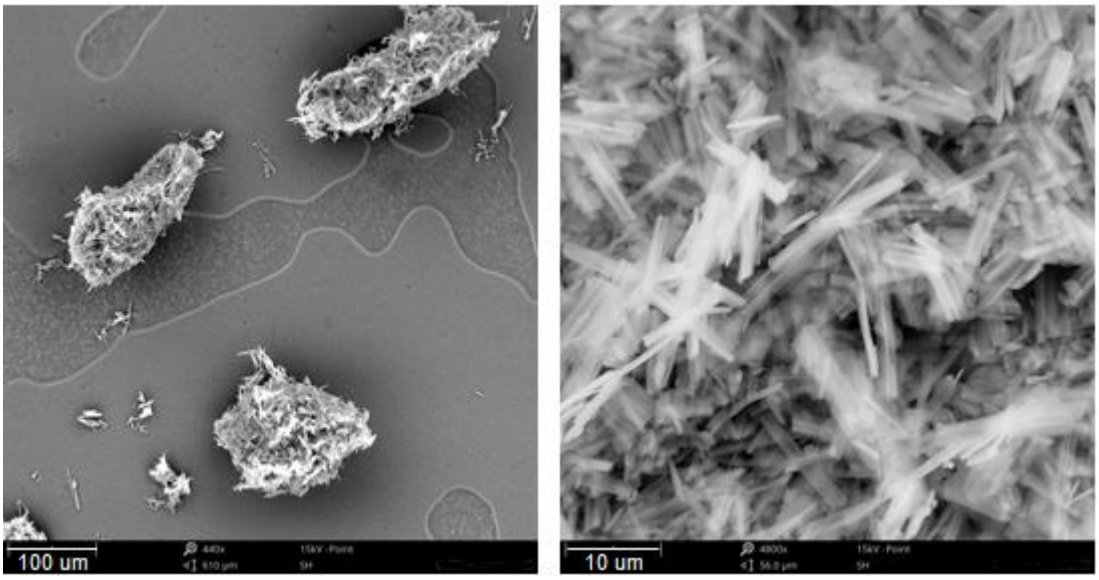

Figure 4.6. SEM images of the morphology of the API crystals obtained after drying (Zoom of 440x and 4800x, respectively).

Analyzing Figure 4.6, it can be seen that the dry crystals seem to be aggregates but no signs of agglomeration are observed. Since FBRM and laser diffraction are sensitive to particle shape, the lack of a more uniform or spherical shape requires caution. For instance, in presence of needle-shaped crystals, an increase in the number of small-sized particles can indicate an increase in the needle length, since the width of long needles has a higher probability of being intersected by the scanning laser beam [24]. Therefore, the measurements can also be influenced by particles' orientation inside the vessel. Hence, for a strict particle shape, in-line monitoring and certainty in the results, a PVM (Particle Vision and Measurement) probe could have provided some insight regarding the shape alterations throughout the process.

4.5. Conclusions

The aim of this study was to investigate the impact of H/C and PV on the PSD parameters (Dv10, Dv50 and Dv90) of an API obtained through an anti-solvent crystallization method.

Assessing the PSD parameters, it was detected that Dv10 and Dv50 are proportional to the H/C, which implies that the particle size is higher when the ratio H/C increases (narrow clearance, C). For instance, the results obtained for Dv50 indicate that, in order to obtain a larger Dv50, higher H/C (lower clearance) and lower PV should be applied during the crystallization. On the other hand, Dv90 seems to be only influenced by the PV applied.

It was found that the nucleation rate seems to moderately influence the particle size parameters Dv50 and Dv90. The models indicated that the particle size parameters Dv50 and Dv90 decrease when the nucleation rate increases, as expected, since higher nucleation rates indicate a low growth rate and

as result, small sized particles are formed. Moreover, collision among crystals, baffles and impeller occur at high agitation, increasing secondary nucleation, which can lead to the formation of smaller crystals

This study indicates that parameters such as clearance and agitation can affect the particle size of the product and therefore these should be investigated during the development phase of anti-solvent crystallization processes.

References

[1] Z. Q. Yu, P. S. Chow, and R. B. H. Tan, “Application of Attenuated Total Reflectance - Fourier Transform Infrared (ATR - FTIR) Technique in the Monitoring and Control of Anti-solvent Crystallization,” *Ind. Eng. Chem. Res.*, vol. 45, pp. 438–444, 2006.

[2] W. Beckmann, *Crystallization: Basic Concepts and Industrial Applications*. Weinheim; Germany: Wiley-VCH, 2013.

[3] X. Y. Woo, R. B. H. Tan, P. S. Chow, and R. D. Braatz, “Simulation of mixing effects in antisolvent crystallization using a coupled CFD-PDF-PBE approach,” *Cryst. Growth Des.*, vol. 6, no. 6, pp. 1291–1303, 2006.

[4] A. N. Saleemi, C. D. Rielly, and Z. K. Nagy, “Comparative investigation of supersaturation and automated direct nucleation control of crystal size distributions using ATR-UV/vis spectroscopy and FBRM,” *Cryst. Growth Des.*, vol. 12, no. 4, pp. 1792–1807, 2012.

[5] H. Grön, A. Borissova, and K. J. Roberts, “In-Process ATR-FTIR Spectroscopy for Closed-Loop Supersaturation Control of a Batch Crystallizer Producing Monosodium Glutamate Crystals of Defined Size,” *Ind. Eng. Chem. Res.*, vol. 42, pp. 198–206, 2003.

[6] A. S. Myerson, *Handbook of Industrial Crystallization*, 2nd ed., no. October. Elsevier Science & Technology Books, 2001.

[7] S. K. Jha, S. Karthika, and T. K. Radhakrishnan, “Modelling and control of crystallization process,” *Resour. Technol.*, vol. 3, no. 1, pp. 94–100, 2017.

[8] M. R. Abu Bakar, Z. K. Nagy, A. N. Saleemi, and C. D. Rielly, “The Impact of Direct Nucleation Control on Crystal Size Distribution in Pharmaceutical Crystallization Processes,” *Cryst. Growth Des.*, vol. 9, no. 3, pp. 1378–1384, 2009.

[9] X. Fu *et al.*, “Effect of Mixing on the Particle Size Distribution of Paracetamol Continuous Cooling Crystallization Products Using a Computational Fluid Dynamics–Population Balance Equation Simulation,” *Cryst. Growth Des.*, vol. 18, no. 5, pp. 2851–2863, 2018.

[10] A. Kaćunić, M. Ćosić, D. Rušić, and N. Kuzmanić, “Effect of impeller off-bottom clearance on crystal growth kinetics of borax in dual-impeller batch cooling crystallizer,” *Chem. Eng. Trans.*, vol. 57, pp. 787–792, 2017.

[11] K. Shimizu, H. Nagasawa, and K. Takahasi, “Effect of off-bottom clearance of a turbine type impeller on crystal size distribution of aluminum potassium sulfate in a batch crystallizer,” *J. Cryst. Growth*, vol. 154, pp. 113–117, 1995.

[12] J. Liu, M. Svärd, and Å. C. Rasmuson, “Influence of Agitation on Primary Nucleation in Stirred

Tank Crystallizers," *Cryst. Growth Des.*, vol. 15, no. 9, pp. 4177–4184, 2015.

[13] L. X. Yu, "Quality by design (QbD): Product and Process Development, Understanding, and Control," *Pharm. Res.*, vol. 25, no. 4, pp. 781–791, 2008.

[14] M. Fujiwara, Z. K. Nagy, J. W. Chew, and R. D. Braatz, "First-principles and direct design approaches for the control of pharmaceutical crystallization," *J. Process Control*, vol. 15, no. 5, pp. 493–504, 2005.

[15] F. X. McConville, *The Pilot Plant Real Book: A Unique Handbook for the Chemical Process Industry*. FXM Engineering and Design, 2002.

[16] H. G. Brittain, *Polymorphism in pharmaceutical solids*, 2nd ed., vol. 192. USA: Informa Healthcare, 2009.

[17] C. Levoguer, "Using laser diffraction to measure particle size and distribution," *Met. Powder Rep.*, vol. 68, no. 3, pp. 15–18, 2013.

[18] S. Pawlowski, C. F. Galinha, J. G. Crespo, and S. Velizarov, "Prediction of reverse electrodialysis performance by inclusion of 2D fluorescence spectroscopy data into multivariate statistical models," *Sep. Purif. Technol.*, vol. 150, pp. 159–169, 2015.

[19] M. S. Reis, "Engenharia de Processos e Sistemas Modelação matemática de base estatística/empírica: Construção de modelos empíricos usando metodologias de regressão linear," 2017.

[20] A. Tulcidas, S. Nascimento, B. Santos, C. Alvarez, S. Pawlowski, and F. Rocha, "Statistical methodology for scale-up of an anti-solvent crystallization process in the pharmaceutical industry," *Sep. Purif. Technol.*, vol. 213, no. December 2018, pp. 56–62, 2019.

[21] J. Henseler, C. M. Ringle, and R. R. Sinkovics, "The Use of Partial Least Squares Path Modeling in International Marketing," *Adv. Int. Mark.*, vol. 20, pp. 277–320, 2009.

[22] J. Bałdyga, "Mixing and fluid dynamics effects in particle precipitation processes," *KONA Powder Part. J.*, vol. 2016, no. 33, pp. 127–149, 2016.

[23] D. O'Grady, M. Barrett, E. Casey, and B. Glennon, "The Effect of Mixing on the Metastable Zone Width and Nucleation Kinetics in the Anti-Solvent Crystallization of Benzoic Acid," *Chem. Eng. Res. Des.*, vol. 85, no. 7, pp. 945–952, 2007.

[24] T. Leyssens, C. Baudry, and M. L. E. Hernandez, "Optimization of a Crystallization by Online FBRM Analysis of Needle-Shaped Crystals," *Org. Process Res. Dev.*, vol. 15, no. 2, pp. 413–426, 2011.

Chapter 5 Statistical methodology for scale-up of an anti-solvent crystallization of an API[3]

[3] This work was published in:

A. Tulcidas, S. Nascimento, B. Santos, C. Alvarez, S. Pawlowski and F. Rocha, "Statistical methodology for scale-up of an anti-solvent crystallization process in the pharmaceutical industry", Separation and Purification Technology, vol. 213, pp. 56 - 62, 2019.

5.1. Scope

The scale-up of crystallization processes is a challenging step in the production of active pharmaceutical ingredients (APIs). When moving from the lab to industrial scale, the mixing conditions tend to modify due to the different geometry and agitation performance, which is particularly important in anti-solvent crystallization where the size of the crystals depends on the mixing and incorporation of the anti-solvent in the solution. The main aim of this study was to further understand the impact of the volume of the mixture occupied in the reactor (%Volume) and mixing parameters such as power per volume (PV) and tip speed (TS), on the particle size of the product and use statistical modeling for a successful scale-up. For this purpose, a scale-down of the production reactor was performed to conduct these studies in a laboratory reactor. The percentage of the volume occupied by the mixture in the reactor was varied during the crystallization to simulate different batch sizes along with the stirring speed and the final particle size of the product was measured. Power per volume and tip speed were maintained constant between the production and lab scales. The results obtained in anti-solvent lab-scale crystallization experiments were used to develop multivariate statistical models predicting Particle Size Distribution (PSD) parameters (Dv10, Dv50 and Dv90) in function of predictors such as percentage of volume, power per volume and tip speed. Firstly, the collinearity among the predictors was assessed using Variance Inflation Factor (VIF) diagnosis. Subsequently, the least squares method was employed to find correlations among the predictors and output variables. The optimization of the models was executed by testing quadratic, logarithmic and square root terms of the predictors and removing the least statistically significant regression coefficient. The quality of the fitting was evaluated in terms of adjusted R^2 (R^2_{adj}).

The modelled Dv10, Dv50 and Dv90 values presented a good fitting to the experimental data, with R^2_{adj} higher than 0.79, either when using power per volume or tip speed along with the percentage of volume as predictors. Afterwards, the particle size distribution parameters of industrial scale production were predicted using the previously developed models. The deviations between predicted and experimental values were lower than 17%. This demonstrates that the statistical models developed in lab-scale conditions can be successfully used to predict particle

size distribution in industrial-size vessels.

5.2. Introduction

The anti-solvent technique is a popular crystallization method employed in the pharmaceutical industry [1]. It is mostly employed when the solubility of the product does not vary significantly with the temperature and it is advantageous for the processing of heat-sensitive substances since it is generally operated at room temperature without additional heating or cooling [2]. However, the scale-up of anti-solvent crystallization process is extremely challenging, since the size of the crystals depends on the mixing conditions and an uniform incorporation of the anti-solvent in the solution [1, 3], as well as the detailed mixing behavior of an industrial-scale full-scale crystallizer cannot be accurately captured with a geometrically similar laboratory-scale experimental model [3]. Laboratory vessels allow significant surface area for heat transfer and approximate well to “perfectly mixed” conditions for mass transfer. As the scale increases, the surface area to volume ratio decreases and gradients of temperature and/or concentration become more significant [4]. Additionally, at larger scales, the power applied to stir the mixture might not be sufficient to achieve homogeneity or it can be too high and cause particle breakage [5]. Consequently, the particle size and the suspension properties are scale dependable, which implies that application in different scales of similar mixing operational conditions, such as stirring speed, might lead to the production of a product out of adequate specification range. Thus, robust methodologies to achieve a successful scale-up of anti-solvent crystallization processes are needed.

Statistical modeling can be used to establish correlations between parameters by using functions to associate the predictor variables with the response variables. Statistical modeling allows to predict processes’ performance, as well as to disclose unobvious relations between parameters, thus to gain additional knowledge and information about processes’ behavior [6]. Different tools and methods, such as Multiple Linear Regression (MLR), Projection to Latent Structures (PLS) or Artificial Neural Networks (ANN), can be used to achieve such purposes [7-10]. In pharmaceutical industry, the typical variables which may influence the in-process materials or final drug product quality (*e.g*. particle size distribution of the crystals) are the material attributes (*e.g*. particle size of the raw material) and the operational parameters such as for example agitation (*e.g*. stirring speed, tip speed, power per volume, etc.) [11].

The main aim of this study is to develop robust multivariate statistical models, which correlate the percentage of the volume occupied by the suspension in the reactor, power per volume and tip speed in order to predict the PSD obtained in an industrial size vessel. A statistical methodology was proposed and the data obtained in scale-down experiments were used to develop statistical models by MLR. Afterwards, the developed models were successfully validated in an industrial scale.

5.3. Materials and experimental procedure

The experimental data used to develop the herein presented statistical models, are based on a study where the impact of the mixing operational conditions on the particle size of the final product was assessed in the lab-scale. The nature of API, as well as used reagents, cannot be disclosed due to confidentiality purposes. Thus, when pertinent, the experimental data were normalized. Nevertheless, the description of the herein proposed statistical methodology for the scale-up of an anti-solvent crystallization process is given with full details.

5.3.1. Anti-solvent crystallization procedure

The anti-solvent crystallization process studies in the lab-scale were done based on a scale-down of the existent plant scale's reactor. The laboratory reactor's features, such as internal diameter, impeller diameter, baffle diameter, vessel bottom to impeller distance and height of reaction mixture were 1/5 of the industrial reactor's characteristics. In addition, the geometric proportions of the reactor were maintained as much similar as possible: the ratio between the reactor internal diameter and impeller diameter (0.66) and the ratio between the height of reaction mixture and internal diameter of reactor (0.46, 0.66 and 0.86, for three different studied batch sizes) were maintained constant between scales. A three-blade retreat curve impeller was employed, which is similar to the one used in the plant reactor. The selected scale-up factors were power per volume (PV in $W \cdot m^{-3}$) and the stirrer' tip speed ($m \cdot s^{-1}$), which were maintained constant between both lab and production scales by adjusting the stirring speed of the stirrer at laboratory scale. PV and tip speed were calculated as follows:

$$PV = \frac{P_0 \, \rho \, N^3 D^5}{V} \tag{5.1}$$

$$Tip\ speed = \pi DN \tag{5.2}$$

where P_0 is the power number which is dependent on the type of agitator [12], ρ is the density of the solution in $kg \cdot m^{-3}$, N the stirring speed in s^{-1}, D the diameter of the impeller in m and V the volume of the solution in m^3.

In the lab-scale study, a 2 L glass reactor was used and the crystallization was performed in semi-batch mode. Three batch sizes (34.4 g, 49.2 g and 64.0 g) were used to mimic the fraction of filling volume of the industrial reactor and the percentage of the volume was varied along with different stirring speed according to the conditions defined (Figure 5.1). The API solution and the anti-solvent were slowly mixed while the temperature was maintained constant (near room

temperature). Afterwards, the slurry was kept under agitation and cooled to increase the yield. Finally, the slurry was filtrated and dried under vacuum to obtain the final product. Each experiment lasted approximately two hours.

The PSD parameters of the final product, such as Dv10, Dv50 and Dv90 were determined through a laser diffraction method [13].

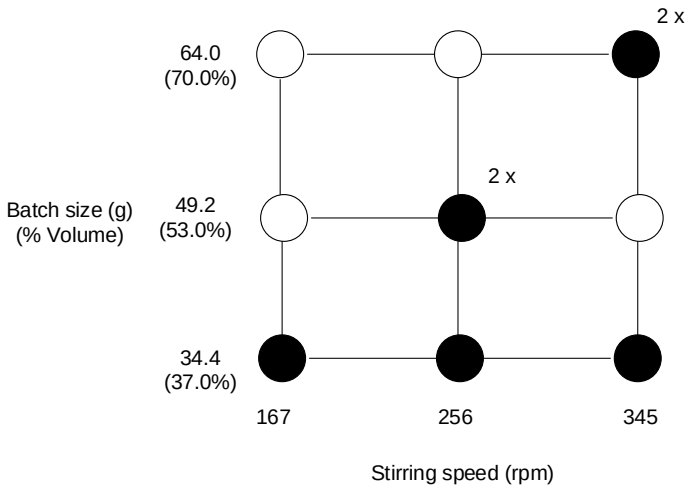

Figure 5.1. Experimental conditions used during the anti-solvent crystallization experiments at lab-scale.

As depicted in Figure 5.1, five different conditions were used, but two of the experimental points (center point and point with %volume of 70% and stirring speed of 375 rpm) were performed in duplicate and therefore, a total number of seven experiments were carried out.

5.3.2. Models' development

All the input and output variables were normalized, by subtracting the average value of the experimental data acquired for each variable and dividing by the respective standard deviation. This procedure eliminates the influence of the variables' units on the models' regression coefficients values and enables to compare the weight of each variable on processes performance [14]–[16].

Collinearity assessment

In order to evaluate if collinearity between possible variables to be included in a model might be an issue, methods such as Condition Indices (CI) and Variance Inflation Factor (VIF) analysis can be employed [17]. In this study the Variance Inflation Factors (VIF) were calculated. Hair *et al.* [18] state that if the VIF values are above 10, collinearity is a problem, whereas Kline

[19] proposes a threshold of five. In the present study, an upper limit of five was considered as a stricter scenario and therefore predictors presenting VIF values above this limit were discarded and were not included in the model.

The VIF values were calculated as follows:

$$VIF_i = \frac{1}{1 - R_i^2} \tag{5.3}$$

where R_i^2 is the coefficient of determination obtained when plotting a predictor X_i against the remaining predictors [20]. When the variation of a predictor is largely explained by a linear combination of the other predictors, the coefficient of determination is closer to one, and the VIF for that predictor is correspondingly large. The inflation is measured relative to an R^2 of zero (no collinearity), and a VIF of one. Alternatively, VIFs are also the diagonal elements of the inverse of the correlation matrix [17]. In this study, the latter method was implemented in MATLAB and used to calculate VIFs.

Data modeling

The method used to obtain the statistical models is described in chapter 4.3.2.

Model validation

A model's predictive capacity should be always tested on an independent dataset that was not used for the model training [21]. In this study, the validation sets consisted of different batches manufactured in the production scale:

- 1st validation set: percentage of volume, power per volume and tip speed used in the production scale are within the model calibration range;
- 2nd validation set: percentage of volume and tip speed used in the production scale are within the model calibration range;
- 3rd validation set: only tip speed used in the production scale is within the model calibration range;

Table 5.1 summarizes the operational percentage of volume, power per volume and tip speed conditions used in each validation set.

Table 5.1 - %Volume, power per volume and tip speed conditions from the production batches used to validate the models. ✓- within the calibration range; ✗- outside the calibration range.

Validation	Batch	%Volume	Power per volume ($W \cdot m^{-3}$)	Tip speed ($m \cdot s^{-1}$)
1st Validation	1 2	36.9 ✓	43.0 ✓	1.71 ✓
2nd Validation	3	44.6 ✓	39.0 ✗	1.48 ✓
3rd Validation	4	72.2 ✗	37.0 ✗	1.71 ✓

Although the models predicting PSD parameters were calibrated in a certain range, thus they are expected to be valid only in that range, the validity of the models was also tested outside the calibration range limits, as shown in Table 5.1. The confidence limits for the predictions were calculated as two times the standard deviation of the experimental particle size distribution data. If the estimated values of the validation set are within these upper and lower limits, the model can be considered valid [22]. Additionally, the deviations obtained between observed and predicted particle size distribution parameters' values were quantified by using the following equation:

$$\%Deviation = \frac{Y_{predicted} - Y_{observed}}{Y_{predicted}} \times 100 \quad (5.4)$$

Figure 5.2 depicts the global statistical methodology applied to develop the models correlating the mixing parameters with the particle size distribution of the API.

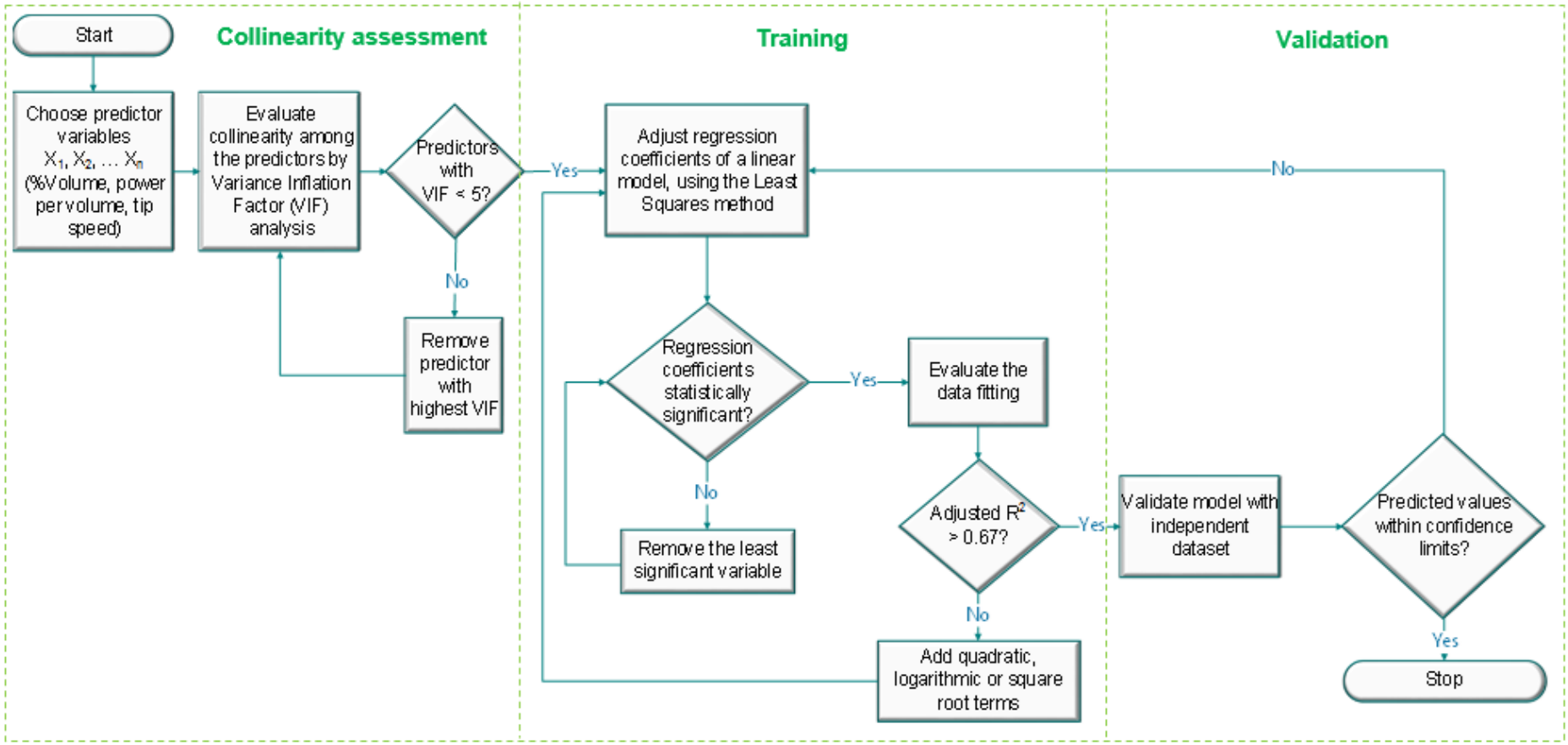

Figure 5.2. Statistical methodology employed to develop statistical models and evaluate the influence of the mixing conditions on the particle size distribution parameters.

5.4. Results and discussion

5.4.1. Collinearity assessment

The VIFs values for each possible predictor' set to be potentially used in the models are presented in Table 5.2.

Table 5.2 - VIF values obtained for each of the predictor variables when regressing them against each other.

Predictor	%Volume	Power per volume	Tip speed
	8	16	25
VIF	1	1	-
	2	-	2

Analyzing the VIF values obtained, it is possible to conclude that it is not adequate to propose a model in which predictors such as percentage of volume, power per volume and tip speed are simultaneously incorporated since their values are above the threshold of five. These results were expected, since both tip speed and power per volume depend on stirring speed, which implies that these are not independent variables. Only independent variables (VIF values below five) should be included in a model. Thus, two sets of predictors were used in the models to predict the response variables Dv10, Dv50 and Dv90:

a) Percentage of volume (%Vol) and power per volume (PV)
b) Percentage of volume (%Vol) and tip speed (TS).

5.4.2. MLR modelling

The models were developed first using only simple linear combinations of the predictors. Then, to improve the values of the R^2_{adj} and thus, the variability explained by the models, the introduction of quadratic, logarithmic and squared root terms was evaluated. The models were further optimized by eliminating the coefficients without statistical meaning. Since PSD measurements were obtained off-line, the developed statistical models predict PSD of the final product and the dynamic behavior during the crystallization has not been studied. Table 5.3 shows the models with the highest R^2_{adj} values.

Table 5.3 – Adjusted R^2 of the simple linear and with interaction parameters (optimized) models.

Predictors		Model	Adjusted R^2
a) %Vol + PV	Linear	$D_{v10} = Coef_{1,Dv10}\%Vol + Coef_{2,Dv10}PV$	0.85
		$D_{v50} = Coef_{1,Dv50}PV$	0.85
		$D_{v90} = Coef_{1,Dv90}PV$	0.88
	Interaction	$D_{v10} = Coef_{1,Dv10}\%Vol^2 + Coef_{2,Dv10}PV$	0.87
		$D_{v50} = Coef_{1,Dv50}PV^2$	0.87
		$D_{v90} = Coef_{1,Dv90}PV^2$	0.91
b) %Vol + TS	Linear	$D_{v10} = Coef_{1,Dv10}\%Vol + Coef_{2,Dv10}TS$	0.83
		$D_{v50} = Coef_{1,Dv50}\%Vol + Coef_{2,Dv50}TS$	0.79
		$D_{v90} = Coef_{1,Dv90}\%Vol + Coef_{2,Dv90}TS$	0.83
	Interaction	$D_{v10} = Coef_{1,Dv10}\%Vol^2 + Coef_{2,Dv10}TS$	0.86
		$D_{v50} = Coef_{1,Dv50}\%Vol^2 + Coef_{2,Dv50}TS$	0.82
		$D_{v90} = Coef_{1,Dv90}\%Vol + Coef_{2,Dv90}\sqrt{TS}$	0.86

As shown in Table 5.3, the R^2_{adj} values were between 0.79 and 0.91. Henseler *et al*. [23] classified values of 0.67, 0.33 and 0.19 of R^2 as substantial, moderate and weak, respectively, thus it indicates that developed models adequately fit the experimental data. It was also observed that introduction of quadratic terms (in comparison to the introduction of logarithmic or square root terms) allowed for the highest improvement of the models, although these differences are small since the linear combinations already strongly described and captured the variance of experimental data. The probability of whether the observed relationship between the variables occurred by chance was determined for the optimized Dv10, Dv50 and Dv90 models. This probability was calculated using the FDIST function in Excel, using the F-value provided by LINEST, the number of data points *n* and the degree of freedom: v_1 = n – degree of freedom obtained by LINEST – 1 and v_2 = degree of freedom obtained by LINEST. The probability values obtained were low: 0.003, 0.001 and 0.0005 for the %volume and PV set and 0.004, 0.007 and 0.004 for the %volume and TS set, respectively, which indicates that there is no random relation between the variables.

Figure 5.3 shows the values of the predictors‘ regression coefficients of the optimized models.

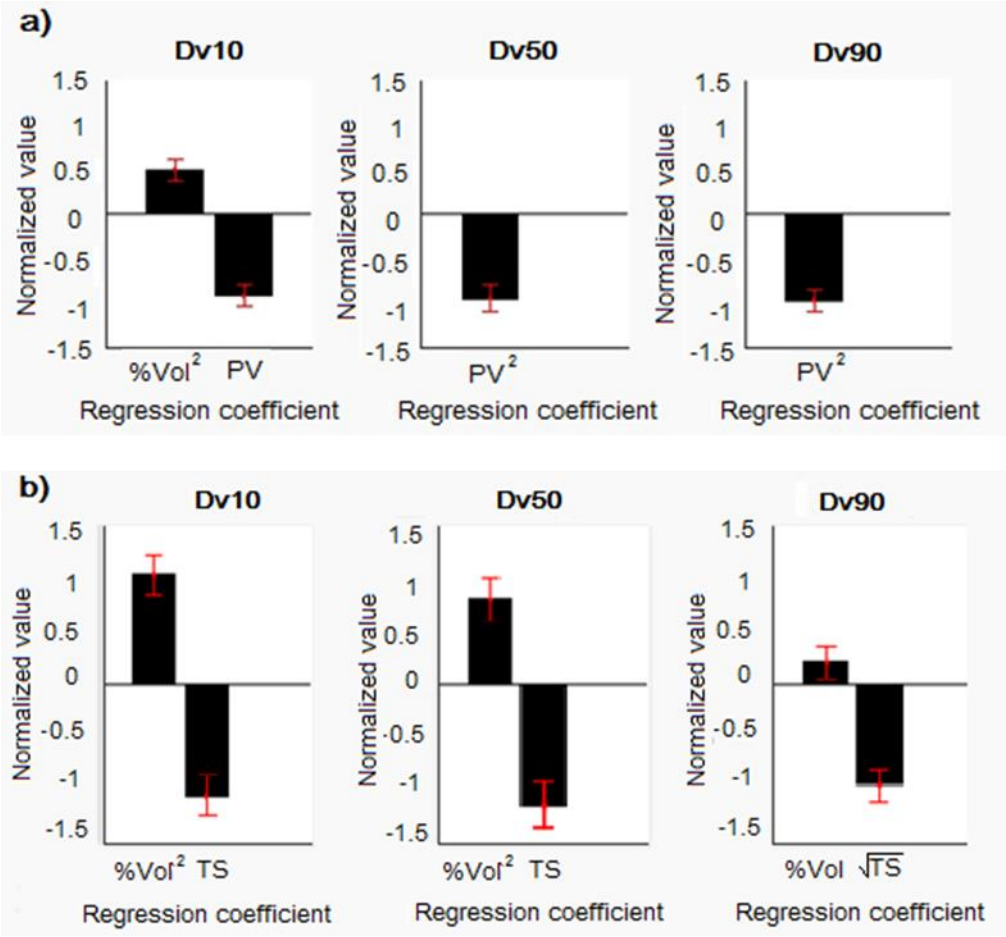

Figure 5.3. Predictors' regression coefficients, and their respective errors, of models predicting PSD parameters (Dv10, Dv50 and Dv90). The predictors' sets were a) %volume and power per volume (PV); b) %volume and tip speed (TS), respectively.

The standard deviation values of the regression coefficients are minor, which shows that the developed models are robust. The regression coefficients' values indicate that the particle size distribution parameters decrease when the mixing parameters power per volume and tip speed increase. In addition, this behavior is expected when the API solution is added into the anti-solvent instead of adding the anti-solvent into the API solution since this procedure promotes the formation of small crystals [24]. Furthermore, an increase in agitation intensity can result in a narrower metastable zone width, due to the increased shear forces and high probability of contact between solute molecules, which promotes nucleation [25]. Increasing the tip speed or the power per volume does seem to maximize this effect. Thus, these results enhance the importance of studying mixing parameters in anti-solvent crystallization to control the particle size of the API.

5.4.3. Models validation

The validation set was based on batches manufactured in the production scale. Some of the validation points (represented by hollow symbols in Figure 5.4) were obtained in conditions out of the models' calibration range, but were also taken into consideration to broaden the analysis performed herein. Figure 5.4 shows the fitting of the optimized models, predicting PSD parameters, for both calibration and validation sets.

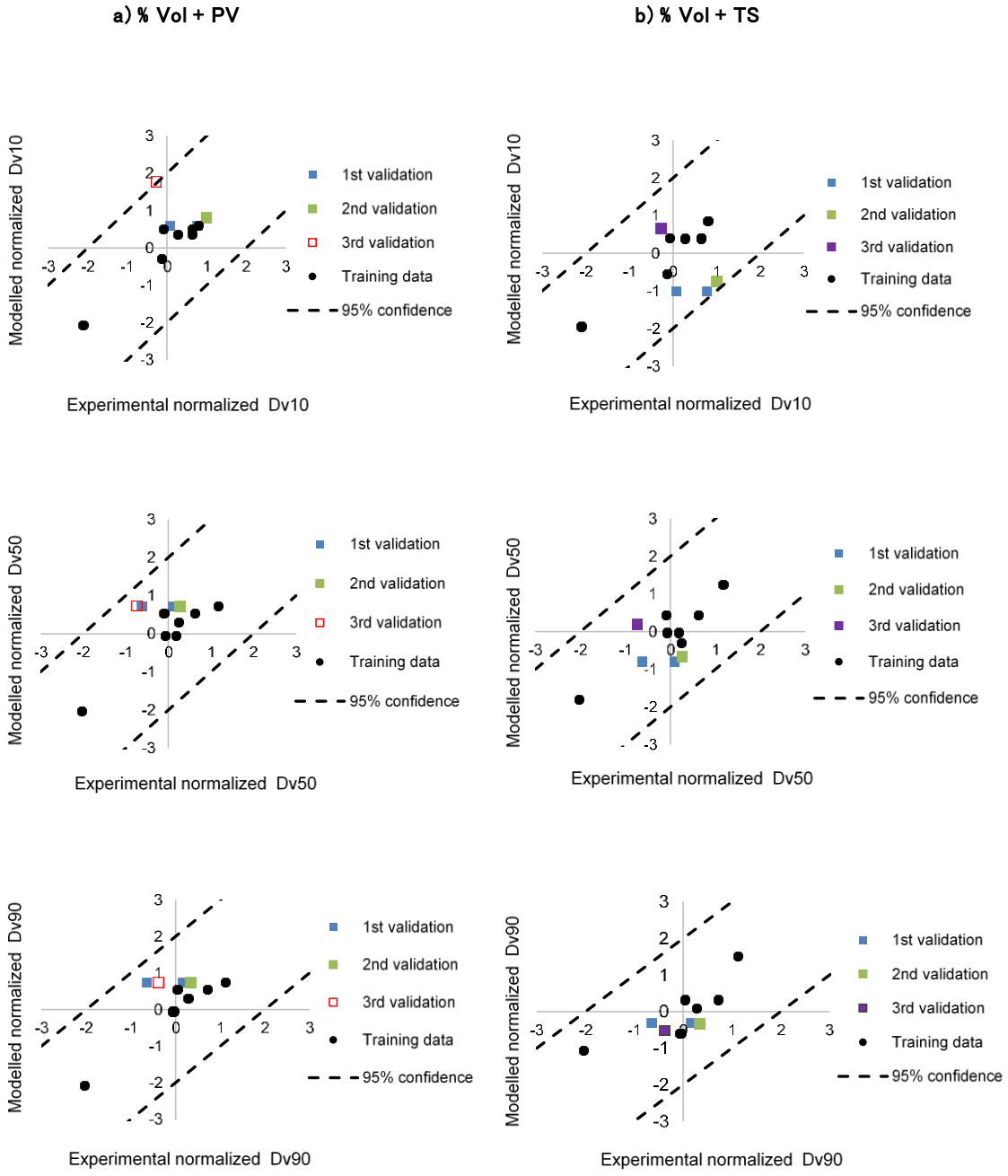

Figure 5.4. Training data, validation points and confidence limits of the optimized models with different predictors: a) %volume and PV; b) %volume and TS. Hollow symbols – conditions out of the calibration range.

By analyzing Figure 5.4, it is possible to see that the predictive ability of the models was successfully validated. All validation points obtained in conditions within models' calibration range are within the confidence limits. Additionally, even the points obtained out of the calibration range conditions, were also well predicted, thus showing strong models' robustness. Obviously, any model should only be used to predict process performance if the values of potential predictors are within the model's calibration range. Thus, for example, and as expected, the prediction of Dv10 parameter in the 3rd validation set for power per volume model was out of the confidence limits, since, most probably, the experimental conditions (and/or their combination) were too different from conditions used to develop the models. Table 5.4 presents the values of deviations (Equation 5.4) between observed and predicted particle size distribution parameters of the validation sets.

Table 5.4 – Deviation values obtained for the particle size distribution parameters obtained experimentally in the production batches (industrial-scale) and estimated by the models developed based on lab-scale results.

Predictors	Set	Batch	Dv10	Dv50	Dv90
a) %Vol + PV	1st Validation	1	4.49 %	11.93 %	13.42 %
		2	1.25 %	5.60 %	5.73 %
	2nd Validation	3	1.33 %	4.22 %	4.10 %
	3rd Validation	4	15.51 %	13.01 %	11.02 %
b) %Vol + TS	1st Validation	1	10.16 %	1.54 %	3.71 %
		2	16.77 %	8.83 %	4.85 %
	2nd Validation	3	16.05 %	8.87 %	6.97 %
	3rd Validation	4	7.89 %	8.82 %	1.26 %

Deviations values resumed in Table 5.4 confirm that the predicted values of Dv10, Dv50 and Dv90 parameters are similar to those obtained in the production scale. For the validation points, which are within models' calibration range, these deviations are lower than 16% and 17% for models with a) %volume and power per volume and b) %volume and tip speed, used as the predictors, respectively.

Nevertheless, for example, although batch 3 does not have the power per volume within the calibration range, the particle size values predicted by models depending on %volume and power per volume, were also still similar to the ones effectively obtained. Similarly, in the case of batch 4, the

particle size obtained is analogous to the ones predicted, despite of experimental %volume being out of the models' calibration range.

5.5. Conclusions

The main aim of this study was to further understand the impact of the volume of the mixture occupied in the reactor and mixing parameters such as power per volume and tip speed, on the particle size of the product and use statistical modelling for a successful scale-up.

Relations among percentage of volume, power per volume, tip speed and particle size distribution parameters were found. It was concluded that the regression coefficients' values indicate that the particle size distribution parameters decrease when the mixing parameters power per volume and tip speed increase. In addition, this behavior was expected when API solution is added into the anti-solvent instead of adding the anti-solvent into the API solution, since this procedure promotes the formation of small crystals. Thus, these results enhance the importance of mixing parameters in anti-solvent crystallizations to control the particle size of the API.

Regarding the model validation, since the main goal was to check if the models obtained at laboratory scale could aid in the prediction of operating conditions at production scale, the validation set used consisted of six batches manufactured in the production. The majority of the models fed with percentage of volume and power per volume were validated successfully within the calibration range. For the models built with percentage of volume and tip speed, the validation was also successful when using the predictors within the calibration range. It was possible to confirm that the Dv10, Dv50 and Dv90 estimated by the model built with percentage of volume and power per volume and the particle size distribution results obtained by the production were similar, with deviation values up to 16%. Regarding the model built with percentage of volume and tip speed, the deviation values obtained were up to 17%.

As final remarks, these results evidence the importance of performing scale-down experiments, develop statistical models for particle size parameters and predict these in the production scale, as long as the predictors such as power per volume and tip speed are maintained constant between scales. Furthermore, this type of statistical study can also help minimize the financial loss caused by issues induced by product with out of specification particle size distribution at scale-up.

References

[1] M. Barrett, D. O'Grady, E. Casey, and B. Glennon, "The role of meso-mixing in anti-solvent crystallization processes," *Chem. Eng. Sci.*, vol. 66, no. 12, pp. 2523–2534, 2011.

[2] J. Cho, J. K. Cho, J. Lee, D. Lee, C. Park, and S. Kim, "Optimization of salting-out crystallization for an efficient in situ separation of synthetic anthraquinone- and azo-type reactive dyes," *Sep. Purif. Technol.*, vol. 68, no. 2, pp. 138–144, 2009.

[3] X. Y. Woo, R. B. H. Tan, P. S. Chow, and R. D. Braatz, "Simulation of mixing effects in antisolvent

crystallization using a coupled CFD-PDF-PBE approach," *Cryst. Growth Des.*, vol. 6, no. 6, pp. 1291–1303, 2006.

[4] H. Y. Wei, "Computer-aided design and scale-up of crystallization processes: Integrating approaches and case studies," *Chem. Eng. Res. Des.*, vol. 88, no. 10, pp. 1377–1380, 2010.

[5] A. S. Myerson, *Handbook of Industrial Crystallization*, 2nd ed., no. October. Elsevier Science & Technology Books, 2001.

[6] L. Breiman, "Statistical Modeling: The Two Cultures," *Stat. Sci.*, vol. 16, no. 3, pp. 199–231, 2001.

[7] M. S. Reis, "Engenharia de Processos e Sistemas Modelação matemática de base estatística/empírica: Construção de modelos empíricos usando metodologias de regressão linear," 2017.

[8] E. C. Alexopoulos, "Introduction to multivariate regression analysis.," *Hippokratia*, vol. 14, no. Suppl 1, pp. 23–8, 2010.

[9] P. Dhillon, Y. Lu, D. P. Foster, and L. H. Ungar, "New Subsampling Algorithms for Fast Least Squares Regression," *Adv. Neural Inf. Process. Syst.*, pp. 1–9, 2013.

[10] J. O. Rawlings, S. G. Pantula, and D. A. Dickey, *Applied Regression Analysis: A Research Tool*, 2nd Editio. New York, 1998.

[11] L. X. Yu *et al.*, "Understanding Pharmaceutical Quality by Design," *AAPS J.*, vol. 16, no. 4, pp. 771–783, 2014.

[12] F. X. McConville, *The Pilot Plant Real Book: A Unique Handbook for the Chemical Process Industry*. FXM Engineering and Design, 2002.

[13] C. Levoguer, "Using laser diffraction to measure particle size and distribution," *Met. Powder Rep.*, vol. 68, no. 3, pp. 15–18, 2013.

[14] S. Sanches, C. F. Galinha, M. T. Barreto Crespo, V. J. Pereira, and J. G. Crespo, "Assessment of phenomena underlying the removal of micropollutants during water treatment by nanofiltration using multivariate statistical analysis," *Sep. Purif. Technol.*, vol. 118, pp. 377–386, 2013.

[15] S. Pawlowski, C. F. Galinha, J. G. Crespo, and S. Velizarov, "Prediction of reverse electrodialysis performance by inclusion of 2D fluorescence spectroscopy data into multivariate statistical models," *Sep. Purif. Technol.*, vol. 150, pp. 159–169, 2015.

[16] B. Santos, C. F. Galinha, J. G. Crespo, M. A. Santos, and S. Velizarov, "Prediction of polar oil and grease contamination levels in refinery wastewater through multivariate statistical modeling," *Sep. Purif. Technol.*, vol. 119, pp. 51–57, 2013.

[17] C. F. Mela and P. K. Kopalle, "The impact of collinearity on regression analysis: The asymmetric effect of negative and positive correlations," *Appl. Econ.*, vol. 34, no. 6, pp. 667–677, 2002.

[18] J. F. Hair Jr, W. C. Black, B. J. Babin, and R. E. Anderson, *Multivariate Data Analysis*, 7th ed. Pearson, 2010.

[19] R. B. Kline, *Principles and Practice of Structural Equation Modeling*. New York: Guilford Press, 1998.

[20] D. A. Belsley, E. Kuh, and R. E. Welsch, *Regression Diagnostics - Identifying Influential Data and Sources of Collinearity*. New Jersey: John Wiley & Sons, 2004.

[21] A. E. Ivanescu *et al.*, "The Importance of Prediction Model Validation and Assessment in Obesity

and Nutrition Research," *Int. J. Obes.*, vol. 40, no. 6, pp. 887–894, 2016.

[22] M. D. Petty, "Calculating and Using Confidence Intervals for Model Validation," 2013.

[23] J. Henseler, C. M. Ringle, and R. R. Sinkovics, "The Use of Partial Least Squares Path Modeling in International Marketing," *Adv. Int. Mark.*, vol. 20, pp. 277–320, 2009.

[24] H. H. Tung, "Industrial perspectives of pharmaceutical crystallization," *Org. Process Res. Dev.*, vol. 17, no. 3, pp. 445–454, 2013.

[25] D. O'Grady, M. Barrett, E. Casey, and B. Glennon, "The Effect of Mixing on the Metastable Zone Width and Nucleation Kinetics in the Anti-Solvent Crystallization of Benzoic Acid," *Chem. Eng. Res. Des.*, vol. 85, no. 7, pp. 945–952, 2007.

Chapter 6 Quality by statistical control: Probability of success of having particle size distribution within specification in an anti-solvent crystallization[4]

[4] Part of this work was published in:

A. Tulcidas, B. Santos, S. Pawlowski and F. Rocha, “Quality by statistical control in crystallization - Assessment of mixing conditions and probability of obtaining the desired particle size”, Industrial & Engineering Chemistry Research, vol. 58, pp. 20162 - 20172, 2019.

6.1. Scope

In the previous chapters, statistical models were developed to correlate the suspension height to clearance ratio (H/C), percentage of volume of suspension occupied in the reactor (%Vol), power per volume (PV) and tip speed (TS) with particle size distribution (PSD) parameters Dv10, Dv50 and Dv90 of an API (Active Pharmaceutical Ingredient), obtained in an anti-solvent crystallization.

The main aim of this study is to build a design space or a region that indicates which operating conditions can lead to PSD parameters within specification. To accomplish the goal, two methodologies were developed. The first methodology consisted in using an indicator function. The second approach considered the existence of correlation among the PSD parameters and therefore Monte Carlo (MC) simulations were performed to calculate the probability of success of having the three PSD parameters within specification. This work allowed to obtain a design space comprising the optimal percentage of volume, power per volume and tip speed operational values to be used in the anti-solvent crystallization process, which can be helpful to support risk based decisions.

6.2. Introduction

Quality by Design (QbD) allows gaining a thorough understanding of a product and its manufacturing process, by evaluating the relationship between a process and a product's critical quality attributes (CQAs) [1]. Design of Experiments (DoE) is a QbD tool that allows defining an operating window that provides a high level of confidence to meet specifications [2] by revealing relationships between input and output factors, and its prevalence over the traditional univariate approach to development studies is the ability to properly uncover how factors collectively affect the output responses [3]. DoE minimizes the number of experiments while allowing the gathering of the most important information [4]. When implementing DoE, the acceptable ranges for critical process parameters affecting the response factors are defined in a design space. The experimental data obtained is used to feed mathematical models in order to predict the response factors and define an operating window that leads to a high probability of the responses being in line with the specification [5]·[6]. For instance, Rozet *et al*. [7] describe how a design space containing the probability of success can be built for analytical methods, with examples involving chromatographic techniques. In the crystallization area, Thirunahari *et al*. [8] developed a design space for cooling crystallization of the desired form I of the polymorphic drug Tolbutamide and Gong *et al.* [9], developed a design space for an ethanol precipitation process using Monte-Carlo simulations. However, no thorough description of the methodology employed was given. Hence, in the crystallization field, there are still few publications reporting a methodology to create a design space quantifying the probability of success of a CQA meeting the specification.

A design space can be obtained by using the posterior probability to meet specifications for all the critical quality attributes jointly [10], [11]. This posterior probability, which is the probability of a certain event occurring based on previous information, can be employed to determine the probability of success (PoS) using Equation 6.1 [11]. In order to account for the correlation among the variables, their joint multivariate distribution should be taken into account [12]. For instance, in multivariate normal distributions, the covariance matrix and the mean vector completely specify the joint distribution [12].

$$PoS = (\tilde{y} \in \lambda \mid x_z, data) \approx \frac{1}{n^*}\sum_{n=1}^{n^*} I(\widetilde{y^s} \in \lambda) \quad (6.1)$$

In Equation 6.1 $(\tilde{y} \in \lambda \mid x_z, data)$ is a new predicted set of responses at a new operating set of input variables x_z. $\widetilde{y^s}$ is a set of values generated on a total of n* Monte-Carlo simulations and λ is the set of specifications [11].

The work presented herein consists of using the statistical models obtained in the previous chapters to develop a methodology that aids in calculating a safe operational zone where an API with particle size within specification could be produced; this methodology can be then employed to models that are more complex. Two approaches were used to obtain a design space, where one of the methods allowed quantifying the probability of simultaneously obtaining the PSD parameters within specification, considering the events as dependent.

6.3. Design space development methodology

6.3.1. Preliminary design space

The values of Dv10, Dv50 and Dv90 estimated by the models were compared against the specification using an indicator function *I* (Equation 6.2). Equation 6.2 is an example of the indicator function based on the models developed using H/C and PV as predictors. To take into account the models attained with %Vol, PV and TS as predictors, the indicator function can be similarly adapted.

$$I\ (Dv10, Dv50, Dv90)\ = \begin{Bmatrix} 1\ if\ \ Dv10_{min\ spec\ value} \leq Dv10((H/C)^2, PV) \leq Dv10_{max\ spec\ value} \\ 1\ if\ \ Dv50_{min\ spec\ value} \leq Dv50((H/C)^2, PV) \leq Dv50_{max\ spec\ value} \\ 1\ if\ Dv90_{min\ spec\ value} \leq Dv90(PV^2) \leq Dv90_{max\ spec\ value} \\ 0\ \ otherwise \end{Bmatrix} \quad (6.2)$$

A preliminary design space was obtained in order to conceptualize a zone where the Dv10, Dv50 and Dv90 meets the specifications.

For scrutiny, the probability of success of obtaining Dv10, Dv50 and Dv90 within specification was quantified considering them as dependent events.

6.3.2. Design space comprising the probability of success

In order to obtain a design space with the probability of success, assuming that Dv10, Dv50 and Dv90 are dependent among one another, Equation 6.1 was employed. The Jackknife resampling method was used to estimate the precision of the regression models. This method allowed the determination of the mean and covariance of the regression coefficients (β) for each Dv10, Dv50 and Dv90 model. Secondly, Monte-Carlo simulations were performed, where new β values (β*) following a multivariate normal distribution were generated for each pair of predictors H/C and PV, using the mean and covariance previously obtained. New values of Dv10, Dv50 and Dv90 were calculated from the generated β* and were compared against the specification and the probability of success was quantified by using Equation 6.1.

The detailed procedure is described in the following sections.

Resampling

Resampling involves constructing subset 'populations' derived from the experimental observations[13]. The half-sample method, used by Mahalanobis in 1946 under the name Interpenetrating samples, is one of the oldest resampling method, where one repeatedly chooses at random half of the data points, and estimates the statistics for each resample[14]. An important variant

is the Quenouille–Tukey Jackknife method. For a dataset with n data points, one constructs exactly n hypothetical datasets each with n − 1 points, each one omitting a different point. This resampling method is a generalization of the leave-one-out approach, where the number left out can range from one observation to half the sample[15]. Another popular resampling method is Bootstrap. In this method, one generates a large number of datasets, each with n data points randomly drawn from the original data. The constraint is that each draw is made from the entire dataset, so a simulated dataset is likely to miss some points and have duplicates or triplicates of others[14] and thus, might not be suitable for small data sets. Considering small datasets, the Jackknife is more adequate.

Since the experimental dataset used in this work is small, Jackknife resampling method was employed. The steps performed are described below[16].

1. One observation from the experimental data (H/C, PV, Dv10, Dv50 and Dv90) was drawn and new regression coefficients β were estimated using the remaining data, for each Dv10, Dv50 and Dv90 model, using the Least Squares' method.
2. The removed data was recovered, the following observation was removed, and a new set of regression coefficients was estimated using the remaining data.
3. Similarly, each remaining data was omitted, and a new set of regression coefficients was estimated. The procedure was repeated until reaching the total number of experimental observations.

A simple outlier analysis was executed using the algorithm 3σ [17]. This method assumes that the data follows a normal distribution and identifies as an outlier any value outside the three-sigma range (mean ± 3σ).

Covariance matrix

As mentioned previously, in multivariate normal distributions, the covariance matrix and the mean vector are necessary to characterize the joint distribution [12]. The multivariate normal distribution of a k-dimensional random vector $X = (X_1, X_2, ..., X_k)^T$ can be written as $X \sim N(\mu, \Sigma)$, where μ is the k-dimensional mean vector and Σ is a k x k covariance matrix [18].

The covariance of two random variables is a measure of their joint variability, or their degree of association and is the average value of the product of the deviation of *X* from its mean and the deviation of *Y* from its mean [19]. The covariance matrix was calculated using the *cov* function of the SciLab program. For instance, the covariance of *X* and *Y* is defined by Equation 6.3.

$$Cov(X,Y) = E[(X - \bar{X})(Y - \bar{Y})] \tag{6.3}$$

where $\bar{X}$ and $\bar{Y}$ are the expected values of the mean values of X and Y, respectively.

In this work, the covariance matrix was obtained with the resampled values of regression coefficients β (Equation 6.4).

$$Cov(\beta_{1,Dv10}, \beta_{2,Dv10}, \beta_{3,Dv10}, \beta_{1,Dv50,}\ \beta_{2,Dv50}, \beta_{1,Dv90}, \beta_{2,Dv90}) \approx E[(\beta_{1,Dv10} - \bar{\beta}_{1,Dv10})(\beta_{2,Dv10} - \bar{\beta}_{2,Dv10})(\beta_{3,Dv10} - \bar{\beta}_{3,Dv10})(\beta_{1,Dv50} - \bar{\beta}_{1,Dv50})(\beta_{2,Dv50} - \bar{\beta}_{2,Dv50})(\beta_{1,Dv90} - \bar{\beta}_{1,Dv90})(\beta_{2,Dv90} - \bar{\beta}_{2,Dv90})] \quad (6.4)$$

Monte-Carlo simulations

Monte Carlo simulation computes random sampling and conducts a large number of simulations [20]. In each experiment, the possible values of a variable (e.g. *X*) are generated according to their distribution. The generated values of *X* are then used to calculate the values of, for instance, a function *Y* (X), whose values can then be used for further statistical analysis [20], [21].

In order to perform Monte-Carlo simulations, *grand* function was used in SciLab. This function is described by Equation 6.5.

$$Y = grand\ (n, \textit{"mn", Mean, Cov)} \quad (6.5)$$

This function generates random values of Y, that follow a multivariate normal (*"mn")* distribution with the respective mean and covariance matrix, n times ($n = n^*$= number of simulations).

The approach presented in [22] was followed to calculate the number of simulations to be performed (n^*) (Equation 6.6).

$$n^* = (1.96\ \frac{\sigma_{high\ number\ of\ simulations}}{precision\ \mu_{desired}})^2 \quad (6.6)$$

This approach consists of estimating the number of simulations needed to obtain generated values with a 95% confidence level, hence the 1.96 in Equation 6.6, corresponds to the standard normal distribution Z value for such level of confidence. Primarily, the standard deviation was quantified for a trial simulation with high number of runs ($\sigma_{high\ number\ of\ simulations}$) to assure a stable value. The mean value desired ($\mu_{desired}$) is the mean value to which the Monte-Carlo simulations should approximate to. For instance, when generating regression coefficients β*, the mean values of β calculated from the resampled data were used. The precision is the deviation from the mean value and a value of 1% was set.

Subsequently, after calculating the optimal number of simulations, new regression coefficients were generated, using the mean and covariance previously obtained (Equation 6.4). The new set of values of Dv10, Dv50 and Dv90 generated from each new regression coefficients for each pair of H/C and PV conditions were compared against the specification and the number of events within the specification were quantified and divided by the number of simulations, in order to calculate the probability of success (Equation 6.1). The steps followed to obtain the probability of success assuming dependent events, are summarized in Figure 6.1.

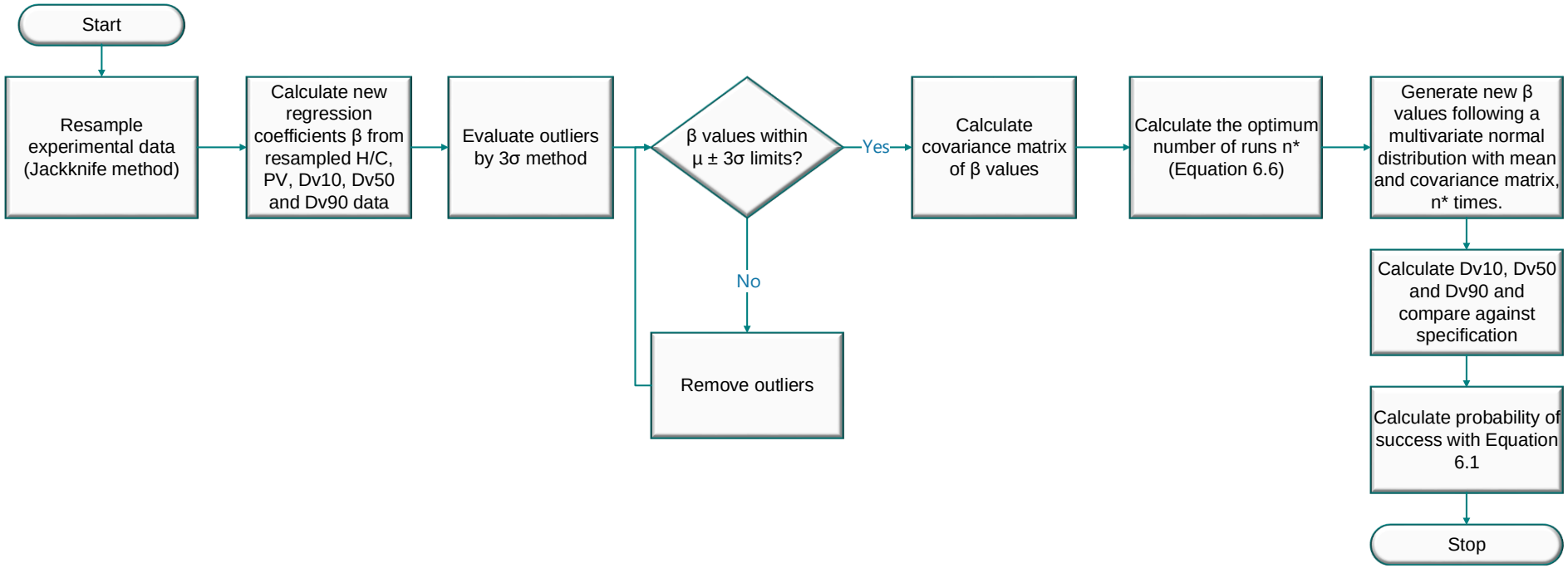

Figure 6.1. Methodology followed to obtain a design space comprising the probability of success of obtaining PSD parameters within specification, considering dependent events.

6.4. Results and discussion

The models used to create the design space are presented in Table 6.1 and were developed in the previous chapters.

Table 6.1 – Models used in this study and the respective adjusted R^2.

Predictors	Model	Adjusted R^2
H/C - PV	$D_{v10} = \beta_{1,Dv10}.(H/C)^2 + \beta_{2,Dv10}.PV + \beta_{3,Dv10}$	0.58
	$D_{v50} = \beta_{1,Dv50}.(H/C)^2 + \beta_{2,Dv50}.PV + \beta_{3,Dv50}$	0.71
	$D_{v90} = \beta_{1,Dv90}.PV^2 + \beta_{2.Dv90}$	0.80
%Volume - PV	$D_{v10} = \beta_{1,Dv10}\%Vol^2 + \beta_{2,Dv10}PV + \beta_{3,Dv10}$	0.87
	$D_{v50} = \beta_{1,Dv50}PV^2 + \beta_{2,Dv50}$	0.87
	$D_{v90} = \beta_{1,Dv90}PV^2 + \beta_{2,Dv90}$	0.91
%Volume - TS	$D_{v10} = \beta_{1,Dv10}\%Vol^2 + \beta_{2,Dv10}TS + \beta_{3,Dv10}$	0.86
	$D_{v50} = \beta_{1,Dv50}\%Vol^2 + \beta_{2,Dv50}TS + \beta_{3,Dv50}$	0.82
	$D_{v90} = \beta_{1,Dv90}\%Vol + \beta_{2,Dv90}\sqrt{TS} + \beta_{3,Dv90}$	0.86

The results presented regarding the design spaces obtained considering the obtainment of Dv10, Dv50 and Dv90 within specification are presented and discussed in the following section.

6.4.1. Preliminary design space

A preliminary design space was obtained in order to conceptualize a zone where the Dv10, Dv50 and Dv90 meet the specifications (Figure 6.2 and Figure 6.3) using Equation 6.2.

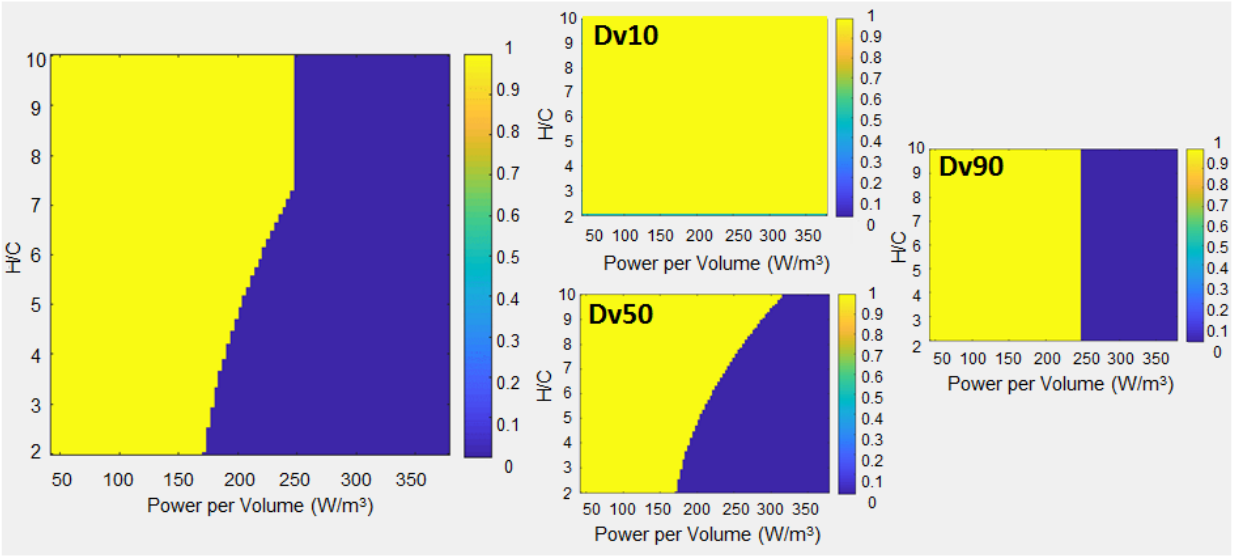

Figure 6.2. Left: preliminary design space indicating the operating zone where Dv10, Dv50 and Dv90 simultaneously meet the specifications (when I (Dv10, Dv50, Dv90) from Equation 6.2 equals to 1; yellow area). Right: preliminary design space for each PSD parameter Dv10, Dv50 and Dv90.

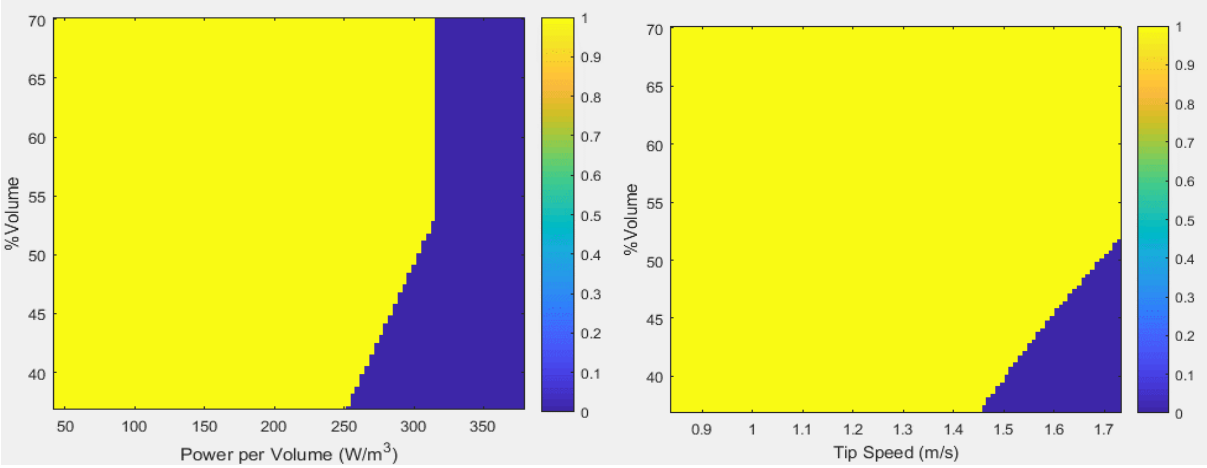

Figure 6.3. Preliminary design space depicting the operating zone where Dv10, Dv50 and Dv90 simultaneously meet the specifications, built from the models developed when using %Vol and PV as predictors (left) and %Vol and TS as predictors (right).

In Figure 6.2 and Figure 6.3, the preliminary design spaces indicate that it is safe to work in the yellow area, which is the area where Dv10, Dv50 and Dv90 are all within specification. The operating region obtained (Figure 6.2 – left) is in accordance with the expected, since it represents an overlay of the design spaces individually built for each PSD parameter (Figure 6.2 – right). Moreover, this design space depicts that the particle size distribution of the product will be within specification regardless of the H/C ratio used and until a power per volume value of approximately 175 W/m^3 is applied. Applying power per volume higher than the aforementioned value with lower H/C ratios seems to lead to out-of-specification product. As explained in chapter 4, low H/C translates to higher clearances, and in these conditions, the impeller is near the supersaturated build-up zone. Applying vigorous agitation in this region can lead to higher nucleation rates induced by secondary nucleation due to particle-particle and particle-impeller collision. Moreover, higher nucleation rates indicate less solute available for the crystals to grow which can generate substantially smaller crystals, which do not meet the particle size specifications. These principles can also explain the interpretation of the design spaces depicted in Figure 6.3. Both design spaces shown in Figure 6.3 indicate that working at higher PV and TS, along with lower values of %volume occupied by the suspension inside the reactor can lead to product that does not comply with the specification.

Although the preliminary design space presented can be useful to gain knowledge about the operating conditions to use in order to obtain particle size within specification, further improvement was considered. Consequently, a more detailed design space comprising the probability of success was generated considering that the events of Dv10, Dv50 and Dv90 being in specification are dependent. The results obtained are presented in the following section.

6.4.2. Design space comprising the probability of success

Resampling and covariance matrix

Jackknife resampling technique was employed to construct a larger dataset derived from the experimental observations for further statistical analysis (mean and covariance matrix determination). Figure 6.4 presents the regression coefficients obtained for each Dv10, Dv50 and Dv90 models using by the Least Squares' method for each pair of predictors (H/C – PV, %Volume – PV and %Volume – TS), as well as the outliers identified by using the 3σ algorithm.

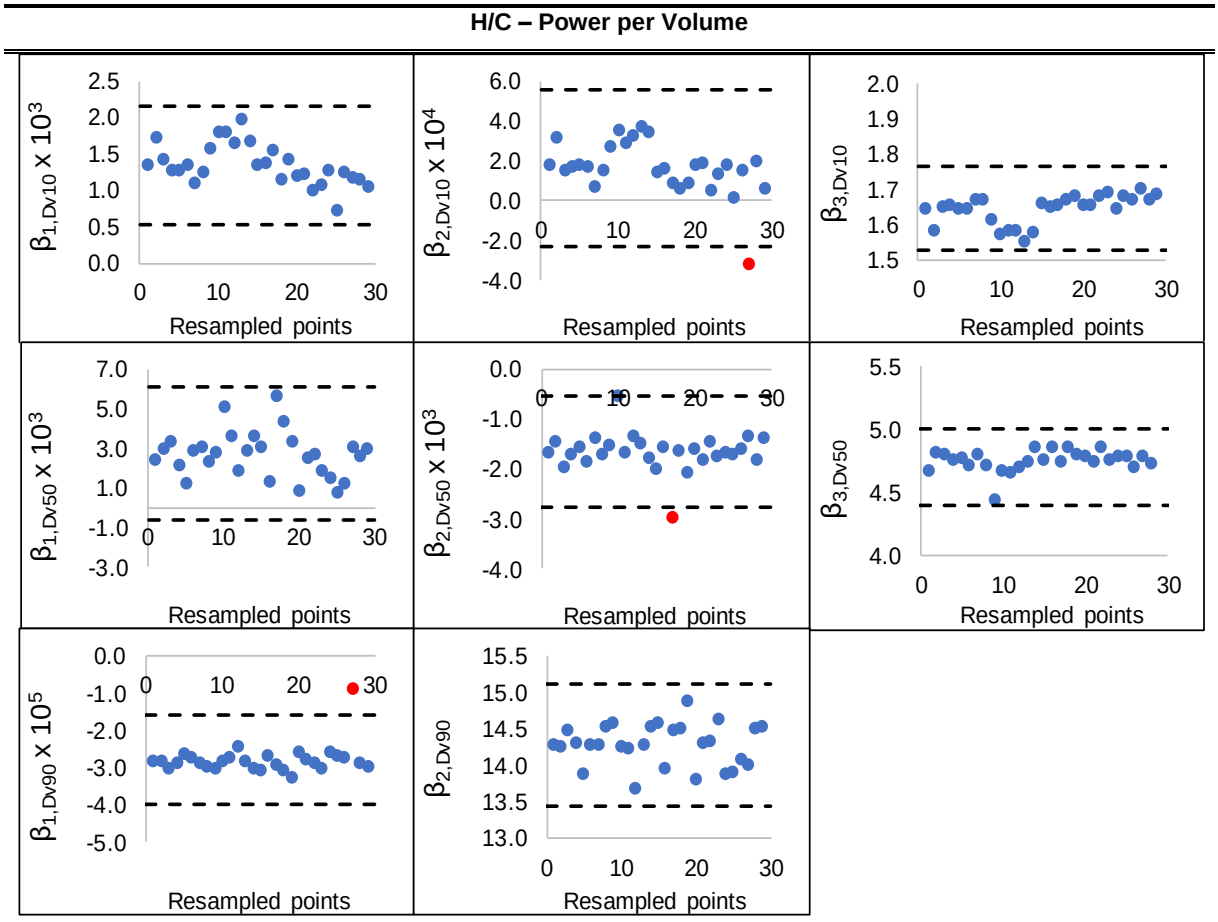

Figure 6.4. Resampled regression coefficients for each models with different set of predictors (H/C – PV, %Vol – PV and %Vol – TS) and the outliers identified as red. Dotted lines are the boundaries (mean value ± 3.standard deviation).

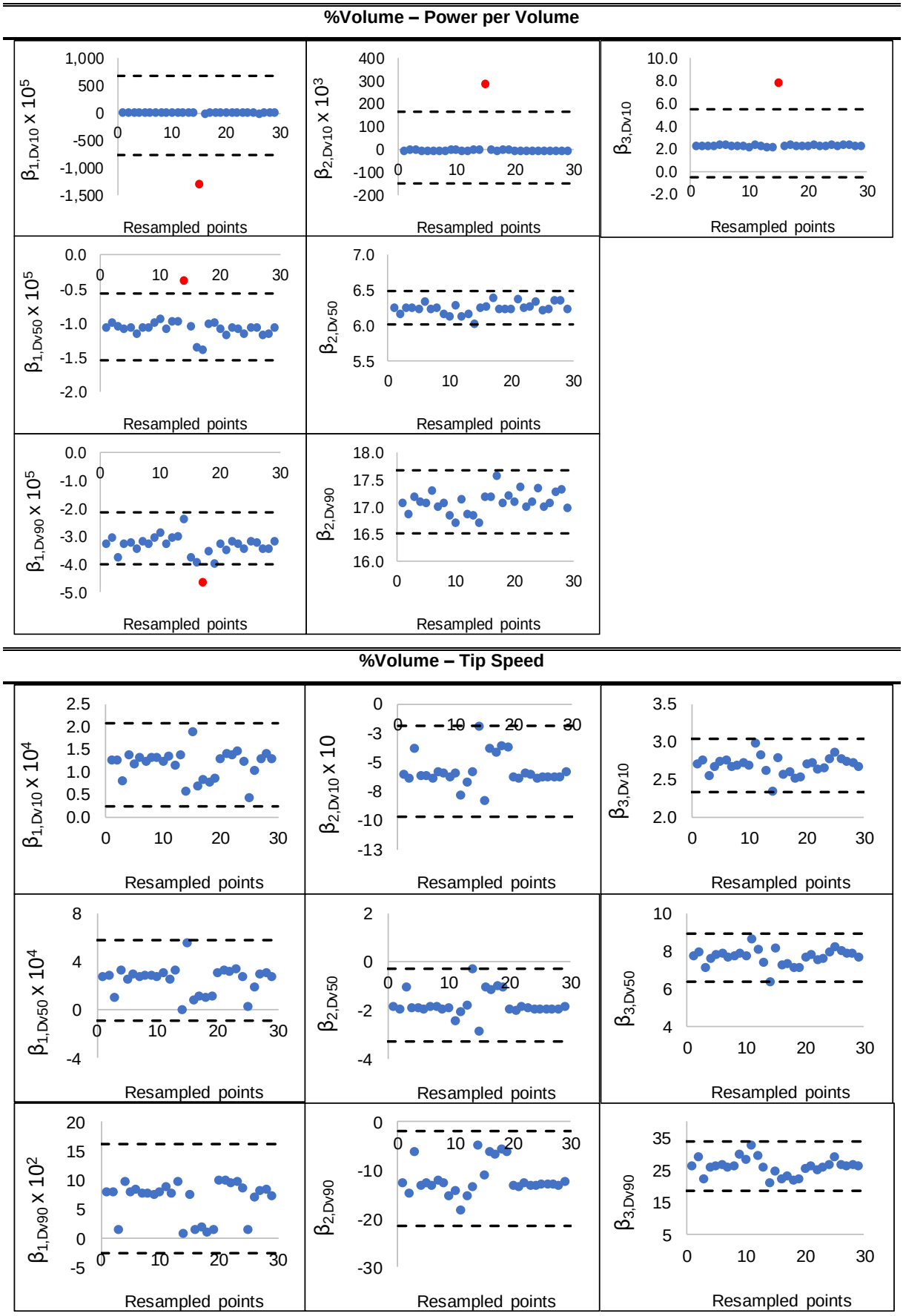

Figure 6.4 (Cont.). Resampled regression coefficients for each models with different set of predictors (%Vol – PV and %Vol – TS) and the outliers identified as red. Dotted lines are the boundaries (mean value ± 3.standard deviation).

From Figure 6.4, it is possible to observe that the resampled data is mostly within the mean ± 3σ boundaries defined to identify outliers. Nevertheless, the few outliers detected were removed.

Monte-Carlo simulations

Prior to performing Monte-Carlo simulations to quantify the probability of having Dv10, Dv50 and Dv90 within specifications, the number of runs needed to obtain generated values of β within a 95% confidence level was calculated for every model using Equation 6.6. The calculated number of runs needed to generate regression coefficients was 11769, 2422 and 8137 for the models developed using H/C and PV, %Vol and PV and %Vol and TS as predictors, respectively. Therefore, an approximate run number of 12000 was defined in order to attain generated values within the desired confidence level.

After performing the 12000 simulations, the following design space was obtained (Figure 6.5).

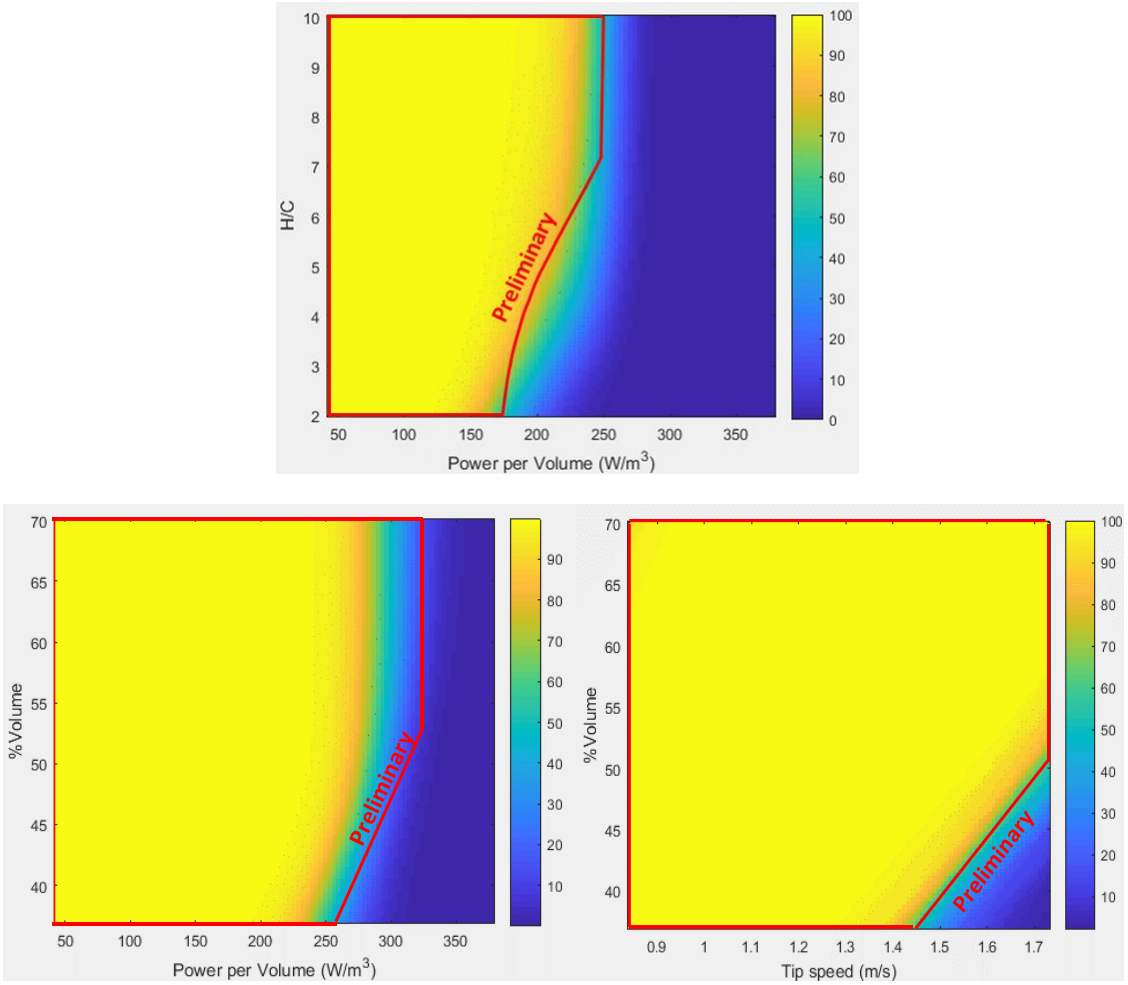

Figure 6.5. Comparison of the design space quantifying the probability of obtaining Dv10, Dv50 and Dv90 within specification, considering dependent events and the preliminary space (red lines) for each developed model.

Through Figure 6.5, the design space indicates that in order to have particle size within specification with a higher probability of success, regardless of the H/C ratio used, a power per volume

value of approximately 125 W/m^3 should be applied, instead of the 175 W/m^3 observed in the preliminary design space (Figure 6.2). Figure 6.5 – bottom compares the design spaces resulting from models developed with the predictors' set %Vol – PV and %Vol – TS with the preliminary design spaces. As stated previously, it can be observed that the design spaces shown in Figure 6.5 (bottom) suggest operating within a narrower region in order to have a higher probability of obtaining product within specification, in comparison with the preliminary design spaces.

Moreover, the tested experimental conditions used to develop each model were plotted in the design space, for further interpretation (Figure 6.6).

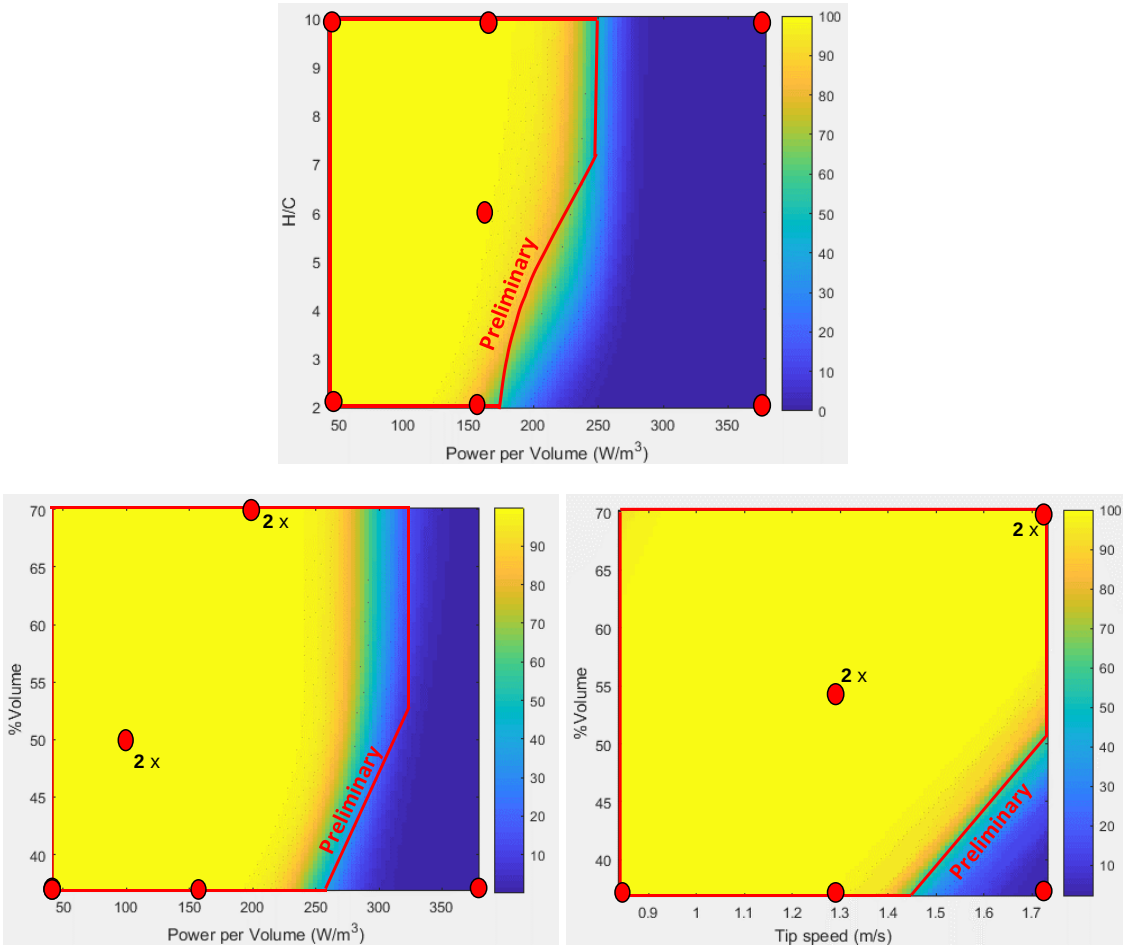

Figure 6.6. Design space depicting the experimental points performed to develop the models (red dots).

Analyzing Figure 6.6 (top), it can be observed that both design spaces are in accordance with the experimental data, since the product obtained in the two crystallization processes performed at 378 W/m^3 did not meet the particle size distribution specifications and the design space does seem to predict similar behavior. This behavior is also observed for the design spaces built from the models developed for the predictor sets %Vol – PV and %Vol – TS (Figure 6.6 – bottom), since these predict that the

product will fail the particle size specification when working at a PV of 378 W/m^3 and a TS of 1.7 m/s, as occurred experimentally.

Overall, comparing the two approaches used to define a design space (preliminary and dependent), the design space estimated considering that obtaining Dv10, Dv50 and Dv90 are dependent events (depicted in Figure 6.6) can be used as a worst case scenario, since it quantifies the probability of success and can be more helpful to support risk based decisions.

6.5. Conclusions

The aim of this study was to develop a methodology to obtain a design space quantifying the probability of success of having PSD (Dv10, Dv50 and Dv90) within specification, which can be useful during the development phase of crystallization processes.

The methodology consisted of executing Monte-Carlo simulations by generating regression coefficient values for each Dv10, Dv50 and Dv90 model developed throughout the thesis. The dependency existent among the PSD parameters was also taken into consideration, by comprising the correlation matrix in the simulations. The newly simulated regression coefficients were then fed into the previously developed models to estimate new values of Dv10, Dv50 and Dv90 for the set of predictors (H/C – PV, %Volume – PV and %Volume – TS) and compared against the specification. The developed methodology enabled to visually perceive the risk of failing when using certain operating conditions (for instance, higher PV and lower H/C and higher PV and TS along with lower %Volume can lead to a lower probability of success, i.e. higher risk of failing the specification).

Moreover, the predicted design spaces were compared with the experimental points used to build the models and it was witnessed that these were in accordance.

Therefore, employing statistical model development and methodologies to generate a more sophisticated design space that quantifies the probability of having the particle size distribution within specification, can be extremely useful to gain further process knowledge and to aid in decreasing the financial costs caused by out-of-specification batches.

References

[1] A. S. Rathore and H. Winkle, “Quality by design for biopharmaceuticals,” *Nat. Biotechnol.*, vol. 27, no. 1, pp. 26–34, 2009.

[2] P. Whitcomb and M. Anderson, “Using DOE with Tolerance Intervals to Verify Specifications,” in *11th annual ENBIS Conference*, 2011.

[3] L. X. Yu *et al.*, “Understanding Pharmaceutical Quality by Design,” *AAPS J.*, vol. 16, no. 4, pp. 771–783, 2014.

[4] D. W. Kim, M. W. Cho, T. Il Seo, and E. S. Lee, “Application of design of experiment method for thrust force minimization in step-feed micro drilling,” *Sensors*, vol. 8, no. 1, pp. 211–221, 2008.

[5] S. A. Weissman and N. G. Anderson, “Design of Experiments (DoE) and Process Optimization. A Review of Recent Publications,” *Org. Process Res. Dev.*, vol. 19, no. 11, pp. 1605–1633, 2015.

[6] S. De Gryze, I. Langhans, and M. Vandebroek, “Using the correct intervals for prediction: A tutorial on tolerance intervals for ordinary least-squares regression,” *Chemom. Intell. Lab. Syst.*, vol. 87, no. 2, pp. 147–154, 2007.

[7] E. Rozet, P. Lebrun, B. Debrus, B. Boulanger, and P. Hubert, “Design Spaces for analytical methods,” *Trends Anal. Chem.*, vol. 42, pp. 157–167, 2013.

[8] S. Thirunahari, P. S. Chow, and R. B. H. Tan, “Quality by Design (QbD) -Based Crystallization Process Development for the Polymorphic Drug Tolbutamide,” *Cryst. Growth Des.*, vol. 11, no. 7, pp. 3027–3038, 2011.

[9] X. Gong, Y. Li, Z. Guo, and H. Qu, “Control the effects caused by noise parameter fluctuations to improve pharmaceutical process robustness : A case study of design space development for an ethanol precipitation process,” *Sep. Purif. Technol.*, vol. 132, pp. 126–137, 2014.

[10] J. J. Peterson, “A Bayesian Approach to the ICH Q8 Definition of Design Space,” *J. Biopharm. Stat.*, vol. 18:5, no. April 2013, pp. 959–975, 2008.

[11] T. Coffey and H. Yang, *Statistics for Biotechnology Process Development*, 1st ed. Florida; US: CRC Press, 2018.

[12] M. Bohdalová and Ľ. Šlahor, “Monte Carlo Simulations of the multivariate distributions with different marginals,” 2007. .

[13] H. T. Hendi, “Jackknife Method to Estimate the Confidence Intervals about an R-squared statistic Using SAS Software,” *Glob. J. Res. Anal.*, vol. 6, no. 5, pp. 679–683, 2017.

[14] G. J. Babu, “Jackknife and Bootstrap,” 2008. .

[15] P. I. Good, *Resampling Methods - A Practical Guide to Data Analysis*, 3rd ed. Birkhäuser.

[16] Z. Y. Algamal and K. B. Rasheed, “Re-sampling in Linear Regression Model Using Jackknife and Bootstrap,” *Iraqi J. Stat. Sci.*, no. 18, pp. 59–73, 2010.

[17] R. K. Pearson, “Outliers in Process Modeling and Identification,” *IEEE Trans. Control Syst. Technol.*, vol. 10, no. 1, pp. 55–63, 2002.

[18] M. Siotani, “Tolerance Regions for a Multivariate Normal Population,” *Ann. Inst. Stat. Math.*, vol. 16, no. 1, pp. 135–153, 1964.

[19] J. A. Rice, *Mathematical Statistics and Data Analysis*, 3rd ed. Duxbury: Thomson Brooks/Cole, 2007.

[20] J. N. Siddall, *Probabilistic Engineering Design*. CRC Press, 1983.

[21] M. Bohdalová and Ľu. Šlahor, “Simulations of the Correlated Financial Risk,” *J. Appl. Math. Stat. Informatics*, vol. 4, no. 1, pp. 89–99, 2008.

[22] W. L. Winston, *Operations Research - Applications and Algorithms*, 4th editio. Thomson Brooks/Cole, 2004.

Chapter 7 Final Remarks

7.1. Conclusions

The main aim of this thesis was to understand and gain knowledge about crystallization processes, which was done firstly at lab-scale (Chapters 3 and 4), and to build models that can aid the prediction of particle size distribution parameters of the API at larger scales, in order to minimize the production of batches that do not comply with the established specification (Chapters 5 and 6).

Chapter 3 gives awareness about the importance of monitoring the crystallization process and how the operating conditions and the system of solvents used affect some of the final properties of the product such as purity, size, crystal habit and polymorphic form. Chapter 4 provides an insight about the impact of the clearance and agitation applied during an anti-solvent crystallization on the particle size distribution parameters of an API. Chapter 5 focuses in building a statistical methodology that can predict the particle size parameters at industrial scale using data from scale-down anti-solvent crystallization experiments performed at the laboratorial scale. Lastly, Chapter 6 highlights the importance of the process risk analysis, where a methodology was developed using the models found in the previous chapters, to build a design space that quantifies the probability of the product meeting the particle size specification.

7.1.1. Characterization at lab-scale of crystal habit, size and polymorphic stability of an API

This chapter aimed to better understand and optimize a crystallization process, where an API presenting a different crystal habit and size with a specific polymorphic form was desired. The process, consisting of an evaporative crystallization in ethanol followed by cooling, was monitored with a FBRM Lasentec probe, where additional steps such as heating and cooling cycles were executed in order to induce the Ostwald ripening phenomenon to assess their impact on the crystal habit and size. As detected by the FBRM probe, and as expected, the fine particles' count slightly decreased when the temperature increased, due to the dissolution of these smaller particles, while the remaining particles' count maintained constant. This was only detected when applying the second heating cycle, which implies that inducing more cycles could result into better results. Moreover, it was also possible to observe that, when applying cooling ramps, only the number of fine particles increased. This increase in the number of counts of small particles could be either due to the supersaturation attained during cooling or due to the stirring speed applied which might additionally induce secondary nucleation. It was also possible to observe that during the agitation at constant temperature, the number of smaller particles increased, which can be interpreted as the existence of secondary nucleation caused by the stirrer (particle-particle collision, particle-baffle-impeller-reactor walls collision).

In order to quantify the supersaturation during the crystallization step, the solubility curve of the API in ethanol was determined using turbidity probes. From the obtained turbidity data, it was possible to conclude that the metastable zone is wider using high cooling rates. Additionally, it was also detected that the metastable zone widens as the saturation temperature decreases. When performing a cooling crystallization experiment with a slow cooling rate and supersaturation ratio lower than the one of the evaporative method, growth and agglomeration of the crystals were observed, which in turn resulted into particles that are more robust.

Polymorphic stability studies of the API were executed in a slurry of the product in a mixture of 1,2-dimethoxyethane:heptane, with different stirring rates and a heating step at 50ºC and 80ºC (higher than the melting point of the product). It was found that the stirring speed did not seem to affect the final form. The new system of solvents showed promising results when performing the heating step of the slurry experiment at higher temperatures (80ºC). Comparing the dimensions of the crystals that resulted from heating the slurry of the API at 80°C with the ones obtained in the remaining tests performed at 50°C, it was visible a significant increase of the size of the particles. In addition, comparing the crystal dimensions with the ones of the starting material, these presented an increase of 480%. The desired polymorphic form was attained as well as an acceptable purity.

These experimental observations are highly promising, particularly in cases where the crystal habit cannot be easily attained by altering the solvent or the supersaturation.

As concluding remarks, the obtained results show how operating conditions such as supersaturation, stirring speed, seeding, and temperature affect the final properties of the product such as crystal habit, size, purity and polymorphic form. In addition, these also show the importance of following the particle size in-situ during the process development phase to understand the impact of minor changes in the operating conditions.

7.1.2. Characterization at lab-scale of the influence of the mixing conditions on the particle size in anti-solvent crystallization of an API

In this work was investigated the impact of suspension height to clearance ratio (H/C) and power per volume (PV) on the PSD parameters (Dv10, Dv50 and Dv90) of an API obtained through an anti-solvent crystallization method.

It was found that Dv10 and Dv50 are proportional to the H/C, which imply that the particle size is higher when the ratio H/C increases (narrow clearance, C). On the other hand, Dv90 seems to be only influenced by the PV applied.

The relation between the particle size and nucleation rate was also evaluated. It was observed that the nucleation rate seems to moderately influence the particle size parameters Dv50 and Dv90. The models indicated that the particle size parameters Dv50 and Dv90 decrease when the nucleation rate increases, as expected, since higher nucleation rates indicate a low growth rate and as result, small sized particles are formed.

7.1.3. Statistical methodology for scale-up of an anti-solvent crystallization of an API

The main aim of this study was to further understand the impact of the volume of the mixture occupied in the reactor and mixing parameters such as power per volume and tip speed, on the particle size of the product and use statistical modelling for a successful scale-up.

Relations among percentage of volume, power per volume, tip speed and particle size distribution parameters were found using multiple linear regression. It was concluded that the regression coefficients' values indicate that the particle size distribution parameters decrease when the mixing parameters power per volume and tip speed increase. In addition, this behaviour was expected when API solution is added into the anti-solvent instead of adding the anti-solvent into the API solution, since this procedure promotes the formation of small crystals. Thus, these results enhance the importance of mixing parameters in anti-solvent crystallizations to control the particle size of the API.

The majority of the models fed with percentage of volume and power per volume were validated successfully within the calibration range, with a deviation value up to 16% between the predicted and production. Regarding the models built with percentage of volume and tip speed, the validation was also successful with deviation values up to 17%.

This work's results show that using the data obtained in scale-down experiments to develop statistical models seem to predict the particle size parameters in the production scale, as long as the predictors such as power per volume and tip speed are maintained constant between scales. Hence, it would be promising to process chemists to follow this methodology during the development of anti-solvent crystallization processes.

7.1.4. Quality by statistical control: Probability of success of having particle size distribution within specification in an anti-solvent crystallization

In this work, two methodologies were used to develop a design space depicting the zone where the predictors H/C, %Volume, power per volume and tip speed studied in the previous chapters can lead to PSD parameters Dv10, Dv50 and D90 within specification.

One approach consisted in using the indicator function. The second approach consisted in calculating the probability of obtaining Dv10, Dv50 and Dv90 simultaneously within the specification, by executing Monte-Carlo simulations by generating regression coefficient values for each Dv10, Dv50 and Dv90 model developed throughout the thesis. The dependency existent among the PSD parameters was also taken into consideration, by comprising the correlation matrix in the simulations. The newly simulated regression coefficients were then fed into the previously developed models to estimate new values of Dv10, Dv50 and Dv90 for the set of predictors (H/C – PV, %Volume – PV and %Volume – TS) and compared against the specification.

The methodologies presented in this work enabled to visually understand the risk of failing the particle size specification when using certain operating conditions. For instance, performing the crystallization process described in chapters 5 and 6 at higher PV and lower H/C and higher PV and TS

along with lower %Volume can lead to a lower probability of obtaining product within the desired particle size, i.e. higher risk of failing the specification.

This work enhances that developing statistical models and methodologies to generate a more detailed design space quantifying the probability of having the particle size distribution within specification, can be useful to gain further process knowledge and to aid taking risk-based decisions, especially when dealing with limited datasets.

7.2. Guidelines for similar process challenges

The actions taken throughout this work that allowed attaining the desired physical product properties were summarized as guidelines, which can be used in similar crystallization processes (Table 7.1).

Table 7.1 – Summary of some actions taken to overcome certain challenges, based on the conclusions of this thesis.

Challenge	Action
Increase crystal size	• Determine the metastable zone width (MSZW) and perform the crystallization process near the solubility curve (low supersaturation conditions). • If low supersaturation does not increase the crystal size, attempt seeding. • Try performing heating and cooling cycles to induce Ostwald ripening phenomenon. • Attempt using low agitation or perform DoE varying agitation and volume of suspension in the reactor and clearance (for anti-solvent crystallization processes).
Modify crystal habit	• Attempt working at a temperature above the melting point of the product (if API has a low melting point). • Change solvent system.
Obtain the most stable polymorph	• Attempt working at a temperature above the melting point of the product (if API has a low melting point).
Maintain particle size during scale-up of anti-solvent crystallization	• Follow the statistical methodology presented in this work based on scale-down experiments.

7.3. Future work

The work developed herein represents a solid base for future work and thus, some recommendations are proposed in this section.

7.3.1. Characterization of crystal habit, size and polymorphic stability

In this work, changes in the crystal habit and polymorphic form were witnessed when performing a slurry test at a temperature above the melting point of an API. A suggested follow-up for this topic is the performance of slurry tests with different low melting point APIs at a temperature higher than the melting point, in order to check if a change in crystal habit and polymorphic form is still attainable with this approach. Furthermore, it would also be intriguing to carry out these tests in different scales and investigate the impact of the scale in the obtained results.

Regarding the evaporative crystallization in ethanol, it would be of interest to attempt to conduct the process at different evaporation rates, in order to observe if it could avoid an abrupt supersaturation increase and therefore allow the crystals to grow and attain a different habit and polymorphic form.

7.3.2. Influence of the mixing conditions on the particle size

In this work the impact of varying mixing parameters such as percentage of volume occupied by the suspension in the reactor (%Vol), the suspension height and clearance ratio (H/C), power per volume (PV) and tip speed (TS) on the particle size distribution was assessed through statistical modeling.

It would be intriguing to check if the inclusion of shear rate, mixing time and/or Reynolds number as models' parameters could lead to improvement of the so far achieved predictions. Computational fluid dynamics (CFD) tools can be eventually used to estimate the local shear rate. The use of probes such as React-IR, which measure *in-situ* the concentration of the API in solution, would also be of interest in order to monitor the supersaturation in real time during the crystallization processes.

7.3.3. Statistical methodology for scale-up of an anti-solvent crystallization process

A statistical methodology to aid the scale-up of an anti-solvent crystallization procedure was developed from the data obtained during tests in which the power per volume and certain geometric features were maintained constant between the laboratory and industrial scales. Therefore, it would be interesting to check if this methodology is also applicable to other APIs by performing similar experiments and subsequently employing the herein developed methodology to predict the particle size parameters of different APIs at an industrial scale.

7.3.4. Detailed validation of the developed design spaces

A methodology was developed to estimate a design space comprising the probability of obtaining product with particle size distribution parameters within specification. A very good agreement was observed between the estimated design spaces and the experimental points obtained previously and used to build the models described in the previous chapters. For research purposes and for a thorough validation, it would be of interest to perform several crystallization experiments at different operating conditions and to check how many of them lead to product within specification and to compare it with the estimated probability of success.